University of Minnesota
St. Anthony Falls Hydraulic Laboratory

Project Report No. 325

METHANE TRACER TECHNIQUE FOR GAS TRANSFER AT HYDRAULIC STRUCTURES

by

John P. McDonald

and

John S. Gulliver

Prepared for the

LEGISLATIVE COMMISSION ON MINNESOTA RESOURCES
St. Paul, Minnesota

March 1992

ABSTRACT

Hydraulic structures have an impact on the amount of dissolved gases in a river system, even though the water is in contact with the structure for a short time. Bubbles become entrained when water flows over a spillway, creating more area for gas transfer. Because of this, the same transfer that normally would require several miles in a river can occur at a hydraulic structure.

It would seem natural to use oxygen to measure gas transfer at a structure. However, there are problems associated with using oxygen for measurement. Many times the dissolved oxygen (D.O.) levels are near saturation. The uncertainty associated with estimates of D.O. saturation concentration and with D.O. measurements then results in a large uncertainty in the gas transfer measurement. Also, if the reservoir is stratified, it is difficult to predict withdrawal from the various layers with the required accuracy.

Methane is produced in the sediments as a by–product of the anaerobic decomposition of organic material. Methanogenesis is the terminal process in a chain of decomposition processes and represents a major mechanism by which carbon leaves the sediments. Although methane is oxidized by bacteria to form carbon dioxide and water, the oxidation rate is insignificant over the short residence time of a hydraulic structure. If methane is present in measurable quantities, it may prove to be an excellent in–situ tracer of gas transfer.

This report investigates using methane as an in–situ tracer of gas transfer at hydraulic structures. There were two major objectives: first, to develop a measurement technique to determine methane concentrations accurately; second, to perform field investigations to determine the applicability of using methane as an in–situ tracer of gas transfer. During an investigation, samples were gathered upstream and downstream of the structure and the transfer efficiencies were calculated for oxygen and methane. The mid–winter sampling technique of Rindels and Gulliver (1987) was used to assure accurate oxygen transfer measurements.

Thene and Gulliver (1989) developed a headspace measurement technique while using propane as a tracer gas for measuring transfer efficiency at hydraulic structures. This measurement technique was adjusted to compute methane concentrations, and is also presented in this report.

Methane was found in sufficient quantities for accurate measurements in all but one river/reservoir, where sulfate reduction inhibited the production of methane. Methane was generally unstratified upstream except under ice cover, providing an excellent tracer for gas transfer. The exception was under ice cover, when methane tends to be stratified and accurate transfer

efficiency measurements were difficult. Under ice cover, however, the mid–winter oxygen measurements will produce accurate transfer efficiency measurements.

The stratification of methane under ice cover created difficulties with the comparison of oxygen and methane measurements because the field conditions required to accurately measure the transfer of the two gases seems to be mutually exclusive, except at a few structures. A technique using oxygen, methane, and temperature measurements with a selective withdrawal routine (Davis, et al, 1987) was developed to compare oxygen and methane transfer measurements. Oxygen and methane transfer efficiencies, after adjustment for diffusivities, were comparable at a given structure except when the entrained air bubbles were pulled to a depth in the tailwater causing the bubbles to experience a higher pressure. Since the partial pressure in air determines saturation concentration of atmospheric gases, the saturation concentration of oxygen is higher as the bubbles are pulled through the stilling basin. Thus, an "effective saturation" concentration must be determined for oxygen at hydraulic structures with a tailwater.

TABLE OF CONTENTS

LIST OF FIGURES

LIST OF PHOTOS

LIST OF SYMBOLS

AC	Area counts from gas chromatagraph
BC_d	Bias in downstream concentration
BC_u	Bias in upstream concentration
B_{EH}	Bias in Transfer Efficiency due to bias in Henry's law constant
C_d	Downstream concentration
C_{HS}	Concentration in headspace
C_i	Concentration in sample $_i$
C_s	Saturation concentration
C_{SYR}	Concentration in syringe
C_u	Upstream concentration
C_W	Concentration in water
D	Molecular diffusivity
D_{eff}	Effective depth
E	Transfer efficiency
f	Constant function
F_D	Dilution factor used by Thene and Gulliver (1989)
FID	Flame ionization detector
H	Tailwater depth
HCF	Headspace correction factor
HLC	Henry's Law constant
K	Transfer coefficient
K_g	Gas transfer coefficient
K_L	Liquid film transfer coefficient
LOD	Limit of Detection
LOQ	Limit of Quantification
M_{HS}	Mass of methane in headspace
M_{inj}	Mass of methane injected
M_m	Molecular mass of methane
M_w	Molecular mass of water

n	Number of moles
n_d	Number of samples downstream
n_u	Number of samples upstream
P	Pressure
P_e	Effective pressure
P_{HS}	Pressure in headspace
Q_a	Air flowrate
Q_w	Water flowrate
r	Deficit ratio
R_u	Universal gas constant
T	Temperature in degrees celsius
U_E	Uncertainty in Transfer Efficiency
U_{MASS}	Uncertainty in mass
V_{HS}	Volume of headspace
V_{INJ}	Volume of headspace injected
v_o	Minimum velocity for air entrainment
V_W	Volume of water
W_{CAL}	Uncertainty due to calibration
WC_d	Uncertainty in downstream concentration
WC_u	Uncertainty in upstream concentration
W_{EP}	Precision uncertainty in sample
W_{HCF}	Uncertainty due to headspace correction factor
σ	standard deviation
ρ	density of water
μ	dynamic viscosity
μg	micro–gram = 10^{-6} gram
μl	micro–liter = 10^{-6} liter

ACKNOWLEDGEMENTS

This work was sponsored by the Legislative Commission on Minnesota Resources and the Reservoir Water Quality Branch, Hydraulic Laboratory, U.S. Army Engineer Waterways Experiment Station, Vicksburg, MS.

This report is based on a thesis submitted to the faculty of the Graduate School of the University of Minnesota for partial fulfillment of the requirements of the degree of Masters of Science by John Preston McDonald.

Special thanks goes to Sylvia Schwartz for help with the gas chromatagraph, and to Carol Harbor for help with the Winkler titrations. Fred Luck and Bob Murdock also assisted in data gathering.

I. INTRODUCTION

Hydraulic structures have an impact on the amount of dissolved gases in a river system, even though the water is in contact with the structure for a short time. While water is flowing over a spillway, bubbles become entrained in the water, thus creating more surface area for gas transfer. Because of this the same gas transfer that normally would require several miles in a river can occur at a hydraulic structure. In addition, if bubbles are transported to various depths downstream of the structure the possibility of supersaturation exists. Supersaturation is normally not a problem with oxygen but dissolved nitrogen supersaturation can cause fish mortality by nitrogen gas bubble disease.

Many times interest lies in the transfer of oxygen from the atmosphere to the water. Therefore it seems logical to use oxygen for measurement. However, there are some problems associated with the measurement of dissolved oxygen. If the dissolved oxygen level is close to saturation, the uncertainty associated with the measurements makes the estimation of the gas transfer useless. Also if the reservoir is stratified. it is difficult to predict withdrawal from the various layers with the required precision.

Rindels and Gulliver (1989) have made accurate predictions of oxygen transfer at hydraulic structures in the winter. Ice cover has an impact on gas transfer. There is a significant upstream oxygen deficit as ice prevents any air–water oxygen transfer, and the saturation concentration increases as water temperature decreases. In addition, formation of ice allows samples to be taken with relative safety. However, not all structures are located where freezing conditions exist (even in Minnesota only half the structures are suitable) so some other measurement technique must be used.

A tracer technique for reaeration measurement in open channels was introduced by Tsivoglou (1968). The basic assumption behind this technique is that there is a constant ratio between the desorption of the tracer gas and the absorption rate of oxygen. Tsivoglou then related tracer gas transfer to the oxygen transfer through results of laboratory experiments or the simultaneous transfer of both gases. Since the driving force of gas transfer is the difference in partial pressures of the gas in the atmosphere and that dissolved in water, tracers can be chosen that have an atmospheric concentration of zero, and thus measurements can be made independent of ambient conditions. Tsivoglou injected radioactive krypton–85 into a river and measured its desorption along the river reach. Tsivoglou's technique worked rather well, but required the use of radioactive materials. Rathbun (1978) modified Tsivoglou's method to avoid the use of radioactive materials in the environment by using propane and ethylene in place of krypton–85. The assumptions made were similar to Tsivoglou's, with changes made for the desorption rates of propane and ethylene.

Thene (1988) and Thene and Gulliver (1989) developed a headspace measurement technique for propane and subsequently found measurable amounts of methane while using propane as a tracer gas. This discovery held promise for use of methane as a tracer gas. Methane is produced in the sediments as a byproduct of the anaerobic decomposition of organic materials. No costly injection of gases if needed, and the uncertainty associated with this injection is eliminated. In addition, methane measured by this headspace technique requires only the equipment found in most GC laboratories as opposed to the more common purge and trap technique, which requires additional training of personnel and significantly more time for each sample.

The purpose of this work is to develop a method to measure methane concentrations in water and then measure the gas transfer at various hydraulic structures. Transfer efficiency has been used to describe the amount of gas transfer at a hydraulic structure (Gameson, 1957)

$$E = \frac{C_d - C_u}{C_s - C_u} \qquad \text{(I–1)}$$

where E is the transfer efficiency, C_s is the saturation concentration, C_u is the upstream concentration, and C_d is the downstream concentration. For gases like methane, that do not have an appreciable concentration in the atmosphere, C_s is zero and E is given as:

$$E = \frac{C_u - C_d}{C_u} \qquad \text{(I–2)}$$

Transfer efficiency thus ranges from zero for no transfer to unity for complete transfer.

This report describes the technique used to measure methane concentrations and the role methane plays in the water column. The results of a survey of various hydraulic structures are given and some conclusions are reported.

II. REVIEW

A. Gas Transfer Theory

Several concepts have been used to describe the interfacial transfer of gases. Lewis and Whitman (1924) assumed the interface between the gas and turbulent liquid is a thin layer of gas and a thin layer of liquid. Gases then pass through both thin films by molecular diffusion. The gas concentration in the liquid is assumed to be constant, and a linear concentration exists in the film. Two objections have been raised to this theory: the validity of the assumption of a stagnant film on a turbulent free surface and the validity of assuming a linear concentration in the thin film.

Higbies Penetration Model (1935) assumed the surface film is first to become stagnant with the absorption and transportation of gases by molecular diffusion. Suddenly, the water is mixed completely and instantaneously. Danckwerts Modified Penetration Theory (1951) assumed the surface film to continuously undergo various degrees of vertical mixing. Particles are exposed to the surface for varying periods of time, picking up oxygen from the air according to Fick's First Law. The chance of a fluid element being removed from the air–water interface and being replaced with another element from below is independent of its time at the air–water interface.

Today, the most accepted theory of gas transfer is Dobbin's (1956) Film Penetration Model. This theory combines the modified penetration theory and the thin film theory. This theory states that a "thin film" of water elements at the air–water interface will absorb gas through molecular diffusion until they are replaced with elements from below. Thus the rate of mass transfer depends on the rate of surface renewal and the rate of molecular diffusion in the thin film. For most civil engineering applications there is little difference between the Film Penetration Model and the Modified Penetration Theory.

The application of the above theory to the gas transfer process leads to a first–order process in which the rate of change of the gas concentration in the water is linearly dependent on the ambient concentration. Mathematically the flux of any dissolved chemical across the air–water interface is given by the equation:

$$F = K\ (C_a/H - C_w) \qquad \text{(II–1)}$$

where F = flux/unit surface area, K = transfer coefficient, C_a = concentration in the air, C_w = concentration of the dissolved chemical in the water, and H = Henry's law constant, an equilibrium constant. C_a/H is often called the saturation concentration, C_s. The transfer coefficient is given by the equation:

$$\frac{1}{K} = \frac{1}{K_L} + \frac{1}{HK_g} \qquad \text{(II–2)}$$

where K_g is the gas film coefficient, representing transport in the air, and K_L is the liquid film coefficient representing transport in the water. Although a film of both air and liquid is assumed to exist at the interface, gas exchange of methane between the two phases is controlled by molecular diffusion through the liquid film layer. That is, $\frac{1}{K_L}$ is much greater than $\frac{1}{HK_g}$.

If we assume the coefficient K_L remains constant over a hydraulic structure, then Equation II–1 may be integrated to give the deficit ratio, r:

$$r = \exp\,(K_L\ a\ t) = \frac{C_s - C_u}{C_s - C_d} \qquad \text{(II–3)}$$

Where C_d = concentration downstream of the structure, C_u = concentration upstream of the structure, t = residence time of the bubbles, a = specific surface area (ratio of total bubble surface area and total surface volume). The terms $C_s - C_u$ and $C_s - C_d$ are often referred to as concentration deficits. A more convenient form of Equation II–3 is as a transfer efficiency, E:

$$E = 1 - \frac{1}{r} = \frac{C_d - C_u}{C_s - C_u} \qquad \text{(II–4)}$$

For gases which do not have appreciable concentrations in the atmosphere (like methane), C_s is zero and transfer efficiency is given as:

$$E = \frac{C_u - C_d}{C_u} \qquad \text{(II–5)}$$

A transfer efficiency of 1.0 means the full transfer up to the saturation value has occurred at the structure. No transfer would correspond to E = 0.0.

The driving force of the gas transfer is the partial pressure of the gas in the atmosphere and the concentration of the gas dissolved in water. At equilibrium no driving force exists and there is no net transfer. At this stage the water is considered "saturated". Henry's Law is given as:

$$P_i = H_i\ C_i \qquad \text{(II–6)}$$

where P_i is the partial pressure of gas i, H_i is a Henry's Law constant for gas i, and C_i is the concentration of the gas dissolved in solution. Saturation concentrations are typically assumed proportional to the concentration of the gas in the atmosphere. Consider, however, a bubble at depth in a stilling basin. The hydrostatic pressure of the depth of the

bubble must be considered in finding the saturation concentration. For example, if the temperature is 20° C, the dissolved nitrogen saturation concentration of water in contact with a bubble at the surface is 15.9 mg/l. At a depth of 33.9 feet (ie, 2 atmospheres pressure), however, the atmospheric pressure is twice that at the surface and correspondingly the saturation pressure is 31.8 mg N_2/l. This is the cause of nitrogen and oxygen supersaturation at hydraulic structures and with respect to nitrogen can cause fish mortality by gas bubble disease.

Saturation concentration of methane can be found by first finding Henry's Law constant. At 20° C, Henry's Law constant is given by:

$$HLC = \frac{M_w \; P}{C_s \; M_m \; \rho} \qquad \text{(II–7)}$$

where HLC is Henry's Law constant in atm l/gram, M_w is the molar weight of water, M_m is the molar weight of methane, ρ is the density of water (from Gebhart and Mollendorf, 1977), and C_s is the saturation concentration of methane under one atmosphere of methane gas in units of mole fraction (from Young, et al, 1981). Assuming 20° C, ρ is 999.689 grams/liter and C_s is 0.2767×10^{-4}. Substituting these values into the equation above yields a HLC value of 40.602 atm l/gram. The partial pressure of methane in the atmosphere is 1.989×10^{-6} atmospheres (Turekain, 1969). Combining these two values the saturation concentration of methane can be found by:

$$C_s = \frac{P_m}{HLC} = \frac{1.989 \times 10^{-6} \text{ atm}}{40.602 \text{ atm l/gram}} = 0.049 \; \mu g/l$$

Because this value is small when compared to the in–situ concentrations of methane, it is assumed to be zero in subsequent calculations.

B. Comparison of Methane and Oxygen Measurements

Gulliver, et al (1990) developed an indexing relationship for liquid phase controlled gas transfer at hydraulic structures. They proposed this relationship be used to index transfer measurements to a common temperature, 20° C, and a gas, oxygen, which is used most often in gas transfer measurements. Given the temperature and the diffusivities of the indexing compounds a relationship was derived describing the transfer efficiency for oxygen at 20°C. The relationship is given as:

$$E_i = 1 - (1-E)^{1/f_i} \qquad \text{(II–8)}$$

where E is the measured transfer efficiency, E_i is the indexed transfer efficiency for the index compound at the index temperature (oxygen at 20° C for this study). The parameter f_i is given as

$$f_i = f_g \; f_t \qquad \text{(II–9)}$$

where f_t is a temperature correction to 20° C given as $f_t = 1 + 0.0210(T-20) + 8.261 \times 10^{-5}(T-20)^2$ where T is in C°. The parameter f_g indexes the transfer to oxygen and is given by:

$$f_g = \left[\frac{D}{D_i} \right]^{1/2} \qquad \text{(II–10)}$$

where D is the diffusivity of the measured compound, methane, and D_i is the diffusivity of the indexed compound, oxygen in this study. Determining these diffusivities was discussed in detail in Thene (1988) and Thene and Gulliver (1989) and will be reviewed here. Daniil (1983) reviewed the prediction, measurement technique and available data for the molecular diffusion of oxygen. Daniil concluded the best method to correlate experimental measurements of molecular diffusivity was the Einstein–Stokes equation:

$$\frac{D\ \mu}{T} = f \qquad \text{(II–11)}$$

where μ = dynamic viscosity of liquid, g cm/sec K, T is the temperature of the system in Kelvin, D is the diffusivity of the liquid in cm^2/sec and f is a function of the diffusing system, which is constant at all temperatures. Daniil concluded the value of Goldstick and Fatt (1970) of 2.13×10^{-5} cm^2/sec is the best value to use in the above equation. Using μ = 0.00894 g/cm sec (dynamic viscosity of water at 25° C) yields $f = 6.38 \times 10^{-10}$ g cm/sec K.

Thene (1988) (and Thene and Gulliver (1989)) searched Chemical Abstracts from 1965 to 1986 for diffusivity data on methane. Analysis of 14 methane diffusivity measurements gave an average f value of 4.94×10^{-10} g cm/s K. Thus f_g is given by

$$f_g = \left[\frac{D}{D_i} \right]^{1/2} = \left[\frac{4.94 \times 10^{-10}}{6.38 \times 10^{-10}} \right]^{1/2} = 0.880 \qquad \text{(II–12)}$$

III. DEVELOPMENT OF LABORATORY TECHNIQUE

This section outlines the sampling procedure used, the data reduction and quality control / quality assurance steps taken.

A. Methane Sampling and Headspace Analysis

All samples were take in 40 ml borosilicate glass vials with teflon faced septa and open top screw caps. The vials were Fisher brand "for EPA water analysis". Each vial was numbered for permanent identification. The volume and mass of each vial was recorded. The average weight of the caps and septa was determined by weighing a large number. The standard deviation of the masses of caps and septa were also recorded for use in an uncertainty analysis to be presented later.

The samples were taken in a dissolved gas sampler as described by Thene (1988) and Thene and Gulliver (1989). This sampler is shown in Photo III–1. When a bubble free sample had been taken, the bottle number and time were recorded. 0.5 ml of 37% formaldehyde solution (often called formalin) was then injected as soon as possible into the sample to stop bacterial action from affecting methane concentration.

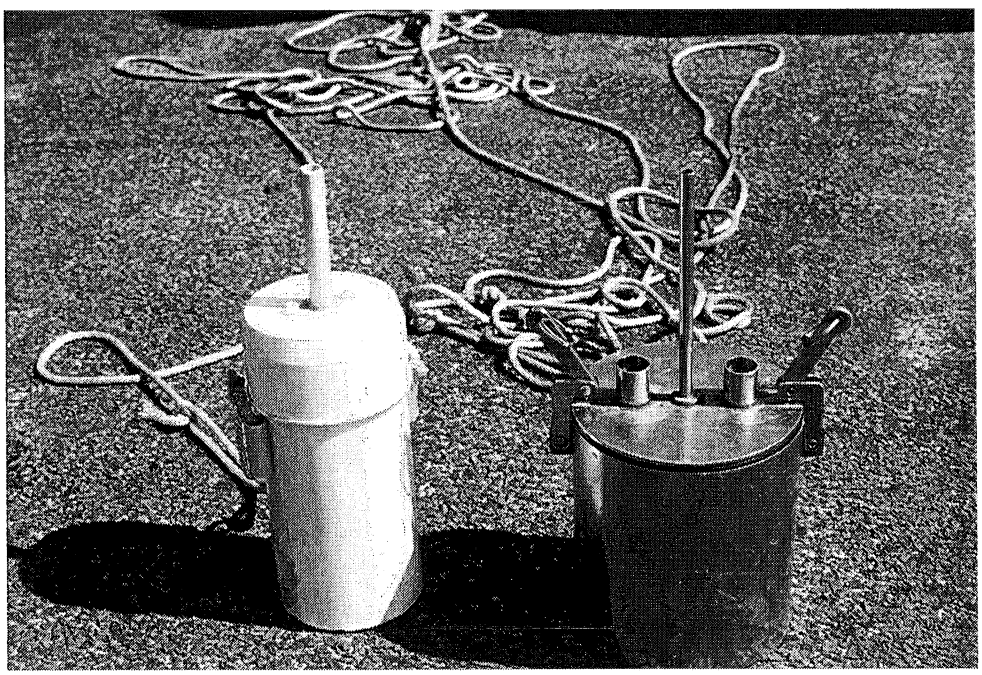

Photo III–1 Methane sampler (left)
and D.O. sampler (right)

Samples were taken to the GC lab after sampling. Samples were transported with the septa side down to prevent any loss of sample by bubble formation during temperature change. At the GC lab a 10 ml headspace was created by inserting a 3 inch needle, open to the atmosphere, to the bottom of the sample bottle and injecting 10 ml of nitrogen gas just underneath the septa thus forcing water out through the large needle. Samples were then shook for 60 seconds to strip the methane into the headspace.

The gas chromatograph used was a Hewlett Packard 5890A equipped with a flame ionization detector, a strip chart recorder and an electronic integrator. The injection port temperature was at 250^{0}C, the FID was at 300^{0}C and the oven was kept isothermal at 90^{0}C. The carrier gas used was nitrogen (Ultra Pure Carrier Grade) flowing at 30 ml/minute. The hydrogen flow was 30 ml/minute and the air flow was 400 ml/minute. The column used was a 4 ft. long 5A 60/80 molecular sieve. Under these conditions the column was able to separate the methane from any imbalance caused by oxygen in the samples. A typical chromatogram is shown in Figure III–1.

The GC was calibrated using commercially prepared and certified gas standards. The standard used was 100.3 ppm by volume methane in nitrogen gas. The concentration was certified to +/– 2% by its manufacturer, Scott Specialty Gases.

Calibration was performed by injecting different volumes of standard into the GC and plotting the results. A second degree curve was then fit through the calibration points to get an equation relating area counts to mass of methane.

The vial with headspace was weighed before headspace sampling. A syringe, open to the atmosphere, containing Mega–Pure water was inserted through the septa into the sample. This was done to prevent any pressure changes occurring across the septa during headspace sampling.

From the headspace of the vial a 250 μl sample was taken using a gas–tight syringe. This volume was quickly injected into the GC. Six samples were analyzed from each headspace. If for some reason one GC result seemed erroneous, another sample was taken so that there would be six "good" samples from each vial.

B. Data Reduction

The data reduction and error analysis is done by use of a FORTRAN computer program. The measured data includes ambient and lab temperature, calibration data, sample vial number, sample weight with headspace, volumes injected and their accompanying GC response in area counts.

Calibration

First the calibration data are converted from a volume of standard injected to a mass of methane:

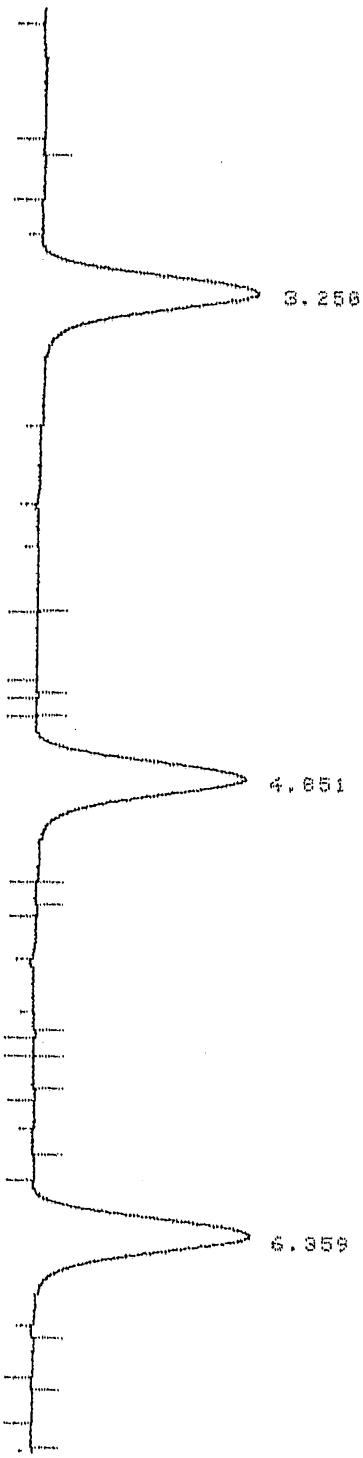

Figure III–1 Typical Chromatagram

$$MINJ = \frac{VINJ \; M \; P \; C}{R_u \; T} \qquad \text{(III-1)}$$

Where MINJ is the mass of methane injected, VINJ is the volume of standard injected, M is the molar mass of methane, P is the pressure, C is the concentration of methane in the standard (100 ppm), R_u is the universal gas constant, and T is the temperature in degrees Kelvin. These masses are then plotted against the GC area count response. Any outlying points are thrown out and a second degree curve is fit through the remaining points. An equation of Mass = A + B*Area Counts + C*Area Counts^2 is obtained. A typical calibration curve is shown in Figure III-2.

Sample analysis

Using the equation from the calibration, the GC response and the volume injected, the concentration of methane in the syringe is found from:

$$CHS_{i,j} = \frac{MINJ}{VINJ} = \frac{A + B*GC + C*GC\hat{}2}{VINJ_{i,j} * 10^{-6} L/\mu l} \qquad \text{(III-3)}$$

where $C_{HS_{i,j}}$ is the concentration of methane in the headspace, MINJ is the mass injected, VINJ is the volume of headspace injected A,B, and C are coefficients obtained from the calibration, and GC is the GC response in area counts. This headspace concentration is then converted to the concentration in the water. The mass of methane in the headspace is given by:

$$M_{HS} = C_{HS} \; V_{HS} \qquad \text{(III-4)}$$

where M_{HS} is the mass of methane in the headspace sample, C_{HS} is the concentration of methane in the headspace, and V_{HS} is the volume of the headspace sample.

Henry's law is given as:

$$P_{HS} = C_W \; H \qquad \text{(III-5)}$$

where P_{HS} is the partial pressure of methane in the headspace (atm), C_W is the equilibrium concentration of methane dissolved in the water ($\mu g/l$), and H is Henry's law constant for methane in water (atm $L/\mu g$). The headspace concentration is converted to a headspace partial pressure by the ideal gas law

$$P_{HS} \; V_{HS} = n \; R_u \; T \qquad \text{(III-6)}$$

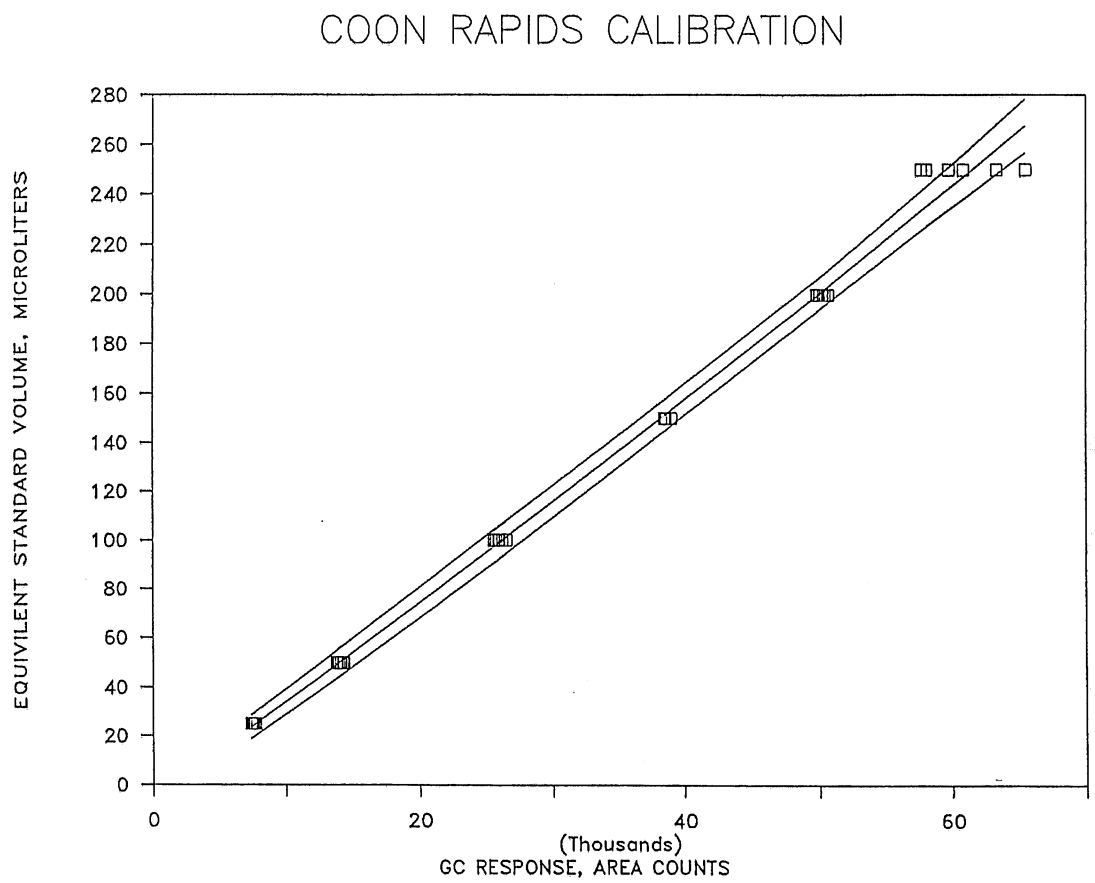

Figure III–2 Typical Calibration Curve with uncertainty

where n is the amount of gas in moles and pressure is given by

$$P_{HS} = C_{HS} \frac{R_u T}{M_m} \qquad \text{(III–7)}$$

The concentration of methane in the water is then:

$$C_W = \frac{P_{HS}}{H} = C_{HS} \frac{R_u T}{M_m H} \qquad \text{(III–8)}$$

Multiplying the concentration of methane in the water by the volume of water yields the mass of methane in the water:

$$M_W = C_W V_W = C_{HS} \frac{R_u T}{M_m H} V_W \qquad \text{(III–9)}$$

By adding the mass of methane in the water to the mass of methane in the headspace and dividing the sum by the volume of water the concentration of methane in the sample is given by:

$$C_W = C_{HS} \left[\frac{R_u T}{M_m H} + \frac{V_{HS}}{V_W} \right] = C_{HS} \text{ HCF} \qquad \text{(III–10)}$$

This equation defines HCF, the headspace correction factor that converts a headspace concentration to the original dissolved concentration.

With all the concentrations converted to original water concentrations, the injections from each vial were averaged. Next all the upstream bottles were averaged to arrive at C_u. Similar calculations were done performed to obtain C_d. Then the transfer efficiency is calculated from:

$$E = \frac{C_u - C_d}{C_u} \qquad \text{(I–2)}$$

The efficiency is then indexed to dissolved oxygen at 20°C using equation (II–9).

$$E_i = 1 - (1-E)^{1/f_i} \qquad \text{(II–9)}$$

C. Quality Assurance/Quality Control

The following section details what QA/QC procedures were followed during development of the laboratory technique.

Preservation Technique

As samples were not analyzed immediately after they were gathered some method of preservation had to be employed. Schultz, et al (1971) concluded 1 ml of 37% formaldehyde solution in a 60 ml solution preserved the sample for seven days. To stop bacterial action other researchers have raised the pH to 11, added HgCl or stored samples on ice. It was decided to test 0.5 ml of 37% formaldehyde solution, commonly called formalin, to preserve the samples. Samples were gathered on May 24, 1988 from the Anoka Dam on the Rum River. Eight pairs of samples were taken upstream and eight samples taken downstream. Four bottles were analyzed each week for four weeks. The results are shown in Table III–1. From the results it is evident the preservation technique stopped bacterial action as no significant drop in methane levels were detected.

Table III–1 Methane Levels at Anoka, samples gathered May 24, 1989

Analysis Date	C_u, $\mu g/l$	C_d, $\mu g/l$	E
5–24	21.99	7.61	0.654
5–31	22.21	6.86	0.691
6–7	22.93	7.23	0.685
6–14	21.32	7.21	0.662

Amount of Formalin

A test was conducted to determine if 1/4 ml of formalin might preserve samples. Twelve samples were taken on June 21, 1989 from the Mississippi River at S.A.F.H.L. Four samples, 2 with formalin and 2 without, were analyzed after 1 day, 2 days, and 1 week. As can be seen from Figure III–3, the methane concentrations decreased with time. Therefore it was decided to use 1/2 ml of formalin as a preservative for this study.

Injection Technique

It was discovered that the manner in which the sample was injected into the GC caused different responses, that is, different speeds of injection gave different results. To test the effects of injection technique (ie, injection speed) different volumes of standard were injected into the GC using different injection techniques. Three speeds were tested. The first speed was to inject as fast as possible. The total time to pierce the septa, depress the plunger, and with drawl the syringe was under 0.5 seconds. The second speed was a three second process. One second was used to pierce the septa and to get the syringe in place. Two seconds were used to depress the plunger and then the syringe was withdrawn quickly. The third speed tested was similar to the second only four seconds were used to depress the plunger. As shown in Figure III–4 the fast injection does not match up with the other injection speeds. The other two plots are virtually identical. Therefore it was decided

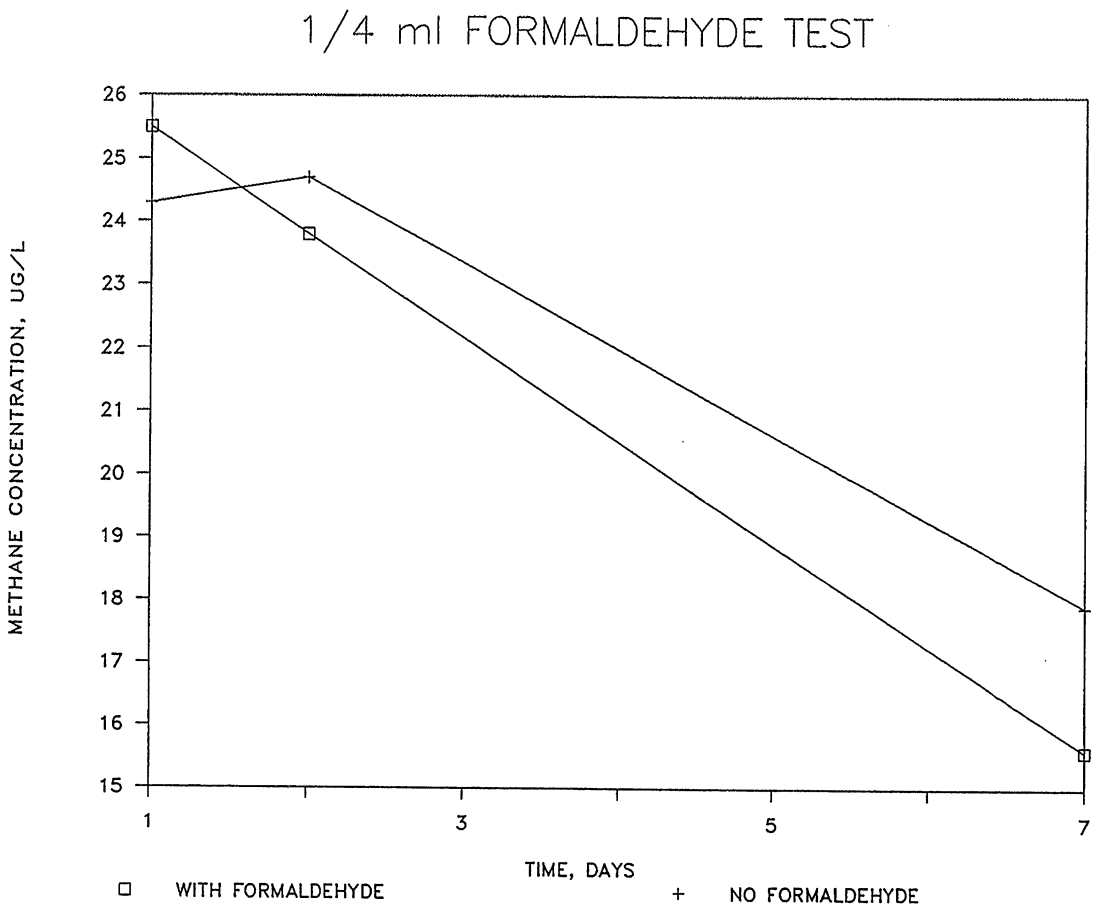

Figure III--3 Amount of Formalin Test

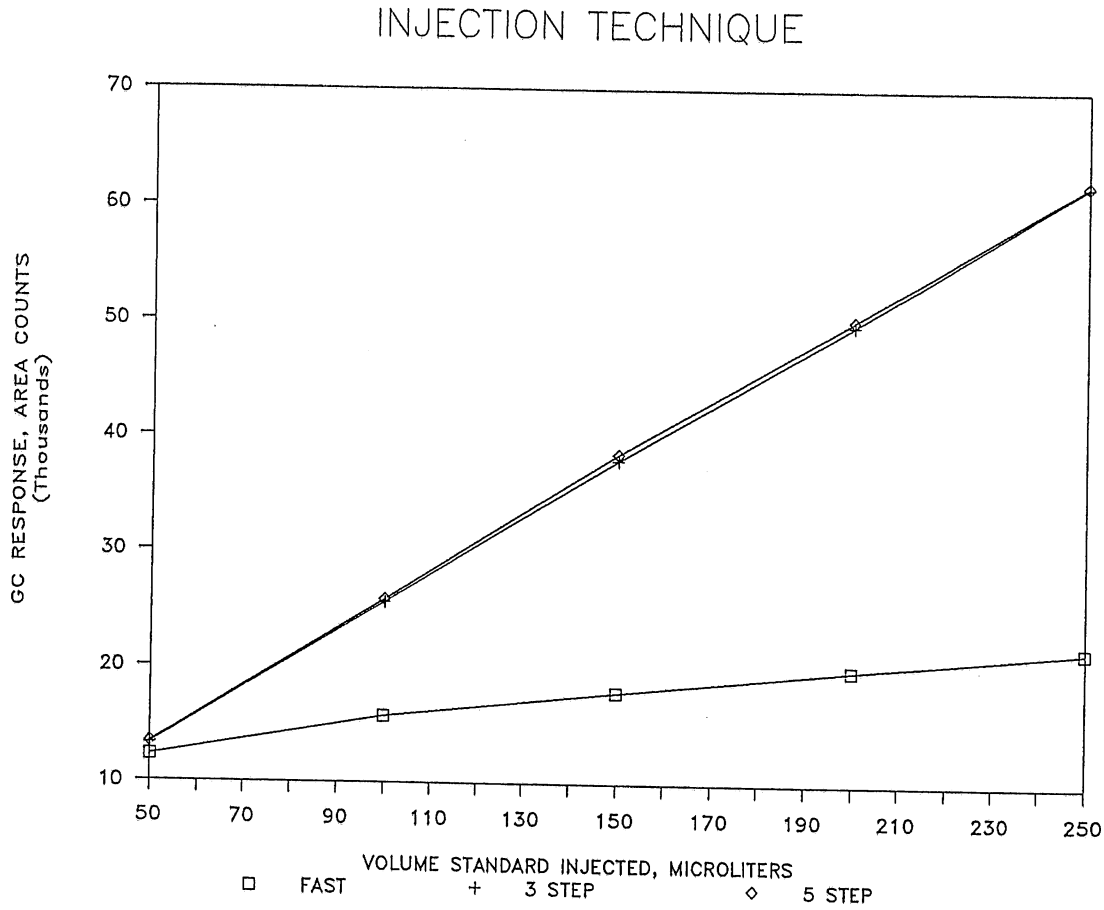

Figure III–4 Injection Test

to use the three step injection for samples. It is thought with the fast injection some of the sample is lost through the pierced septa in the injection port of the GC.

Pressure Change due to Headspace Sampling

It was noted in the early sampling that the area counts decreased with each injection. This was due to a pressure change in the headspace. Six 250 μl samples are taken from a 10 ml headspace thus decreasing the volume by 1.5 ml or 15%. This is accounted for in Thene's (1988) and Thene and Gulliver's (1989) computations by a headspace dilution factor

$$F_D = \prod_{i=1}^{j} \left[1 + \frac{V_{INJ,i,i}}{V_{HS,i}} \right] \qquad \text{(III-11)}$$

However, Thene had a larger headspace, ranging from 40–50% of the total volume of sample bottle, so he didn't encounter such a severe pressure drop. To test for a better headspace sampling technique three different styles were studied. The first technique consists of replacing the volume of sample removed with nitrogen gas, thus keeping the pressure constant. However this technique dilutes the headspace concentration which can be accounted for in the headspace dilution factor described above. The second technique consists of replacing the sample volume with water that contains no methane. A 10 ml syringe filled with methane–free water and equipped with a long needle is inserted to the bottom of the sample vial. When the samples are removed from the headspace, water from the syringe replaces the volume extracted from the headspace. Using this technique the headspace is not diluted and there is no pressure differential. The third method checked was to withdrawal the samples from the headspace without replacement which is what Thene did. This method causes a pressure differential but does not dilute the headspace. It was decided to use the second technique (volume replacement with methane–free water) as it was easy to perform. Most importantly, with this technique all the area counts should be the same (because the headspace is not diluted) which makes it easy to identify outliers. The water concentration, already low because of methane's high volatility, will be reduced slightly, but the effect on headspace methane concentration would be insignificant. A photo of the headspace sampling technique is shown in Photo III–2. The water used to replace the sample volume must not contain methane. Bottles of de–ionized water, tap water, and Mega–Pure water were filled and a 10 ml nitrogen headspace created. Samples were shaken for 60 seconds and headspace samples injected into the GC. Only the Mega–Pure water sample did not give a response. It is thought the exposing of ultra–violet light to the Mega–Pure water "burns" off any methane in the water.

To check if formaldehyde would give a response, 0.5 ml of formalin was added to a sample vial containing Mega–Pure water. A 10 ml nitrogen headspace was created, the sample was shook for 60 seconds, and a headspace sample was injected into the GC. As no response was garnered from the GC it was concluded addition of formalin doesn't affect the GC response.

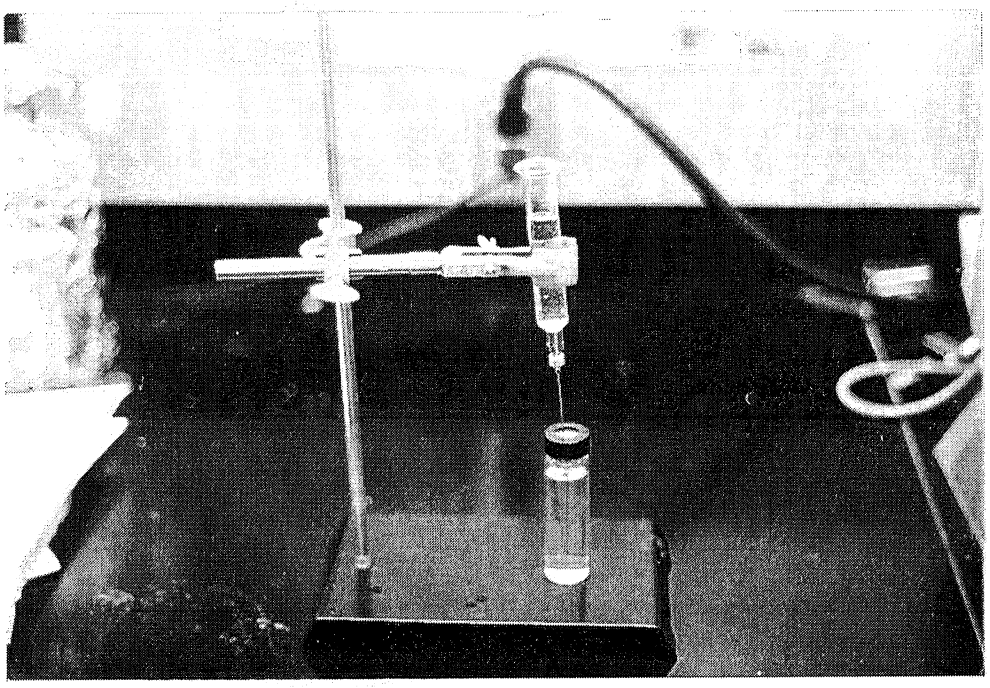

Photo III–2 Headspace Sampling Setup

Septa Analysis

An analysis was run to determine if there would be a significant drop of methane through use of used septa. Four pair of samples were gathered from the Mississippi River at the St. Anthony Falls Hydraulic Lab. Four samples had new septa and the others had used septa in various conditions. The result of the analysis is shown in Table III–2. Even though used septa gave results similar to new septa, it was decided to use only new septa in sampling, because the high expense of a field study did not justify taking a chance with a used septa.

Table III–2 Septa Analysis

Bottle No.	Methane Concentration, μg/l	Septa Condition
1	12.85	new
61	12.48	3 holes
16	12.51	new
15	12.67	16 holes
54	12.49	3 holes
62	11.98	new
30	12.49	new
18	11.98	16 holes

Bubble formation

Bubbles may be formed in the samples as the samples are transported from cold temperatures to warmer temperatures. To check if the bubbles formed would significantly affect the methane concentration in the sample, the following assumptions were made: methane concentration in water = 20 μg/l, water temperature of 20° C, bubble size of 3 mm in diameter. At 20° C Henry's Law constant is given by:

$$H = \frac{M_w \; P}{C_s \; M_m \; \rho} = 40.60 \text{ l atm/gram} \qquad \text{(III–10)}$$

where M_m = molar mass of methane, M_w = molar mass of water, C_s = saturation concentration of methane as given by Young, et al (1981), P = atmospheric pressure, and ρ is the density of water.

In performing the calculation of methane in water, C_w is given as

$$C_w = C_{HS} \left[\frac{R_u \; T}{M_m \; H} + \frac{V_{HS}}{V_W} \right] \qquad \text{(III–11)}$$

where $\frac{R_u \; T}{M_m \; H}$ is that portion of methane in the liquid phase and $\frac{V_{HS}}{V_W}$ is that portion in the gas phase. Using the above value for H, $\frac{R_u \; T}{M_m \; H} = 0.0372$. For a 3 mm diameter bubble, $\frac{V_{HS}}{V_W} = 0.000357$. Thus the percentage of methane in the gas phase is:

$$\frac{\text{methane in gas phase}}{\text{total methane}} = 0.94\%$$

The bubble would remain in the vial upon headspace injection and would become a part of the headspace. If 10 ml of water is removed, while 30 ml remain, the headspace concentration for this example would be higher by:

$$\frac{1}{4} (0.94\%) = 0.24\%$$

This percent difference is insignificant compared to the precision of the GC analytic technique for methane (see Chapter IV).

Limit of Detection / Limit of Quantification

The EPA Treatability Manual (1988) defines LOD and LOQ as:

> LOD – The lowest concentration of the pollutant that will give a signal on the analytical instrument that can be distinguished from the background noise with a known degree of confidence.
>
> LOQ – The concentration above which one can state with a known degree of confidence that a pollutant is present at a specific concentration in the sample tested.

Given these rather vague definitions it was decided to determine the LOD and LOQ by injecting various masses of the standard gas each 10 times into the GC and calculating the standard deviation of each sub–set of injections. Then the LOQ was defined as the point where ten times the standard deviation of a set of injections equaled the average area count of the set of injections. Similarly the LOD was defined as the point where three times the standard deviation equaled the average area count.

Using this definition and the information gathered from the injection of standard gas, Table III–3 was prepared. This table shows the LOQ to lie between the mass contained in 3 and 5 μl of standard gas. By linear interpolation between these two points the mass of LOQ was equal to 0.000211 grams. Assuming a 250 μl sample injection (typical in this analysis) the headspace concentration would be:

$$C_{HS} = \frac{\text{mass}}{\text{volume}} = \frac{0.000211\text{g}}{250\ \mu\text{l}} = 0.84\ \mu\text{g/l} \qquad \text{(III–12)}$$

A typical headspace correction factor is 0.40, then the water concentration is:

$$\text{LOQ} = C_W = C_{HS}\ \text{HCF} = 0.34\ \mu\text{g/l} \qquad \text{(III–13)}$$

This is the value for LOQ. LOD is defined as 3/10 of the LOQ so then:

$$\text{LOD} = 3/10\ \text{LOQ} = 0.10\ \mu\text{g/l} \qquad \text{(III–14)}$$

Table III–2 LOQ ANALYSIS

Volume Std.	Mass, grams	Mean AC	10σ	10σ/mean
150	0.009963	35045.1	5539.3	0.16
100	0.006642	22996.1	7456.6	0.32
50	0.003321	12192.9	4356.6	0.36
10	0.000664	2886.8	1658.2	0.57
5	0.000332	1891.4	1118.3	0.59
3	0.000199	1007.1	1047.5	1.04

D. Dissolved Oxygen

During the summer sampling dissolved oxygen measurements were taken with a YSI Model 54 Oxygen Meter. These results were calibrated against samples taken in a dissolved oxygen sampler as described in *Standard Methods* (1980) and shown in Photo III–1. Samples were analyzed for dissolved oxygen using the Modified Winkler Method (*Standard Methods,* 1980). Winter dissolved oxygen levels were determined by following the mid–winter oxygen technique as developed by Rindels and Gulliver (1986).

IV. UNCERTAINTY ANALYSIS

Inadvertently, measurement uncertainty occurs due to the accuracy of the instruments, the repeatability of the measurements, or operator error. The total uncertainty of any measurement is a combination of the precision uncertainty, or the repeatability of the measurements, and bias uncertainty, or the possible error that would effect each measurement in the same manner (Abernathy, et al 1985). Therefore,

$$U_E = (W_E^2 + B_E^2)^{1/2} \qquad \text{(IV–1)}$$

where U_E = total uncertainty in the measurement, W_E = precision uncertainty in the measurement, and B_E = bias uncertainty in the measurement. All uncertainties will be quoted to the 95% confidence interval, that is, if 20 measurements are taken, 19 will fall within this interval.

A. Dissolved Oxygen Uncertainty

Rindels and Gulliver (1986) attempted to quantify all significant measurement uncertainties in the D.O. procedures, such as the chemical titrant purity or the buret accuracy. They determined the uncertainty in the transfer efficiency as measured by the dissolved oxygen measurements to be:

$$U_E^2 = \left[\frac{WC_d}{C_s - C_u}\right]^2 + \left[\frac{WC_u\,(1-E)^2}{C_s - C_u}\right]^2 + \left[\frac{0.02\,C_s\,E}{C_s - C_u}\right]^2 + \left[\frac{0.01\,C_s\,(C_d - C_u)}{(C_s - 1.01C_u)(C_s - C_u)}\right]^2 \qquad \text{(IV–2)}$$

where U_E is the uncertainty in the transfer efficiency, WC_d is the uncertainty in the downstream concentration = $\sigma\, t(n-1)/\, n_d^{1/2}$, where σ is the standard deviation of the downstream measurements, $t(n-1)$ is a student's t–score and n_d is the number of downstream measurements, WC_u is the uncertainty in the upstream concentration = $\sigma\, t(n-1)/\, n_u^{1/2}$, E is the measured efficiency, C_s is the saturation concentration, C_d is the downstream concentration, and C_u is the upstream concentration. The third term is a bias uncertainty due to the fact that saturation concentration in a natural river is not known precisely. Rindels and Gulliver (1989) determined that C_s should be approximated as (to the 95% confidence interval)

$$C_s = 0.98 +/- 0.2\ C_s^* \ (P=0.95) \qquad \text{(IV-3)}$$

where C_s^* is the distilled water value of C_s. The fourth term in Eq. IV-2 accounts for the bias due to inprecision in the D.O. titrant, which manufacturers quote as +/- 1%.

Further details of the uncertainty analysis can be found in Rindels and Gulliver (1989). The saturation concentration used was estimated by measuring the atmospheric pressure before and after sampling at the St. Anthony Falls Hydraulic Laboratory barometer and the water temperature measured at the site.

B. Methane Uncertainty Analysis

The uncertainty analysis described herein draws heavily from the analysis as described in Thene (1988) and Thene and Gulliver (1989). They examined the possible errors in their experiment due to bias in the syringe, Henry's Law, and standard gas along with the precision uncertainty associated with the experiment. They concluded if one syringe is used throughout the experiment there is no need to consider the syringe bias.

Precision Uncertainty

The defined the uncertainty in the transfer efficiency in the transfer efficiency due the precision uncertainty in samples is:

$$W_{EP}^2 = \left[\frac{\partial E}{\partial C_u} WC_u\right]^2 + \left[\frac{\partial E}{\partial C_d} WC_d\right]^2 \qquad \text{(IV-4)}$$

or

$$W_{EP}^2 = \left[\frac{C_d}{C_u^2} WC_u\right]^2 + \left[-\frac{1}{C_u} WC_d\right]^2$$

where W_{EP} = uncertainty in the transfer efficiency due to precision uncertainty in the samples, C_d = concentration downstream, C_u = concentration upstream, WC_u = precision uncertainty in upstream samples, WC_d = precision uncertainty in downstream samples.

Precision uncertainty of the upstream and downstream samples (WC_u and WC_d) are found two ways and the larger value is used in the equation above. Uncertainty in the upstream samples can be found by:

$$WC_u^2 = \frac{1}{n_u^2} \sum_{i-1}^{n_u} WC_i^2 \qquad \text{(IV-5)}$$

where n_u = number of bottles upstream, WC_i = uncertainty in individual bottle given by $\sigma t(n-1)/n^{1/2}$, with σ = standard deviation of concentration in bottle i,t(n–1) = student's t–score for n–1 degrees of freedom, and n = number of samples in bottle.

The above equation assumes the concentration of methane in the bottles should be the same. That is, the concentration of methane in all the samples upstream (or downstream) should be equal. However if this is not true (all upstream concentrations are not equal), then this equation does not apply. The procedure used to find the precision uncertainty then is to use the upstream (or downstream) bottle averages to find an uncertainty. The equation is given as:

$$WC_u = \sigma t(n-1)/n_u^{1/2} \qquad \text{(IV–6)}$$

where σ = standard deviation of bottle averages, n_u = number of bottles upstream, and t(n–1) = student t–score for n–1.

Calculations are similar for finding uncertainty in downstream samples. The larger of the uncertainties is used to compute the precision uncertainty via equation IV–3.

Bias Due to Headspace Correction Factor

Concentration of methane in the samples has been given as:

$$C_W = C_{HS}\ HCF \qquad \text{(IV–7)}$$

where C_W is the methane concentration in the water, C_{HS} is the methane concentration in the headspace, and HCF is the headspace correction factor. The headspace correction factor was defined as:

$$HCF = \frac{R_u\ T}{M_m\ H} + \frac{V_{HS}}{V_W} \qquad \text{(IV–8)}$$

where R_u = universal gas constant, T = temperature, M_m = molar mass of methane, H = Henry's Law constant, V_{HS} = volume of headspace in the sample, V_{HS} = volume of headspace in the sample, V_W = volume of water in the sample. This factor converts a gas phase concentration to an original water concentration. Thene defined uncertainty in the transfer efficiency due to bias in the headspace correction factor as:

$$W_{HCF}^2 = \left[\frac{C_d\ \ 0.01}{C_u^2\ n_u^{1/2}}\ C_u \right]^2 + \left[\frac{1\ \ 0.01}{C_u\ n_d^{1/2}}\ C_d \right]^2 \qquad \text{(IV–9)}$$

where W_{HCF} = uncertainty due to headspace correction factor, n_d = number of samples downstream, n_u = number of samples upstream, C_d = concentration downstream, C_u = concentration upstream.

Bias Due to Henry's Law Constant

The uncertainty in the saturation concentration of methane is given from Young, et al (1988) as 0.5% for 36 points. The 95% confidence interval is then 0.5 $(t(35))/36^{1/2}$ = 0.17%. The bias in the upstream concentration is then given by:

$$BC_u = \frac{\partial C_u}{\partial H} BH = \sum_{i=1}^{n_u} (CHS_i \; R_u T/M_m H \; 0.0017) \qquad \text{(IV–10)}$$

where BC_u is the bias in the upstream concentration due to bias in Henry's Law, BH is the bias in Henry's Law Constant which was defined above, CHS_i is the headspace methane concentration for the ith sample. Computations are similar for the downstream samples.

Then the bias in E due to H is given by:

$$B_{EH}^2 = \left[\frac{C_d}{C_u^2} BC_u - \frac{BC_d}{C_u} \right]^2 \qquad \text{(IV–11)}$$

where C_d and C_u are the methane concentrations downstream and upstream respectively, BC_u and BC_d are bias in concentration due to bias in H.

Uncertainty Due to Calibration

A second order curve was fit through the plot of mass of methane injected versus the GC response in area counts. Even though the second order term is small the curve fit the points much better than a straight line. A plot of the residual versus the predicted value gave a curved set of points for a straight line. A similar graph for a second degree curve resulted in a plot that had a more random scatter and therefore was a better fit. A search of statistic books revealed an equation of uncertainty for a multivariable line(Brownlee, 1960), this is given as:

$$U_{MASS} = \frac{C \; \sigma \; M_m \; P}{760 \; R_u \; T} \; t(n-3) \left[\frac{1}{n} + \right.$$

$$\left. \frac{(AC_i - \overline{AC})^2 \Sigma AC^4 - 2(AC_i - \overline{AC})(AC_i^2 - AC^2)\Sigma AC^3 + (AC_i^2 - \overline{AC})\Sigma AC^2}{\Sigma AC^2 \Sigma AC^4 - (\Sigma AC^3)^2} \right] \qquad \text{(IV–12)}$$

where U_{MASS} = uncertainty in mass, C = concentration of methane in standard gas, σ = standard deviation of volumes injected, M_m = molar mass of methane, T = temperature, P = pressure in mm Hg, R_u = universal gas constant, t(n–3) = student t–score, n = number of calibration points, AC_i = area counts of sample injection, other symbols refer to sums and averages of area count responses during calibration. This formula indicates the farther a point is from the mean response the larger the uncertainty, which is visible from the plot of the Coon Rapids calibration as shown in Figure III–1.

Concentration in the syringe is given by:

$$C_{SYR} = \frac{Mass}{V_{INJ}} \qquad \text{(IV–13)}$$

Then the uncertainty in the concentration is given by:

$$W_C = \frac{\partial C}{\partial Mass} W_M = \frac{1}{V_{INJ}} W_M \qquad \text{(IV–14)}$$

where W_C is the uncertainty in concentration due to uncertainty in mass, W_M is the uncertainty in the mass from equation IV–12. The concentration of methane in the sample is given by:

$$C_W = C_{HS}\ HCF \qquad \text{(IV–15)}$$

so the uncertainty in C_W due to uncertainty in calibration is:

$$W_{C_w} = \frac{\partial CW}{\partial C_{HS}} W_C = HCF\ W_C \qquad \text{(IV–16)}$$

The concentrations for each bottle are averaged. The uncertainty in the mean concentration due to calibration uncertainty is:

$$W_{CAL}^2 = \sum_{i=1}^{n_{inj}} \left[\frac{\partial C}{\partial C_i} \right]^2 \left[WC_w \right]^2 = \frac{1}{n_{inj}^2} \left[\sum_{i=1}^{n_{inj}} W_{C_w}^2 \right] \qquad \text{(IV–17)}$$

where W_{CAL} is the uncertainty in the averaged concentration, W_{C_w} is the uncertainty in the ith sample due to calibration uncertainty, and n_{inj} is the number of injections. Then the mean concentrations for each bottle are averaged to get a mean concentration upstream and downstream. The uncertainty in C_u due to calibration uncertainty is:

$$W_{Cu_{cal}} = \frac{1}{n_u} \left[\sum_{i=1}^{n_u} WC_w^2 \right]^{1/2} \qquad \text{(IV–18)}$$

where $W_{Cu_{cal}}$ is the uncertainty in the upstream concentration due to calibration and n_u is the number of samples upstream. Calculations are similar for the downstream samples. Uncertainty in E due to calibration uncertainty is given by:

$$W_{ECAL}^2 = \left[\frac{1}{C_u} W_{C_d} \right]^2 + \left[\frac{C_d}{C_u^2} W_{C_u} \right]^2 \qquad \text{(IV–19)}$$

To summarize, the following uncertainties are calculated:

$$U_E = (W_{EP}^2 + W_{HCF}^2 + B_{EH}^2 + W_{ECAL}^2)^{1/2} \qquad \text{(IV–20)}$$

where U_E = Overall uncertainty in transfer efficiency, W_{EP} = Precision uncertainty in the measurement, W_{HCF} = Precision uncertainty in the headspace correction factor, B_{EH} = Uncertainty due to bias in Henry's Law Constant, W_{ECAL} = Uncertainty due to uncertainty in calibration. Bias due to Henry's law constant and uncertainty in the headspace correction factor are typically much smaller than the precision uncertainty and uncertainty in calibration

V. METHANE IN THE WATER COLUMN

Methane is produced as a byproduct of the anaerobic decomposition of organic material. Methanogenesis is the terminal process in a chain of decomposition processes in the anaerobic hypolimnion and represents a major mechanism by which carbon and electrons leave the sediments (Sawyer and Tiedje, 1978). Methane transfer out of the sediments and hypolimnia is by vertical diffusion and, if enough methane is produced, by bubble ebullion. This section of the paper discusses how methane is formed and its role in the water column.

Methane Production

Formation of inflammable gases in nature has been known for quite some time. In 1776 Volta concluded the gas, composed chiefly of methane, owes its origins to rotting vegetable matter. Discovery of the microbial processes that produce methane was done by Popoff and Hoppe–Seyer in the late 1800's (Barker, 1936).

Methane production is a two stage process. In the first stage a group of faculative and obligate bacteria, termed acid formers, turn proteins, carbohydrates and and fats into fatty acids by hydrolysis and fermentation. Methane producing bacteria then convert these acids into methane. Some alcohols from carbohydrate fermentation can also be converted to methane by methane producing bacteria.

The concentration of acetate, H_2, and CO_2, the major substrates for methane production, are highly variable and are dependent upon the organic material. Acetate is the preferred substrate for methanogenesis at low partial pressures of H_2, as the partial pressure of hydrogen rises bicarbonate is the preferred substrate.

The reaction of methane production from the reduction of carbon dioxide is given as:

$$CO_2 + 8H^+ \rightarrow CH_4 + 2H_2O \qquad (V\text{–}1)$$

In the second process, the production of methane from acetic acid can be shown as:

$$CH_3COOH \rightarrow CH_4 + CO_2 \qquad (V\text{–}2)$$

The later process is thought to produce about 70% of methane in the water column with much of the remainder coming from the reduction of CO_2. Fermentation of other acids are of less importance.

Bacteria that produce methane are strictly anaerobic. Even slight traces of oxygen are toxic to these bacteria. They consists of four major genra: rod–shaped non sporulating Methanobacterium, rod–shaped sporulating Methanobacillus, the spherical Methanococcus and Methanosurcina.

It has been shown (Wolin, E.A, et al, 1988) the formation of methane is pH dependant with the optimum pH being 7.0. The rate of methanogenesis was significantly altered by the reduction of pH. Methane formation was found to continue at a pH of 5.6, but at a much lower rate. In addition, Baker–Blocker, et al, (1976) indicate methane will not be produced unless the redox potential is –250 mV or less.

Methanogenesis is severely limited by sulfate reduction. Waters that have high methane concentration have low sulfate concentrations and vice versa. This is because the sulfate reducing bacteria outcompete the methane producing bacteria for H_2 and acetate, both precursors of methane production. The reduction of sulfate in the sediments is described by:

$$SO_4^- + 9H^+ \rightarrow HS^- + 4H_2O \qquad \text{(V–3)}$$

Millimolar quantities of sulfate will inhibit methane production. The sulfate reducing bacteria have a higher affinity for hydrogen and acetate than methane producing bacteria thus keeping the pool of these substrates at a level too low to be used by the methane producing bacteria (Lovely, et al, 1982). In addition, thermodynamic calculations can be used to predict the exclusion of methane production in sulfate containing sediments.

The bacteria responsible for methanogenesis have a wide temperature range for growth. Zeikus and Winrey (1976) found methanogenesis occurring at temperatures from 4° C to 45° C. The maximum in–situ sediment temperature, 23° C, was below the temperature optimum range of 35–42° C they observed for methanogenesis. Although methanogenesis occurred at 4° C the rate was far below that at 23° C. A change of 12° C in the temperature of the sediments during the change of seasons was associated with a 100 to 400 fold increase in the rate of methanogenesis.

Methane Oxidation

Very little of the methane produced escapes to the atmosphere. Rudd (1979) measured evasion rates at 5% of the total methane produced, whereas in Lake Mendota, Wisconsin an evasion rate of 9% was measured (Fallon, et al, 1980). The small evasion rates are due to the presence of methane oxidizing bacteria. Aerobic methane oxidation is given by:

$$5CH_4 + 8O_2 \rightarrow 2(CH_2O) + 3CO_2 + 8H_2O \qquad \text{(V–4)}$$

This reaction has a free energy yield of 195 kcal per mole. The best known methane oxidizing bacteria is Methanomonas methanica which in addition to methane can oxidize numerous other compounds (Wetzel, 1988).

Various factors seem to control the position and activity of these bacteria. Rudd and Hamilton (1976) found during summer stratification in lakes the highest rate of methane oxidation occurs in the lower metalimnion where O_2 concentrations are below 1 mg/l. Above this layer methane oxidation rates can drop by 40%. They postulated that this occurs as methane oxidizing bacteria cannot operate in high O_2 unless there is available dissolved inorganic nitrogen (DIN) available for fixation by the bacteria. During the summer, epilimnetic DIN levels are low so that N_2 fixation is low. Higher rates of methane oxidation have been observed after turnover. This is due to DIN being swept throughout the water column thus alleviating the problem with N_2 fixation. However at Lake Mendota, Wisconsin, Harrits and Hanson (1988) also found the bacteria were limited to a narrow zone during stratification but that methane oxidation rates were dependent on the methane concentration in aerobic waters, rather than on DIN levels. Kuivila et al (1989) found that little, if any, methane oxidation occurs in the water column of Lake Washington; the methane oxidation occurred with in top 6–7 mm of sediments.

Oxidation of methane under anaerobic conditions has been observed. Sulfate is thought to be responsible. The net reaction is:

$$SO_4^- + CH_4 \rightarrow HS^- + HCO_3^- + H_2O \qquad (V\text{–}5)$$

It has been observed in area of high sulfate reduction there is a corresponding high anaerobic methane oxidation rate (Iversen, 1987). However, there is some debate as to the significance of anaerobic methane oxidation and the organism responsible for methane oxidation. Zender and Brock (1979) have suggested methanogenic bacteria may be responsible for methane consumption. Nevertheless, the zone in which anaerobic methane consumption occurs coincides with one of sulfate reduction which suggests the involvement of sulfate reducing bacteria (Iversen, et al, 1987).

Sulfate reducing bacteria in the sediments can utilize methane as an excellent energy and carbon source. Generation of H_2S serves as an efficient means to maintain anoxic conditions against intrusions of aerated water.

Because the residence time over a hydraulic structure is short, no significant amount of methane oxidation would occur over the time it takes a methane molecule to pass through a structure. That is, the only pathway for a methane molecule to leave the water column during the retention time over a structure is by evasion to the atmosphere.

Methane in the Atmosphere

The presence of methane in the earth's atmosphere was first discovered by Migeotte in 1948 who measured its infared absorption band in the solar spectrum. The distribution of methane in the atmosphere is rather uniformly distributed vertically and exhibits a slight gradient with latitude in the stratosphere. The average concentration of methane in the northern hemisphere is 1.72 ppm and 1.62 ppm in the southern hemisphere (Cicerone and Shetter, 1981). Rainwater analyses have shown methane in rain is in equilibrium with methane in the atmosphere.

The largest contributor to atmospheric methane is the entric fermentation of animals, producing roughly 25% of the total methane in the atmosphere. Freshwater lakes are thought to produce any where from 0.24 – 3% of the total atmospheric methane (Ehhalt and Schmidt, 1978).

The methane production must be balanced by destruction in the troposphere. The reaction of methane and a hydroxyl radical is the likely mechanism. This and other smaller reactions are the major sink of methane and a major source for carbon monoxide. The resulting reaction products are important to the water and ozone budgets. The methane cycle is closed at the earth's surface, where CO_2 and H_2O (the ultimate reaction products of CH_4) are photosynthesized to plant matter.

VI. FIELD INVESTIGATIONS

This section discusses the field investigation sites and the results obtained. The objective was to measure the methane and dissolved oxygen concentrations upstream and downstream of the structure, compute and compare the efficiencies via the indexing equation developed by Gulliver, et al (1990).

A. Byllesby Dam

The Byllesby Dam is located on the Cannon River on the border between Dakota and Goodhue Counties, approximately 1 mile upstream from the city of Cannon Falls, Minnesota. The dam is shown in plan view in Figure VI–1 and consists of the following structures: an Ambursen fixed crest spillway, main dam, and powerhouse. The cross sections downstream vary greatly due to the rock outcropping on the right bank.

One site survey was performed on August 22, 1989. A storm had passed through the area the night before which deposited two inches of rain accompanied by strong winds. This development most probably had an impact on the results. Upstream samples were taken at a cross section approximately 600 ft upstream of the dam. Downstream samples were taken as shown in Figure VI–1. All water was passing through the powerhouse and none flowing over the spillway.

Dissolved oxygen isopleths of the survey is shown in Figure VI–2. Concentrations were determined by use of an oxygen probe calibrated with Winkler samples. No anaerobic zone was observed. This profile is similar to a profile measured on August 26, 1987 by Thene, et al (1988).

The temperature profile is also shown in Figure VI–2. No significant stratification was observed. This lack of stratification may be explained by the storm which had passed though the area the night before.

Methane isopleths are shown in Figure VI–2. Very little methane was found. All readings are less than 1.0 μg/l. The results are very consistent throughout the cross–section as the storm from the night before mixed the reservoir. The low methane levels may be explained by the presence of sulfate in the sediments. Sulfate and its implications to methanogenesis were discussed previously in Section V. No sulfate measurements were taken but Thene (1988) recalled smelling the rotten egg odor associated with hydrogen sulfide while inside the dam.

No transfer efficiencies were calculated as no water was flowing over the spillway.

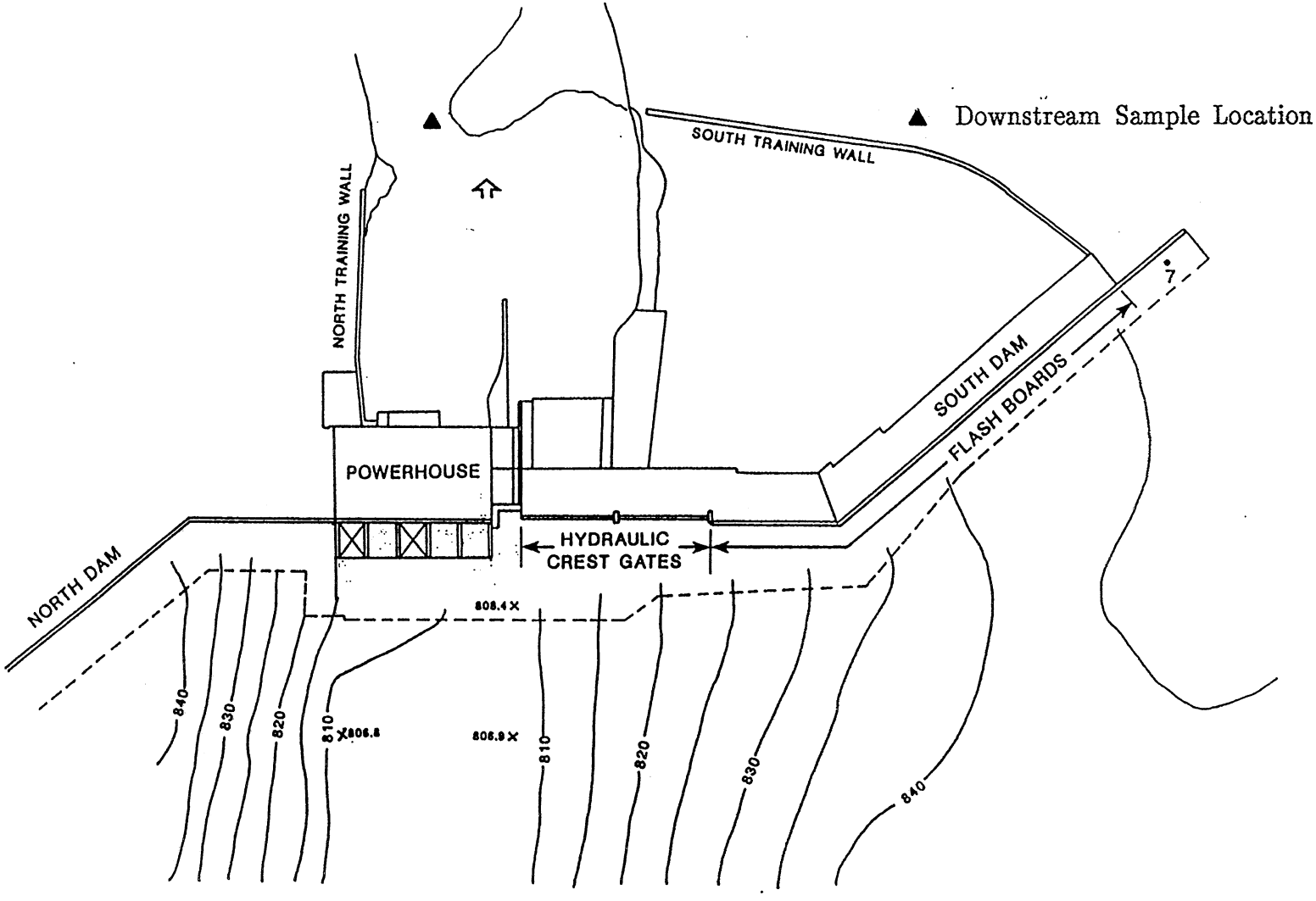

Figure VI -1 Plan view of Byllesby Dam

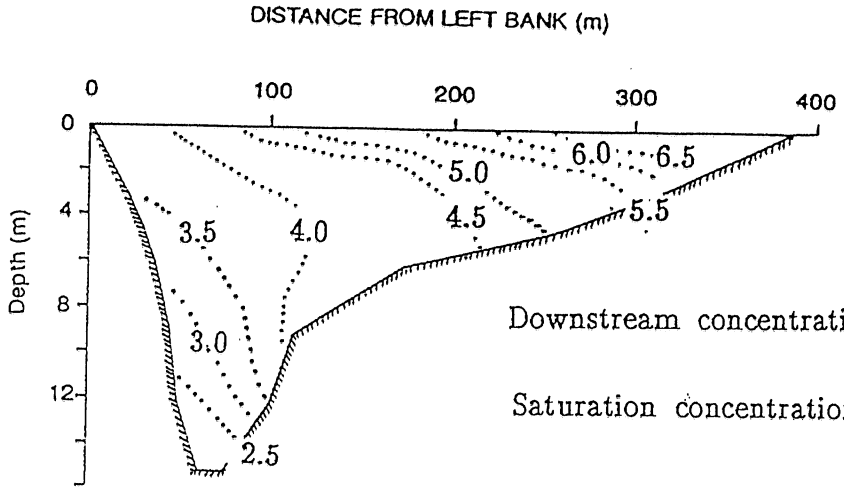

Downstream concentration = 5.4 mg/l

Saturation concentration = 7.67 mg/l

Dissolved Oxygen isopleths, mg/l

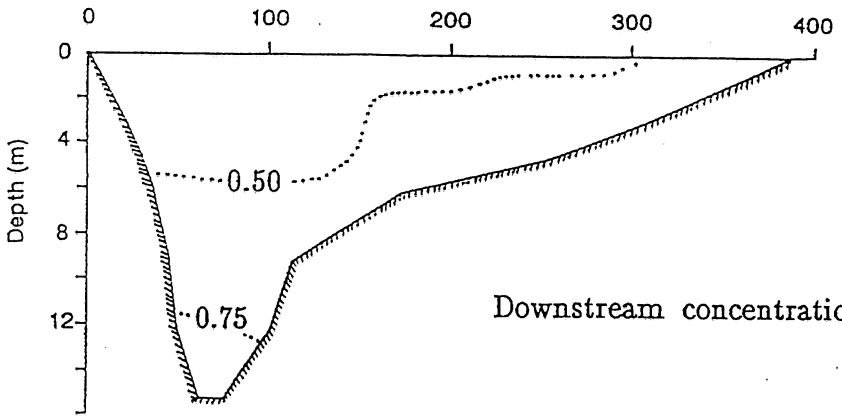

Downstream concentration = 0.78 μg/l

Methane isopleths, μg/l

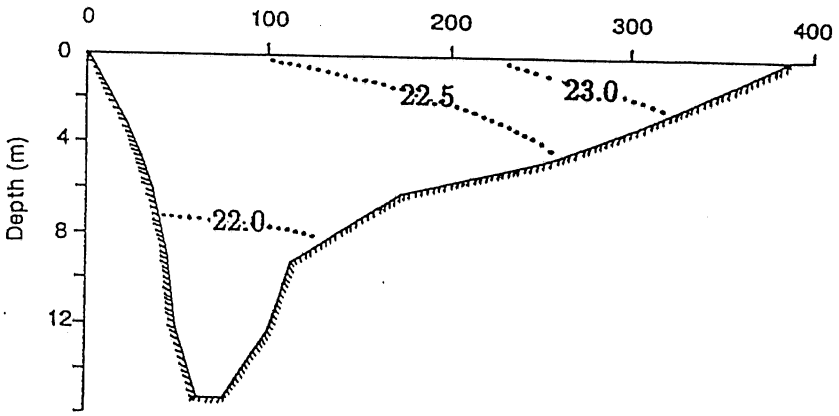

Temperature isopleths, ^{0}C

Figure VI–2 Various isopleths at Byllesby Dam August 22, 1989

B. Faribault Woolen Mill Dam

The Faribault Woolen Mill Dam is an earthen dam flanked by a north gated control structure and a south fixed crest gravity spillway. The dam is located on the Cannon River just upstream of the Second Avenue Bridge over the Cannon River in Faribault, Minnesota. A location plan of the dam is shown in Figure VI–3. Today the dam's primary purpose is to serve as a source of cooling water for the adjacent Woolen Mill and maintain a small reservoir for recreational purposes.

The structure of interest in this study was the fixed crest gravity spillway to the south. The spillway consists of a broadcrested weir, sloped spillway and a flip bucket stilling basin. This structure is shown in plan view in Figure VI–4 and in cross section in Figure VI–5.

The site was investigated on September 20, 1989. Samples from three cross sections across the structure were taken. Samples were also taken on the spillway with a spillway sampler. Spillway samples are taken to show the gas transfer occurs when bubbles are entrained in the flow. This is done by sampling on the spillway just above where bubbles are being entrained into the flow. Samples were also taken 300' downstream of the dam.

Results from the survey are shown in Table VI–1. The samples gathered 300' downstream of the dam had more methane than the upstream samples thus the transfer efficiency is negative. The results are suspect as it was very difficult to get a sample without an enormous amount of debris in it. In addition, the flow was very low, only 0.35 cfs/ft.

Table VI–1 Faribault Results

September 20, 1989	
Upstream Water Surface	100.25
Downstream Water Surface	86.50
Tailwater Depth	0.50 ft.
Discharge	0.35 cfs/ft
Pressure	741.1 mm Hg
Saturation Concentration	8.33 mg O_2/l
Water Temperature	23° C

Location	Right	Center	Left
Upstream			
D.O.	1.68 mg/l	1.42 mg/l	1.99 mg/l
CH_4	119.97 μg/l	113.78 μg/l	147.86 μg/l
Spillway			
D.O.	2.07 mg/l	1.68 mg/l	1.80 mg/l
CH_4	125.57 μg/l	88.98 μg/l	152.99 μg/l
Downstream			
D.O.	3.68 mg/l	2.92 mg/l	4.71 mg/l
CH_4	85.87 μg/l	80.46 μg/l	76.17 g/l
300' downstream	D.O. 3.57 mg/l	CH_4 148.06 μg/l	

E values, all indexed to O_2 at 20°C

	Upstream–Downstream	Upstream–300' Down	Spillway–Downstream	Spillway–300' Down
Right Side				
CH_4	0.304	–0.234	0.338	–0.166
D.O.	0.286	0.270	0.244	0.277
Center				
CH_4	0.314	–0.331	0.103	–0.456
D.O.	0.205	0.176	0.170	0.270
Left Side				
CH_4	0.513	–0.01	0.531	0.035
D.O.	0.409	0.236	0.421	0.214

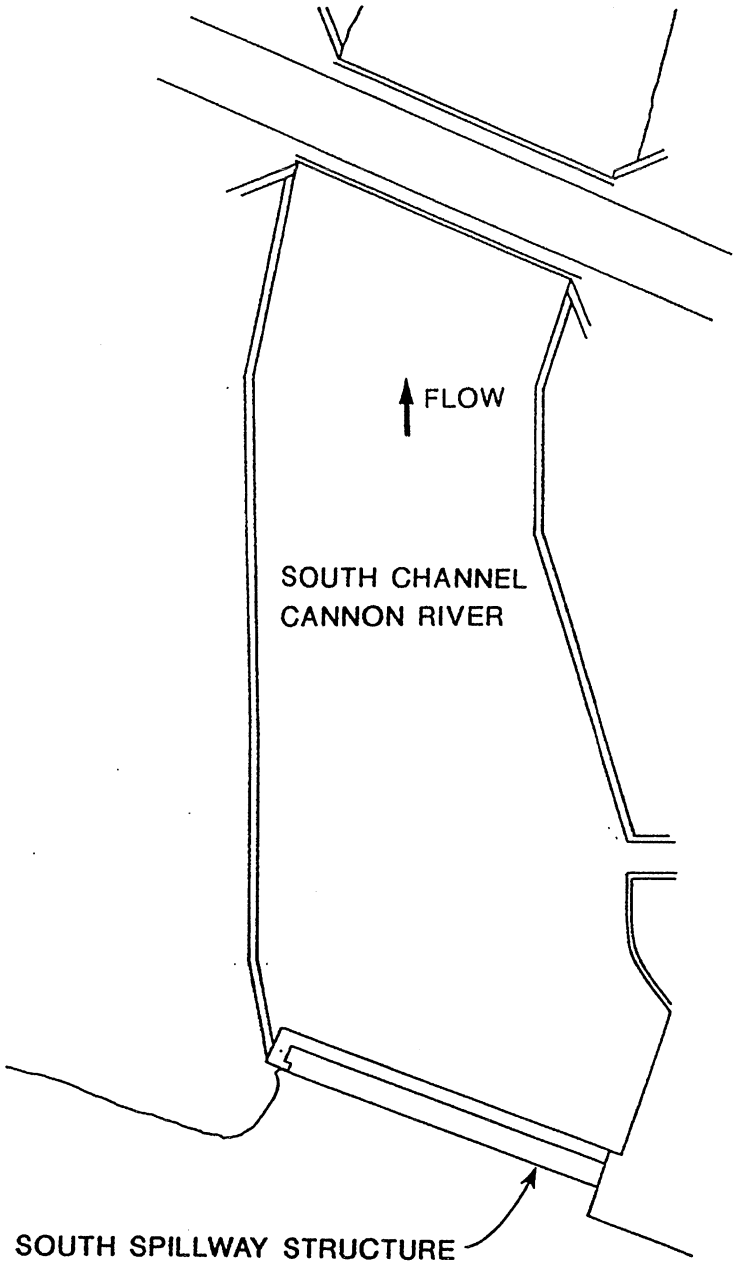

Figure VI–3 Location of Faribault Woolen Mill Dam

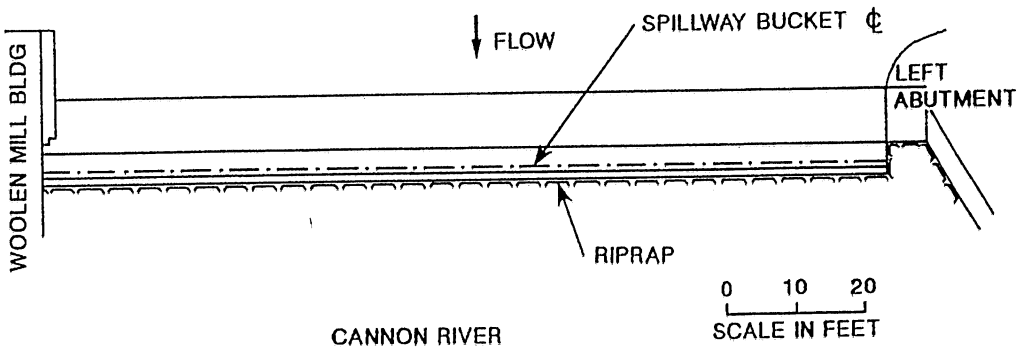

Figure VI–4 Plan view of Faribault Woolen Mill Dam

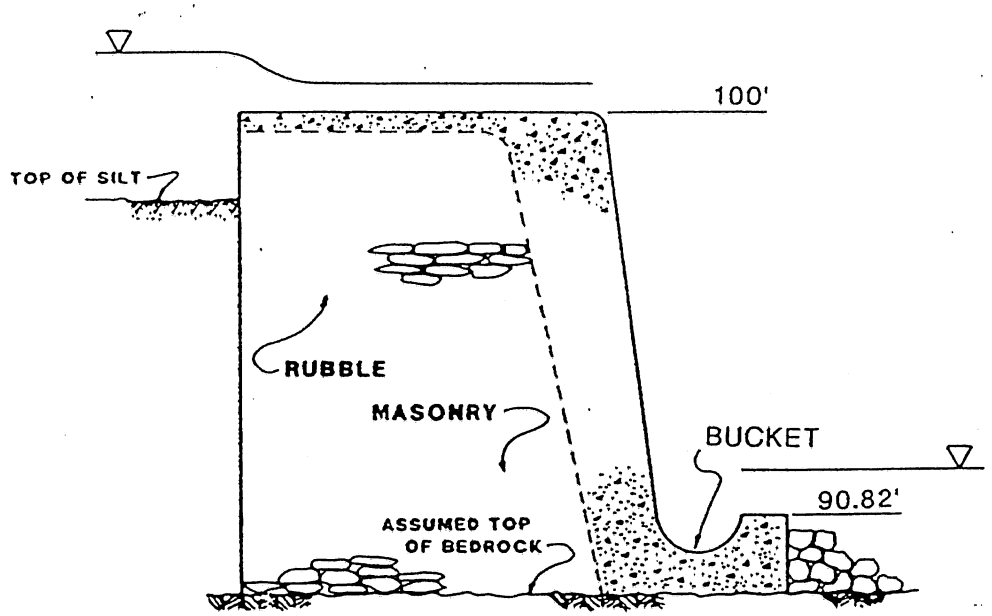

Figure VI–5 Cross section of Faribault Woolen Mill Dam

C. Coon Rapids Dam

The Coon Rapids Dam is located approximately 13 miles upstream from Minneapolis, Minnesota, at river mile 865.5 on the Mississippi River. The structure, upstream pool and surrounding area is owned and operated by the Hennepin County Parks Commission for recreational purposes.

The Coon Rapids Dam consists of several hydraulic structures separated by an earthen dam as shown in Figure VI–6. Gas transfer at this structure was investigated on the tainter gate control structure on the right side of the dam. This control structure consists of 28, 33 ft. wide tainter gate spillways. Downstream of this structure two different types of stilling basins are used to dissipate the energy of the flow. Figure VI–7 shows the stilling basin of bays 1 through 13 and Figure VI–8 illustrates the stilling basin in bays 13 – 28. A simple hydraulic jump was found in bays 1 – 12 and a hydraulic jump run up against the spillway was found in bays 13 – 28. A photo showing the difference in the two types of jumps is given in Photo VI–5.

Four times this site was investigated; August 1, October 6, December 14, 1989 and March 27, 1990. During the first two visits, as well as the last survey, upstream samples were taken directly off the structure and the downstream samples taken off the banks. The isopleths of the first two site investigations are shown in Figures VI–9 to VI–13. During the last survey the tainter gates were fully open and the flow was very high; therefore no samples could be taken with depth. A cross section of the concentrations is given in Figure VI–14.

The methane isopleths have a similar shape, with there being more methane on the left side of the structure than on the right side. There was more methane in the water during the August survey than in the October survey. This may be due to the lower temperatures and to the increased stream flow. As pointed out in Section V, a drop in sediment temperature will cause a drop in the production of methane. Also, during the spring survey there was more methane on the left side of the dam than on the right side. On both survey dates, however, methane concentrations were sufficient for accurate measurements, especially considering the LOQ of 0.35 μg/l.

It is impossible to relate transfer efficiencies for either of the first two visits as the dissolved oxygen is saturated upstream. During the December investigation samples were taken upstream approximately 300 ft. from the dam as shown in Figure VI–6. The results are shown in Table VI–2. A major gradient was observed from the left to the right. No ready explanation for this is available. As this was unexpected, it was decided to study smaller structures in the winter where samples upstream and downstream could be gathered easily.

During the March 27 investigation transfer efficiencies were computed using samples from Gate 1 and Gate 28 as the upstream concentrations left and right sides respectively. As can be seen from the results of the survey (Table VI–2) the dissolved oxygen concentrations are very close to saturation and therefore the uncertainty is very high. The methane results have a much lower uncertainty.

Table VI–2 Coon Rapids Results

December 18, 1989	
Upstream Water Surface	823.16
Downstream Water Surface	809.40
Pressure	750.4 mm Hg
Saturation Concentration	13.73 mg O_2/l
Water Temperature	0.0° C

Location	Left	Right
Upstream		
D.O.	12.10 mg/l	12.09 mg/l
CH_4	32.44 µg/l	2.54 µg/l
Downstream		
D.O.	12.49 mg/l	13.49 mg/l
CH_4	3.36 µg/l	2.10 µg/l
Transfer Efficiency		
D.O.	0.239	0.853
Uncertainty	0.110	0.186
CH_4	0.896	0.176
Uncertainty	0.036	0.214
E values converted to D.O. at 20° C		
D.O.	0.352	0.952
Uncertainty	0.149	0.238
CH_4	0.983	0.295
Uncertainty	0.010	0.330

Table VI–2 (Continued)

March 27, 1990	
Upstream Water Surface	824.91
Downstream Water Surface	812.31
Pressure	747.3 mm Hg
Saturation Concentration	13.31 mg O_2/l
Water Temperature	1.8° C
Flow rate 10,000 cfs	

Location	Left	Right
Upstream		
D.O.	11.27 mg/l	11.68 mg/l
CH_4	32.44 μg/l	3.09 μg/l
Downstream		
D.O.	12.05 mg/l	12.87 mg/l
CH_4	3.36 μg/l	1.80 μg/l
Transfer Efficiency		
D.O.	0.382	0.730
Uncertainty	0.288	0.454
CH_4	0.484	0.416
Uncertainty	0.054	0.133
E values converted to D.O. at 20° C		
D.O.	0.525	0.867
Uncertainty	0.342	0.591
CH_4	0.688	0.610
Uncertainty	0.058	0.132

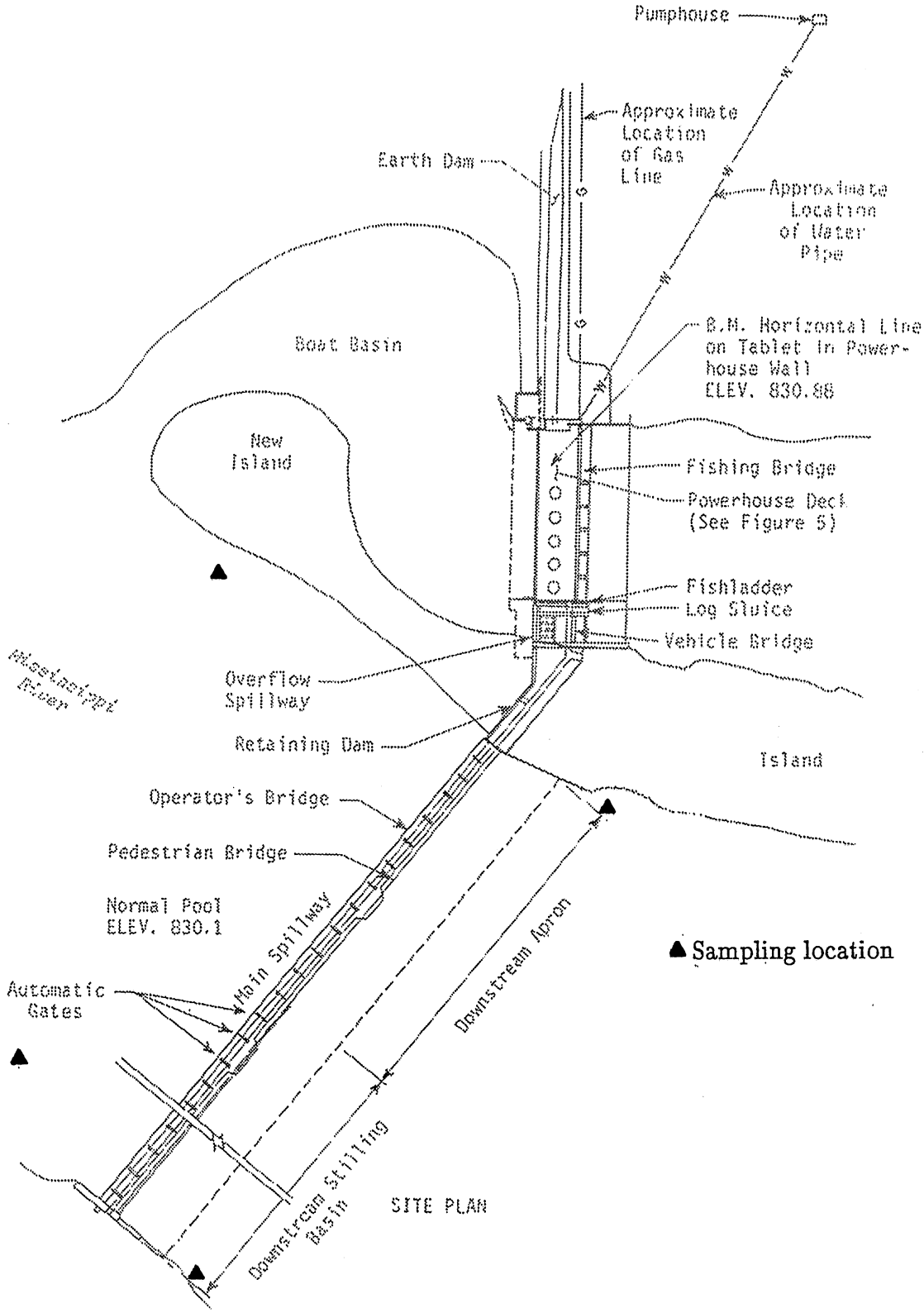

Figure VI–6 Plan view Coon Rapids Dam and sampling locations

December 18, 1989

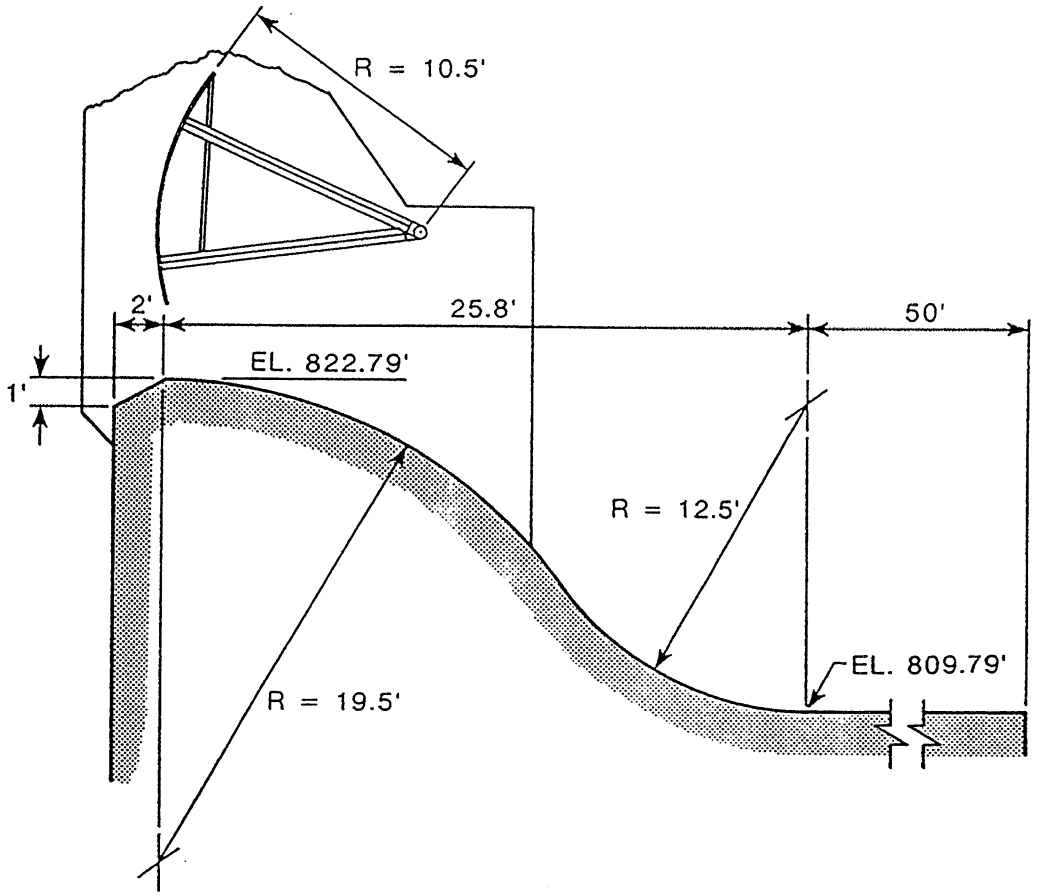

Figure VI–7 Cross section of tainter gate spillway bay 1–12, left bank

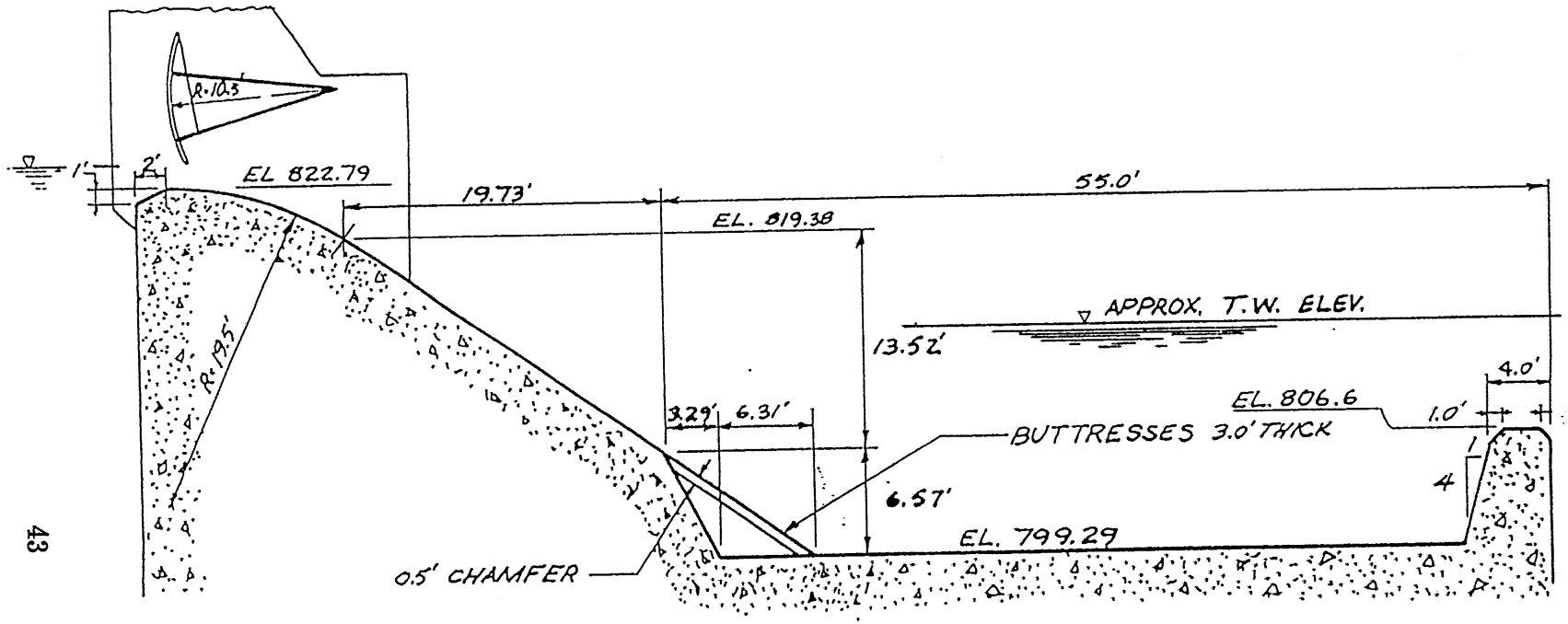

Figure VI–8 Cross section of tainter gate spillway Bay 13–28, right bank.

Downstream left bank = 3.32 μg/l

center = 3.89 μg/l

Downstream right bank = 3.83 μg/l

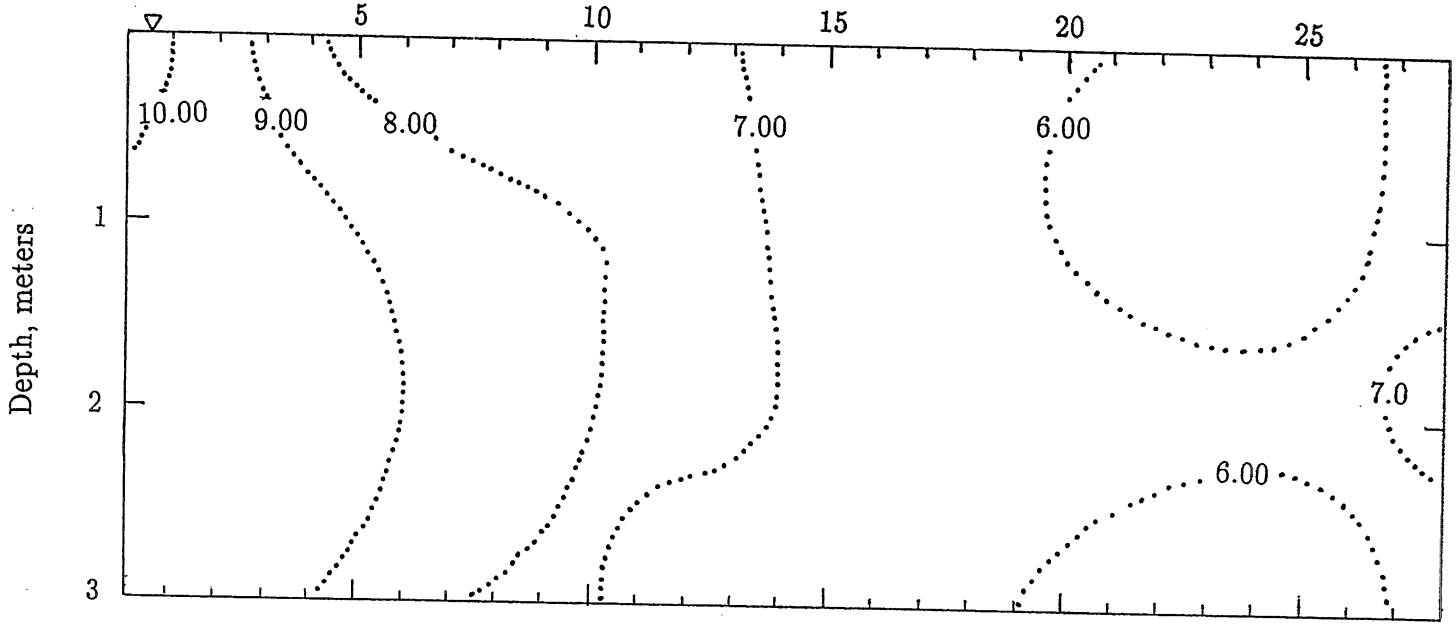

Figure VI–9 Methane isopleths at Coon Rapids Dam, August 1, 1989

Downstream left bank = 8.11 mg/l Downstream center = 8.46 mg/l Downstream right bank = 9.18 mg/l

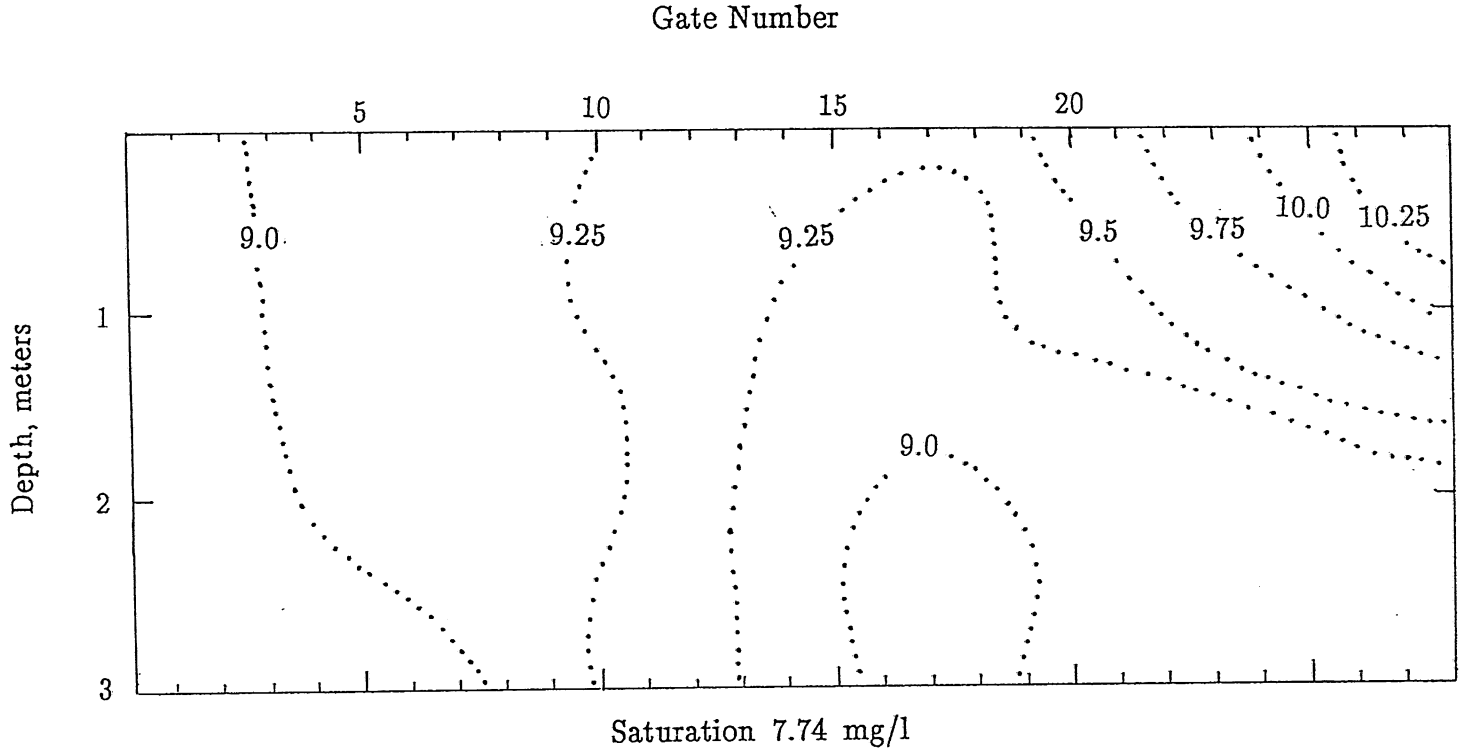

Figure VI–10 D.O. isopleths August 1, 1989

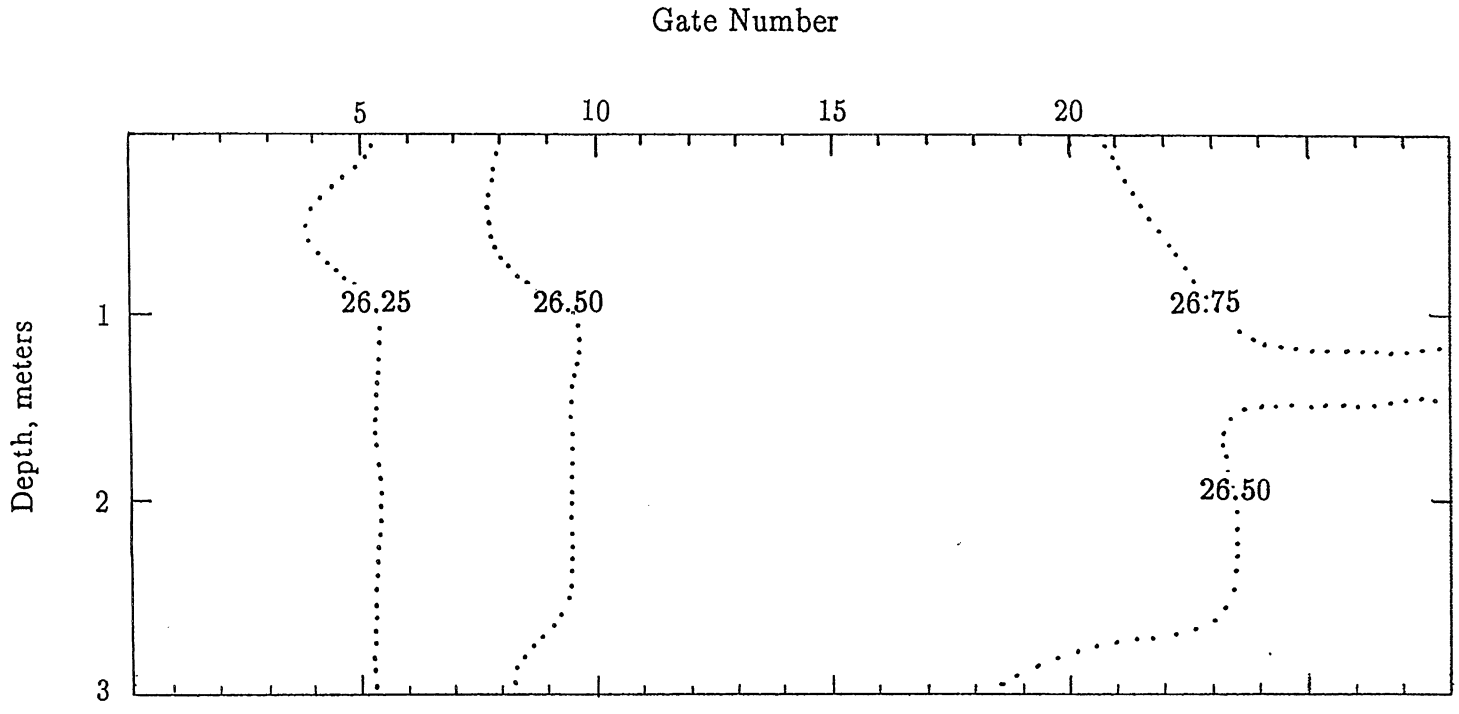

Figure VI–11 Temperature profile August 1, 1989

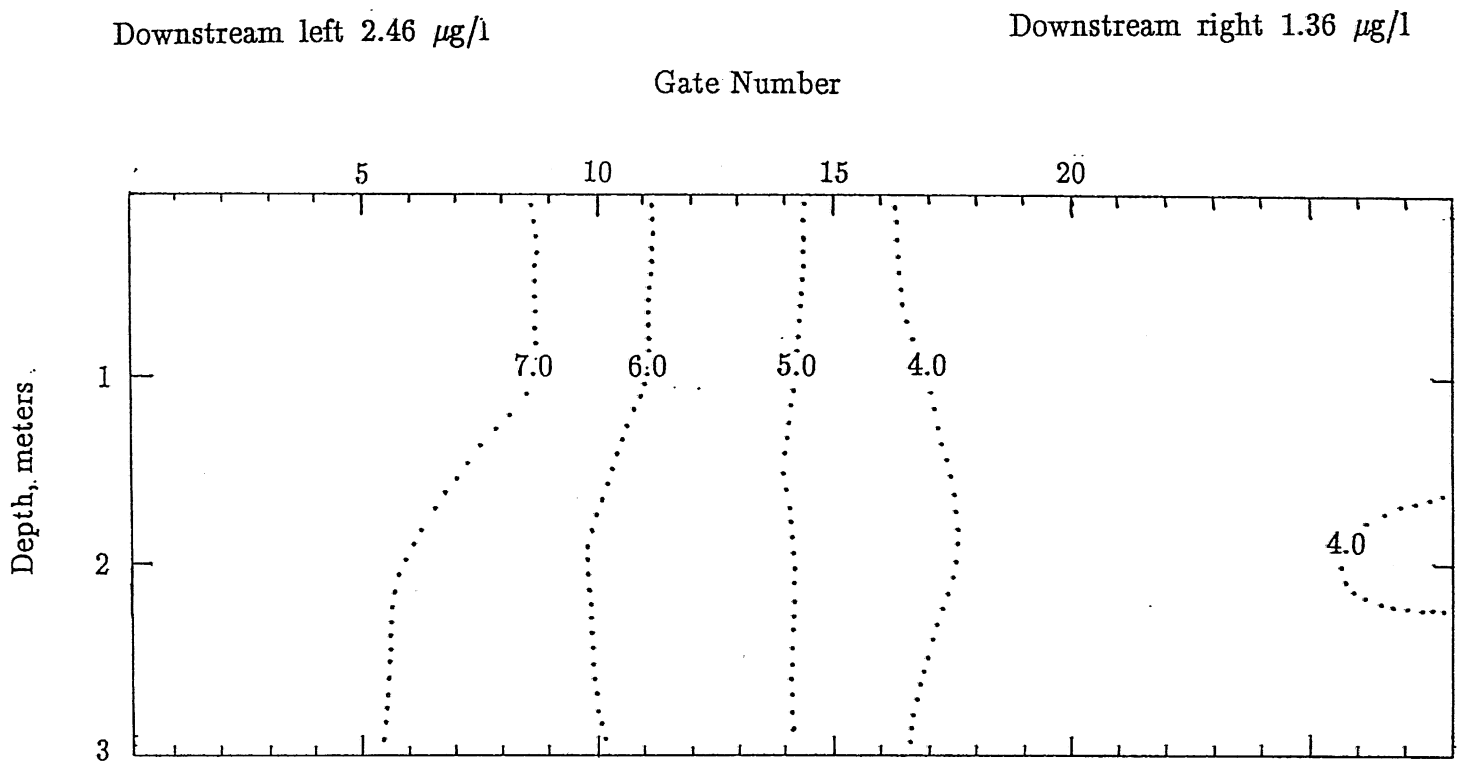

Figure VI–12 Methane isopleths October 6, 1989

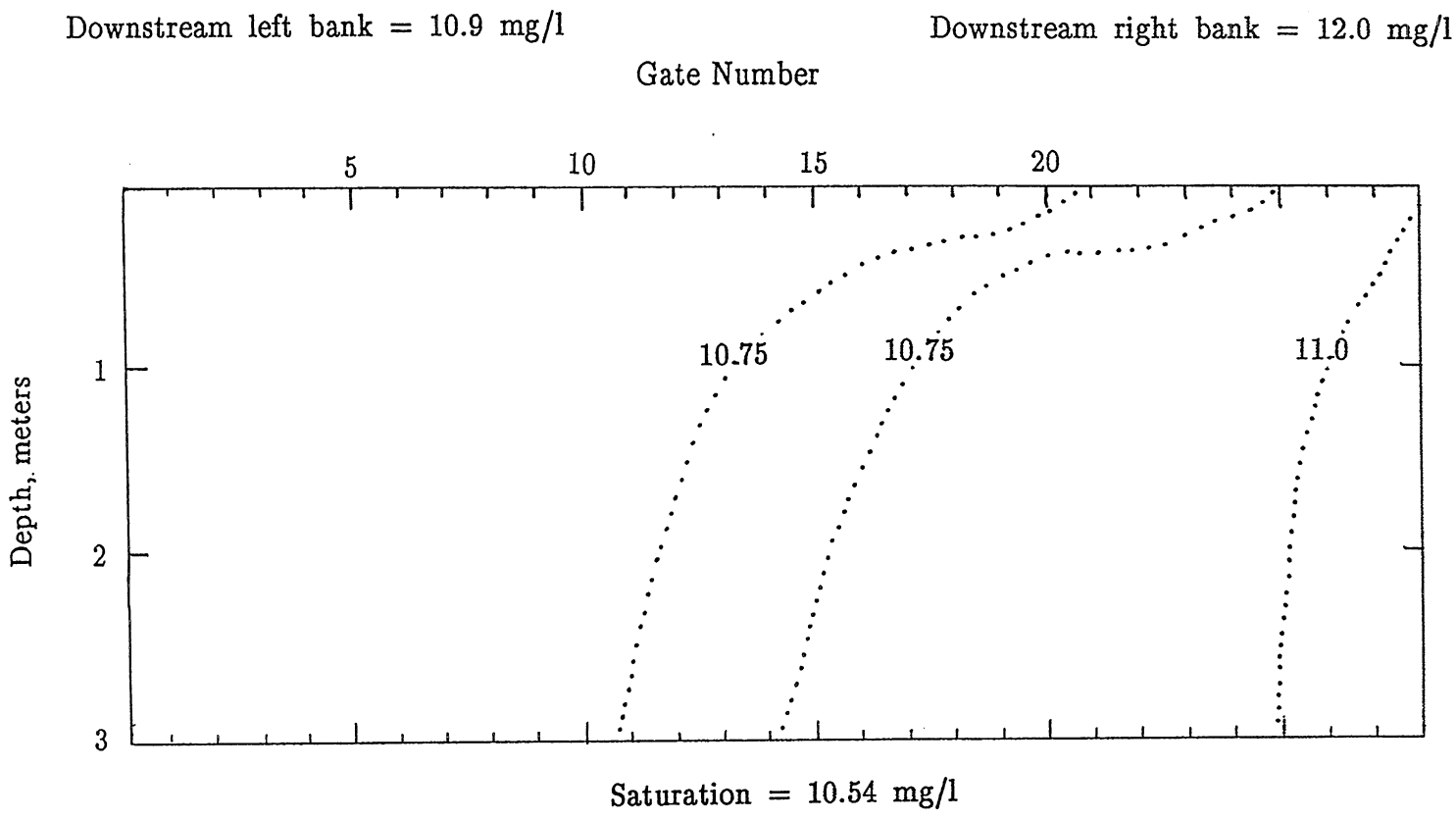

Figure VI–13 D.O. isopleths October 6, 1989

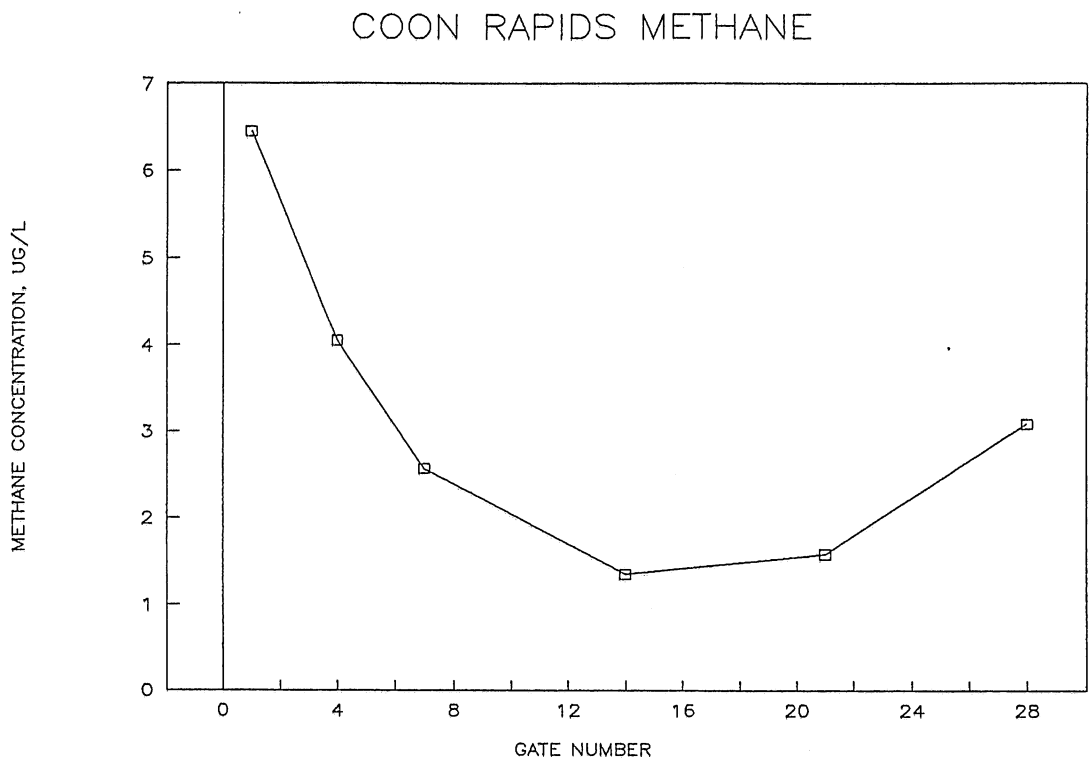

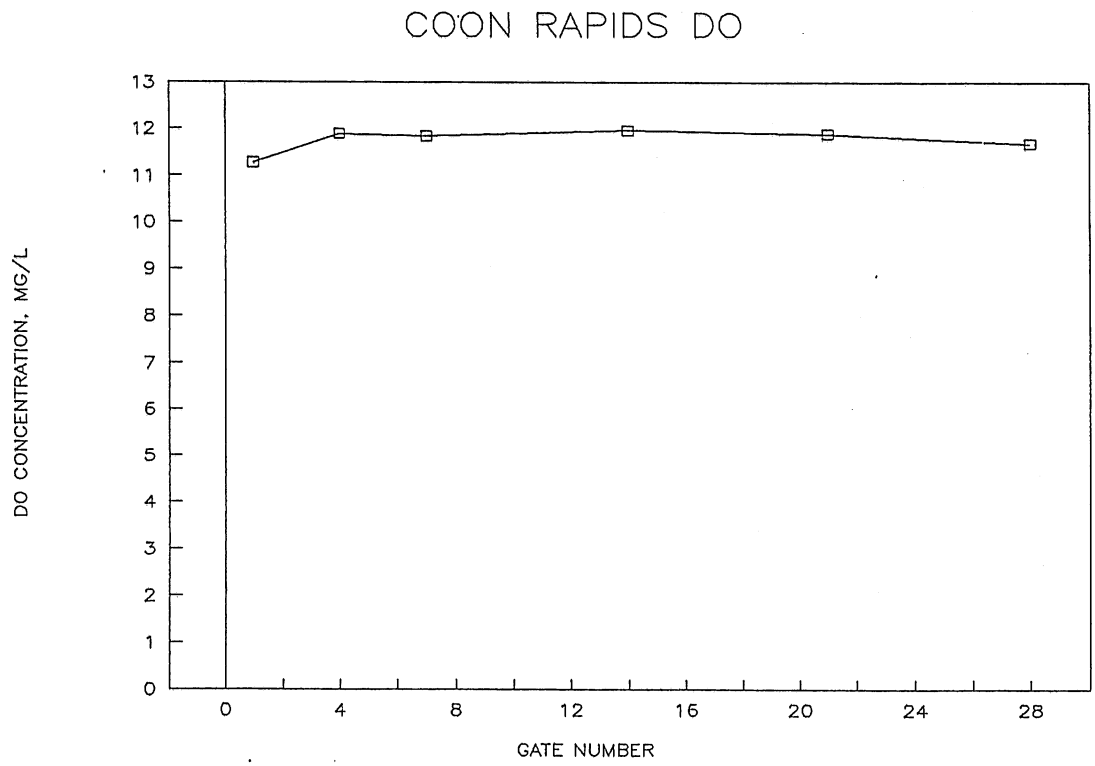

Figure VI–14 Dissolved gas concentrations 3–27–90

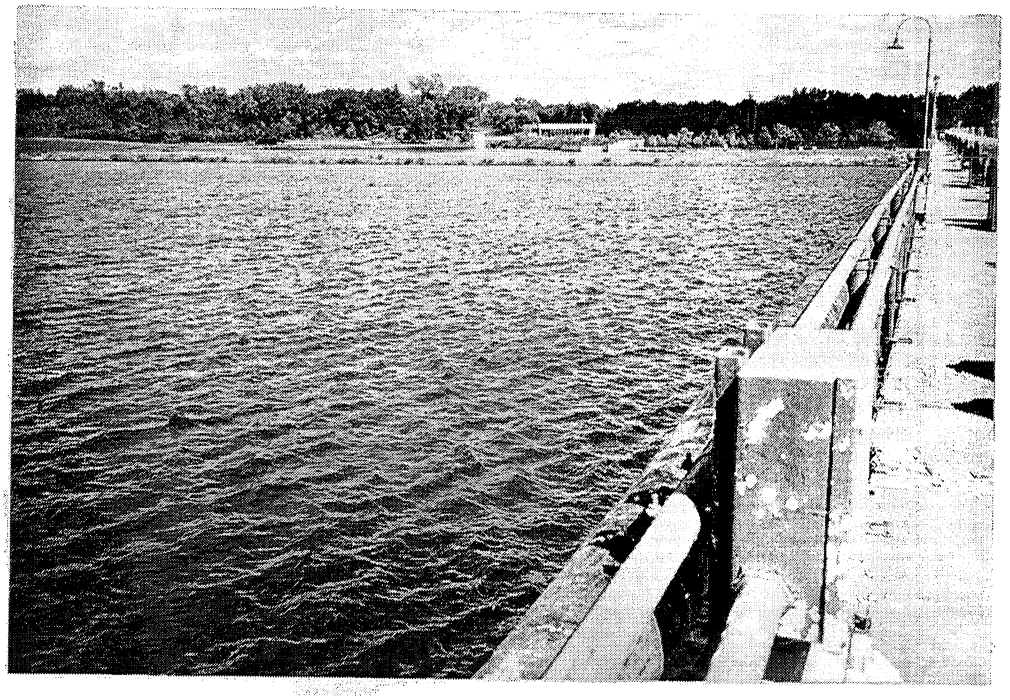

Photo VI–1 Upstream Coon Rapids Dam 8–1–89.

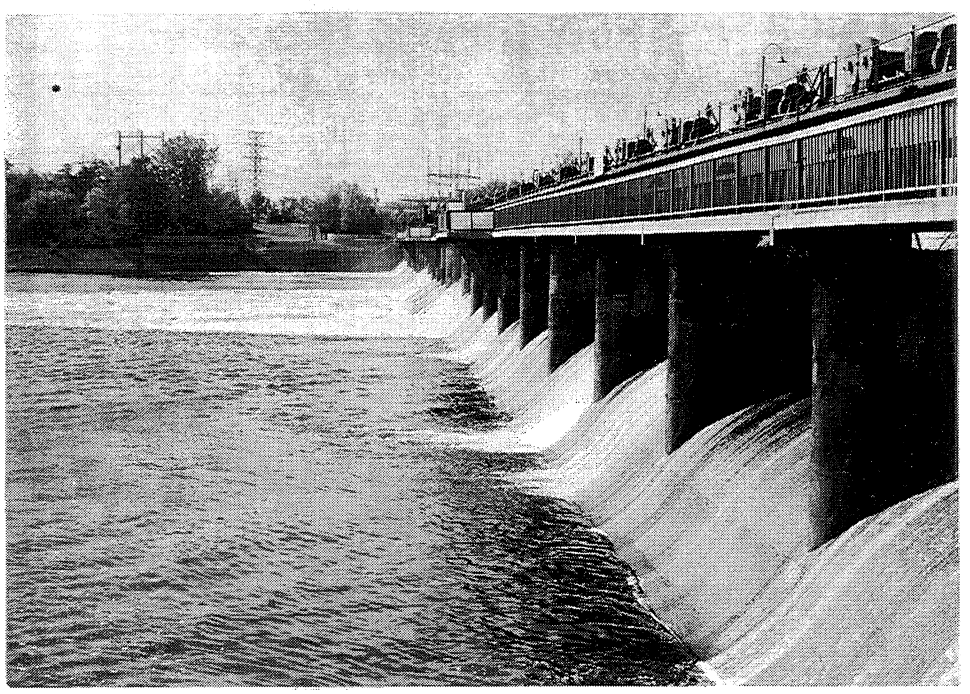

Photo VI–2 Downstream Coon Rapids Dam 8–1–89.

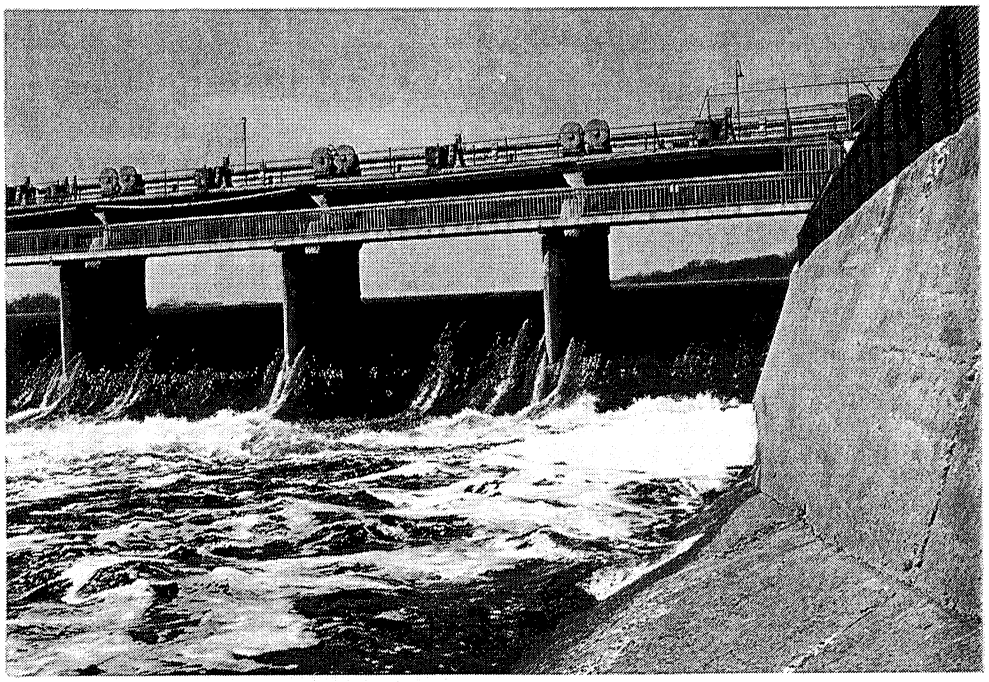

Photo VI–3 Downstream Coon Rapids Dam 12–14–89.

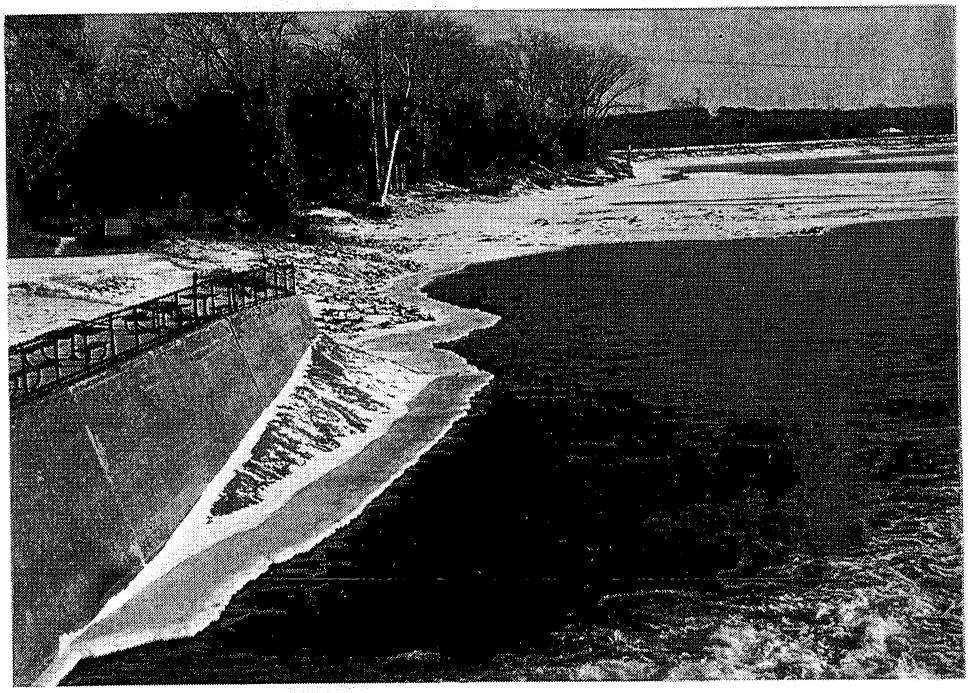

Photo VI–4 Coon Rapids Dam downstream sampling location.

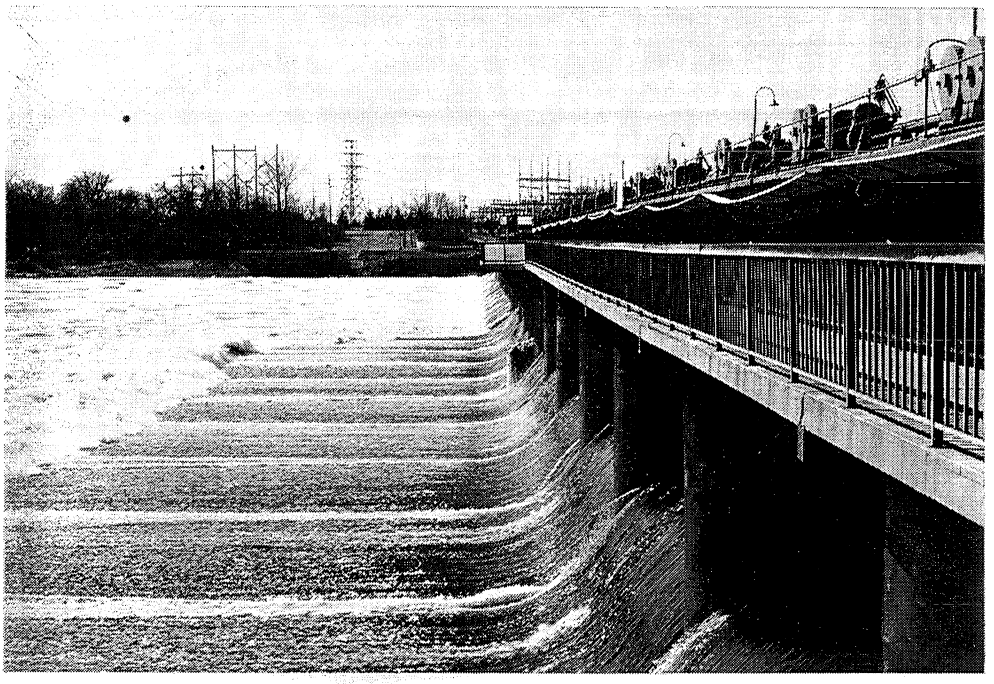

Photo VI–5 Downstream Coon Rapids Dam 3–27–90.

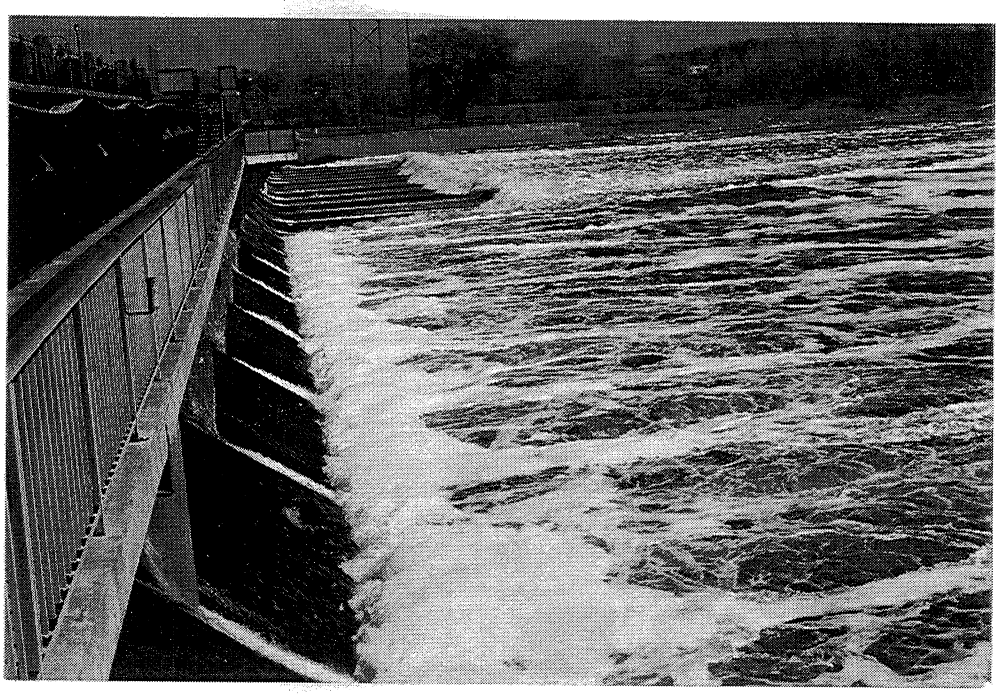

Photo VI–6 Downstream Coon Rapids Dam 3–27–90.

D. Elk River Dam

The Elk River Dam is located on the Elk River approximately 20 ft. upstream of the Main Street Bridge on the southwestern edge of Elk River, Minnesota. The dam maintains a small reservoir as a source of cooling water for the Elk River municipal electric power plant and for recreational purposes.

The dam consists of two fixed crest modified ogee spillways separated by three tainter gate bays as shown in plan in Figure VI–15 and in cross section in Figure VI–16. Gas transfer was investigated at the main 116 ft. northern spillway. The dam is shown in Photos VI–7 to VI–10.

The site was investigated on January 19, 1990. Three cross sections on the spillway were investigated. There was open water across the lip of the spillway so to sample upstream safely two holes were cut through the ice approximately 10 ft. from the spillway. Samples on the left side of the structure were gathered from the concrete base on the side of the structure. Approximate sampling locations are shown in Figure VI–15.

The concentration and temperature profiles are shown in Figures VI–17 to VI–21. The shaded portion signifies ice. The methane results from the samples gathered under the ice exhibit a strong gradient from the ice to the sediments. The ice free sample location also had a similar gradient but not as pronounced. The D.O. also exhibited a gradient however it was not as pronounced as the methane. This gradient made it difficult to perform transfer efficiency calculations as it is hard to predict the amount of each layer that is contributing to the total flow over the spillway. A program developed by the USCOE, called SELECT, was used to compute the upstream concentrations. Using the temperatures recorded as a control, upstream concentrations of methane and D.O. were computed. This seemed to work satisfactorily for the two sections with ice cover, however for the ice free section SELECT computed an upstream methane concentration higher than the measured downstream concentration. Clearly there is something amiss here. The methane transfer efficiencies converted to D.O. at 20°C do not match the D.O. results converted to 20°C. This could be due to lateral mixing on the spillway. Because of the large methane gradient some water with a high methane concentration could have mixed with the low methane concentration water and caused the transfer efficiencies, as predicted by methane and D.O., not to agree. The dissolved oxygen profiles do not exhibit such a large gradient and therefore the transfer efficiencies for oxygen from cross section to cross section are very uniform.

A major difference between the oxygen and methane transfer measurements is likely due to the pressure difference that bubbles undergo when they are dragged under the surface. As a bubble gets deep into the stilling basin the hydrostatic pressure increases, thus raising the saturation concentration of the water in contact with the bubble. Therefore the measured oxygen transfer efficiency using C_s at atmospheric pressure is higher than the actual efficiency. Assuming the methane results are correct, a "corrected" saturation concentration for D.O. can be computed. The E value is converted from methane at the measured temperature to oxygen at the measured temperature using equation I–15.

$$E_i = 1 - (1 - E)^{1/f_i} \qquad \text{(I–15)}$$

where E_i is the transfer efficiency for D.O. at the measured temperature, E is the measured transfer efficiency for methane, f_i is the correction term for gases and temperature equal to $f_g \times f_t$. In this equation $f_t = 1.0$ as methane and oxygen are at the temperature. As explained in Section III, $f_g = 0.88$. The corrected "saturation concentration" is then found from the definition of E, Equation I–5.

$$E = \frac{C_u - C_d}{C_s - C_d} \qquad \text{(I–5)}$$

where E is the corrected transfer efficiency computed above. This combined with the measured C_d and the C_u value from SELECT, the corrected saturation concentration, C_{se}, is found by:

$$C_{se} = \left[\frac{C_u - C_d}{E} \right] + C_d \qquad \text{(VI–1)}$$

The effective depth is the water depth at which the saturation concentration is equal to the effective saturation concentration computed above. This is given by:

$$P_e = C_{se} \left[\frac{1 \text{ atm.}}{C_s \text{ (at 1 atm)}} \right] \qquad \text{(VI–2)}$$

where P_e is the saturation pressure in atmospheres, C_{se} is the effective saturation concentration calculated above, and C_s is the saturation concentration at 1 atmosphere. The saturation pressure is then converted to an equivalent depth of water by:

$$\text{DEFF} = (P_e - 1) \left[\frac{33.9 \text{ ft}}{1 \text{ atm}} \right] \qquad \text{(VI–3)}$$

where P_e is the saturation pressure calculated above and DEFF is the effective depth in ft. The concept of effective depth is irrelevant when the transfer efficiency as determined by the methane is higher than the transfer efficiency as determined by oxygen. That is, when E determined by methane is higher than the E determined by oxygen, the effective depth is negative.

The effective depth was calculated for each cross section. The results are shown in Table VI–4. The effective depths are not consistent. It is felt lateral mixing on the spillway is responsible for the differences.

Table VI–4 Elk River Results

January 19, 1990			
Upstream Water Surface	871.67		
Downstream Water Surface	856.47		
Tailwater Depth	3.67 ft.		
Discharge	1.10 cfs/ft		
Pressure	740.5 mm Hg		
Saturation concentration	13.40 mg O_2/l		
Location	Right	Center	Left
Upstream (from SELECT)			
D.O.	5.12 mg/l	5.84 mg/l	3.94 mg/l
CH_4	9.63 μg/l	10.80 μg/l	3.22 μg/l
Downstream			
D.O.	10.86 mg/l	11.06 mg/l	10.54 mg/l
CH_4	4.22 μg/l	6.96 μg/l	4.32 μg/l
Temp. from SELECT	1.42° C	1.52° C	1.92° C
Measured Temp.	1.4° C	1.5° C	1.9° C
Transfer Efficiencies			
D.O.	0.693	0.693	0.711
Uncertainty	0.010	0.028	0.016
CH_4	0.562	0.359	–0.301
Uncertainty	0.013	0.013	0.032
E indexed to D.O. at 20° C			
D.O.	0.844	0.843	0.834
Uncertainty	0.012	0.022	0.015
CH_4	0.770	0.547	–0.554
Uncertainty	0.015	0.016	0.051
DEFF, ft.	2.95	14.24	—

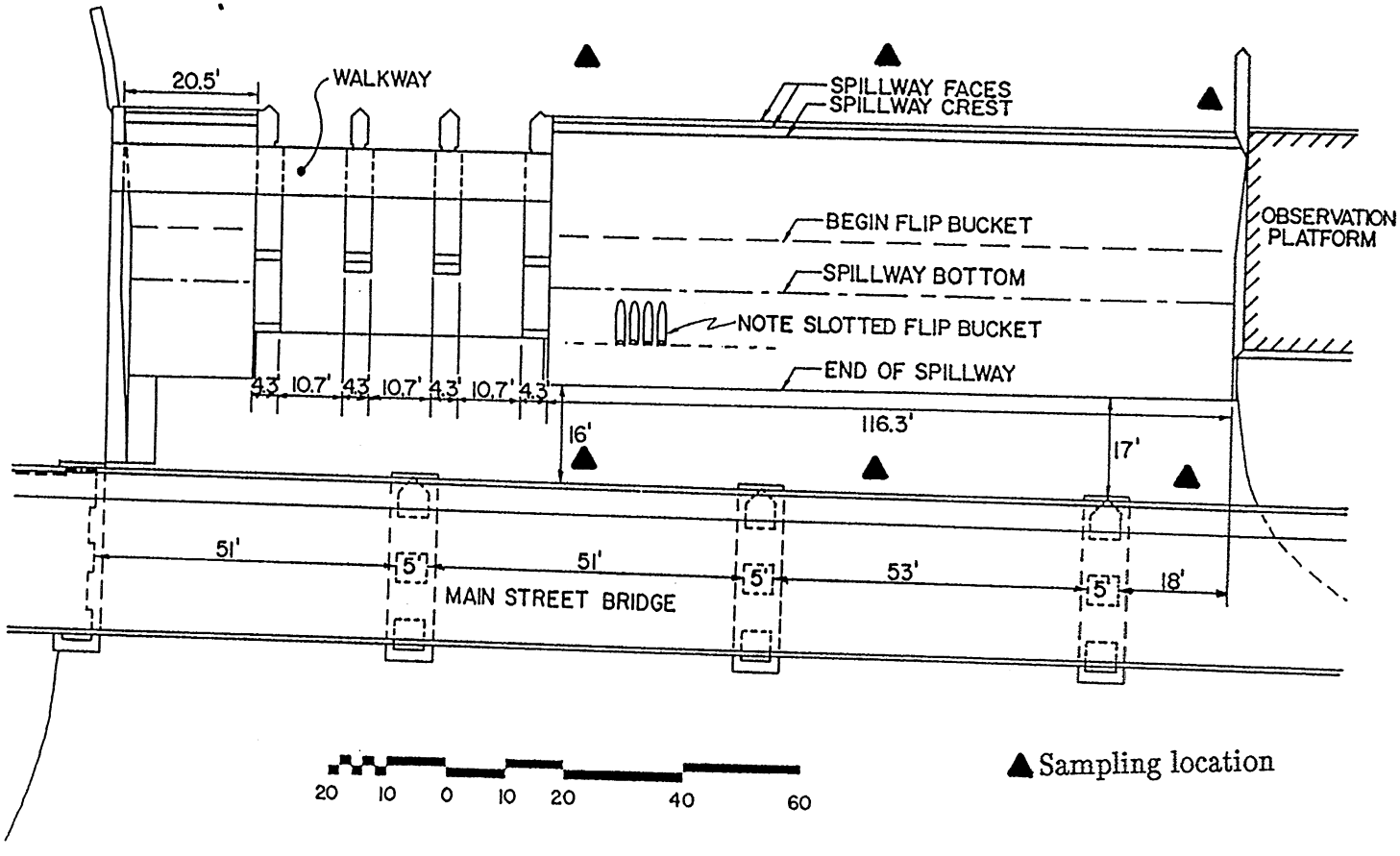

Figure VI–15 Plan view Elk River Dam and January 19, 1990 sampling location

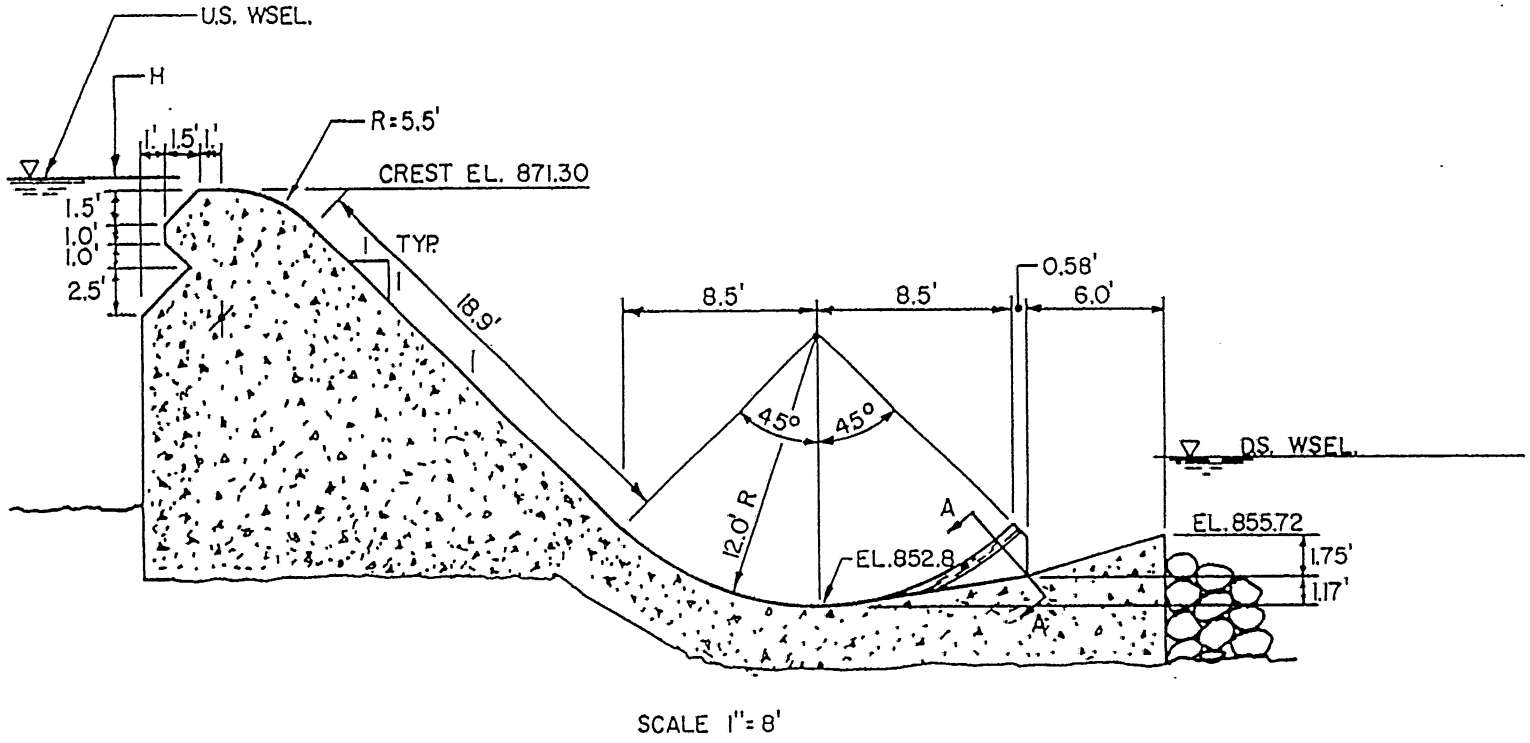

Figure VI–16 Cross section Elk River Dam

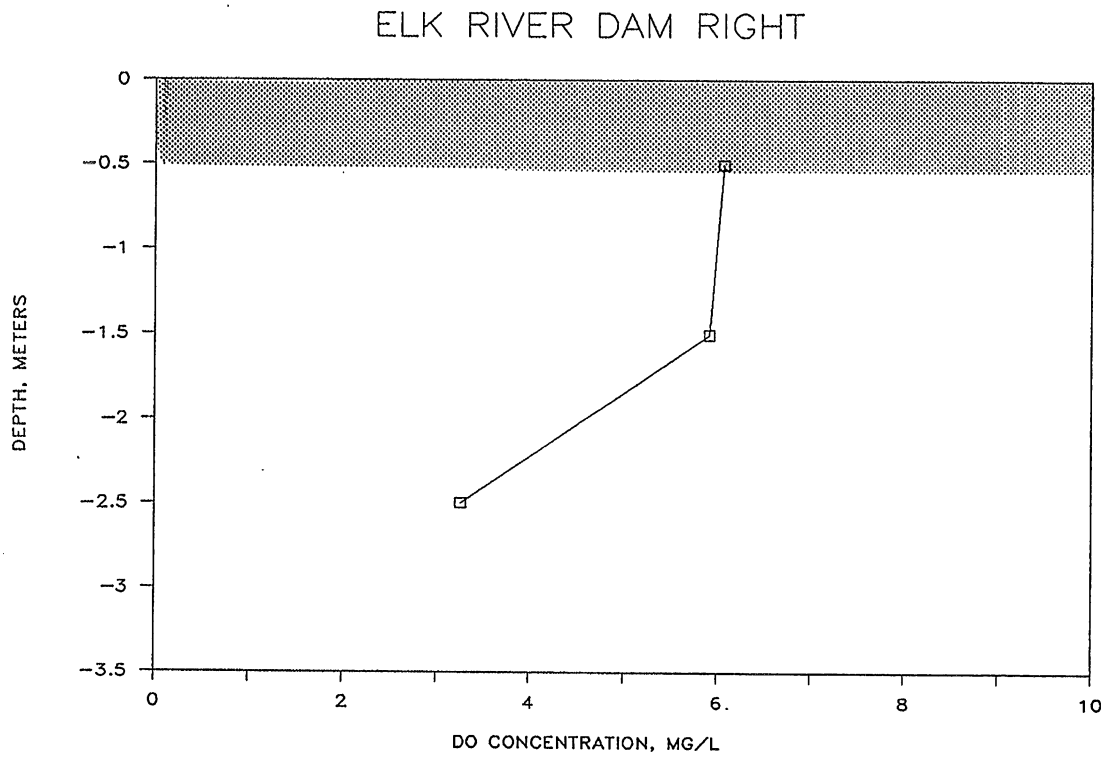

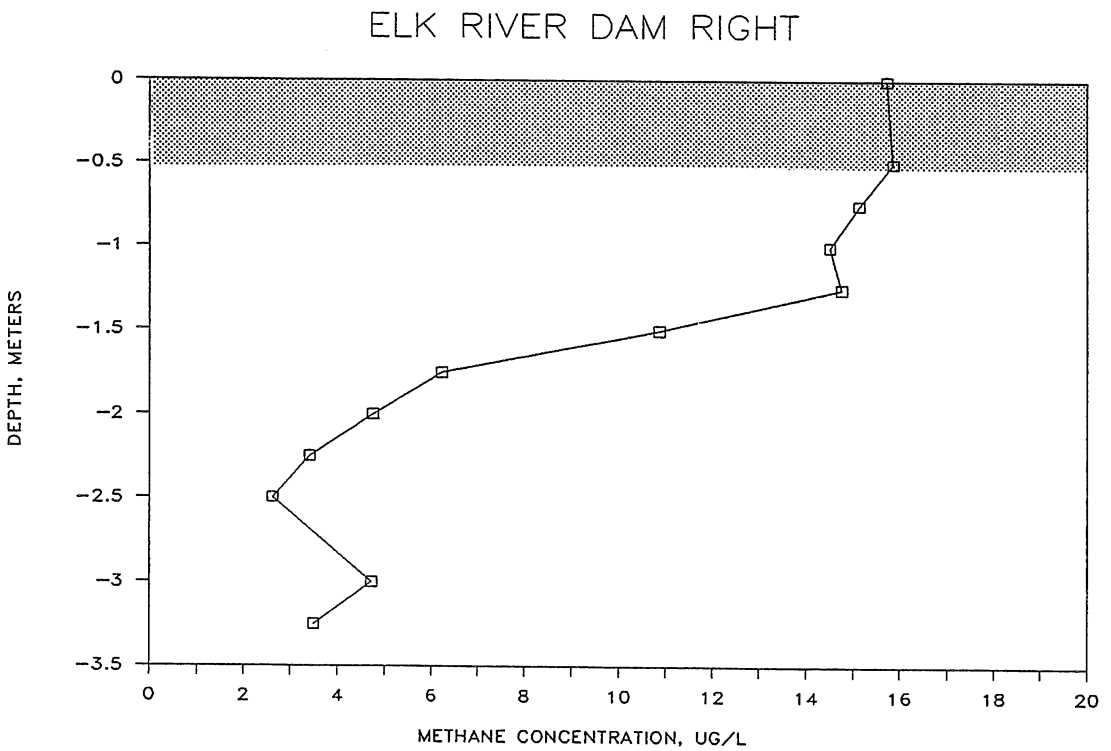

Figure VI–17 D.O. and Methane profiles for right side

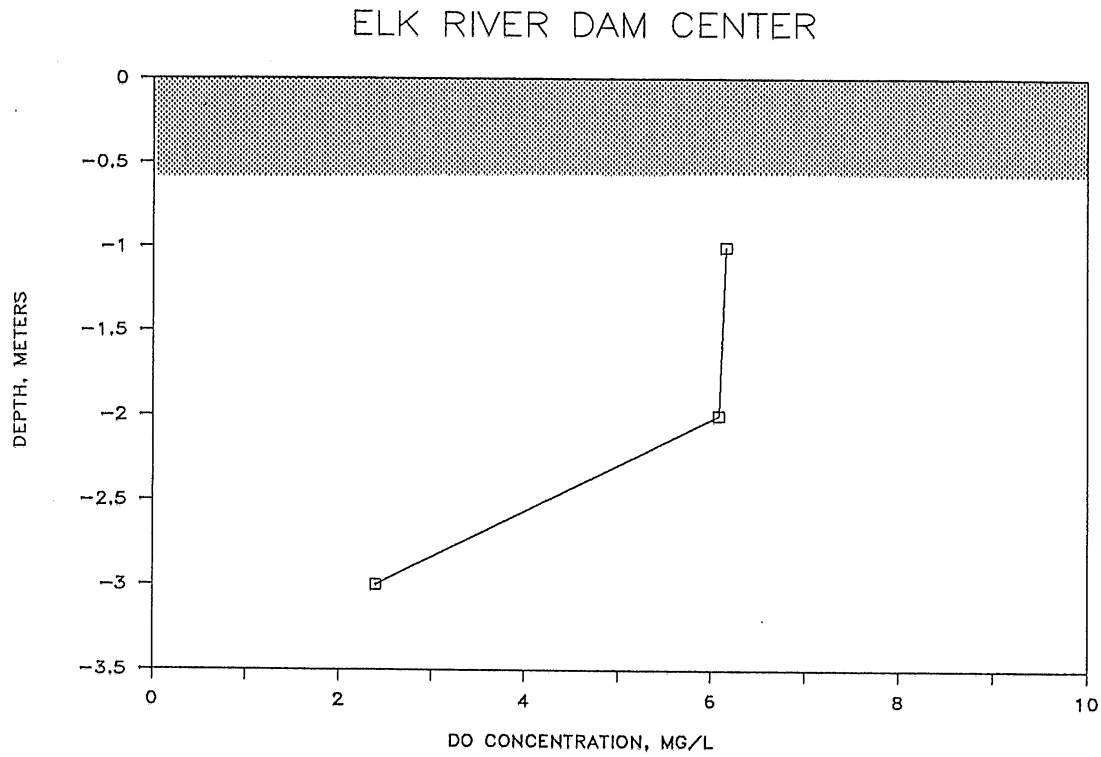

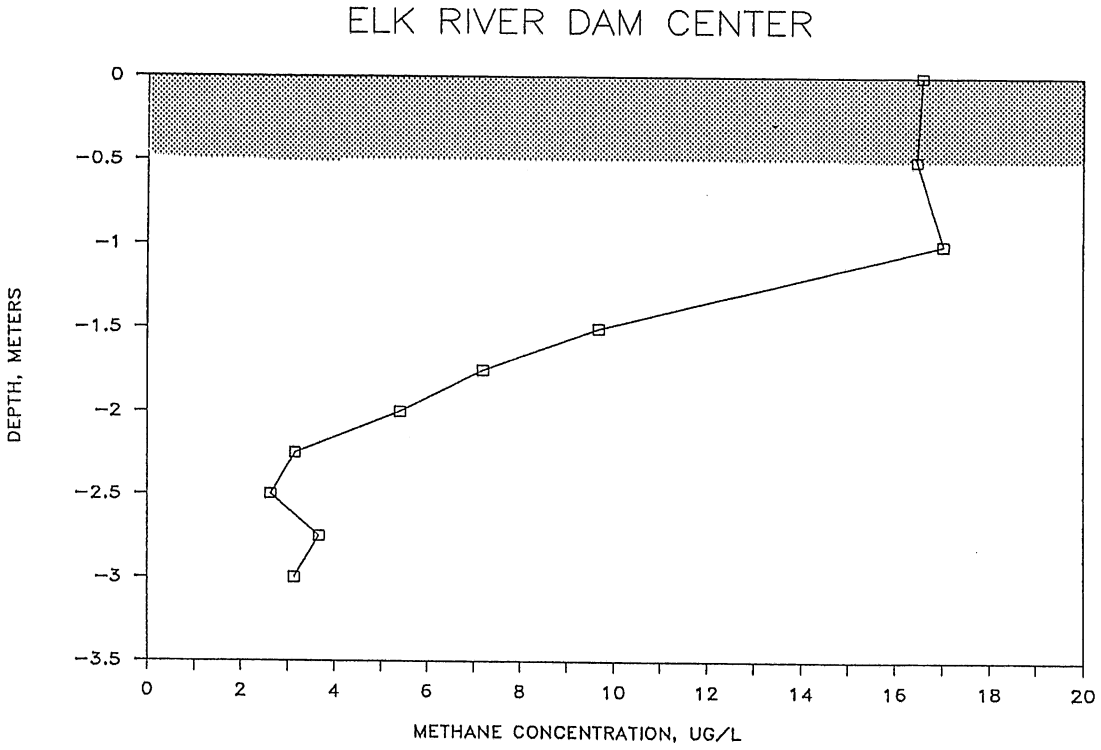

Figure VI–18 D.O. and Methane profiles for center

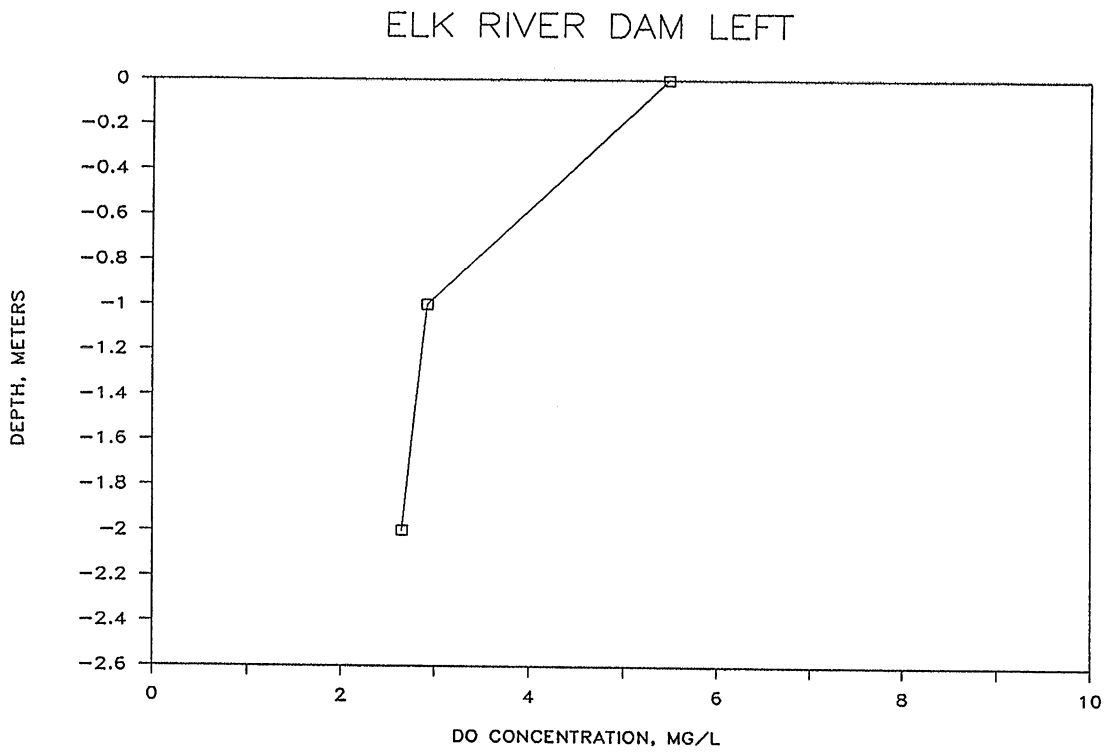

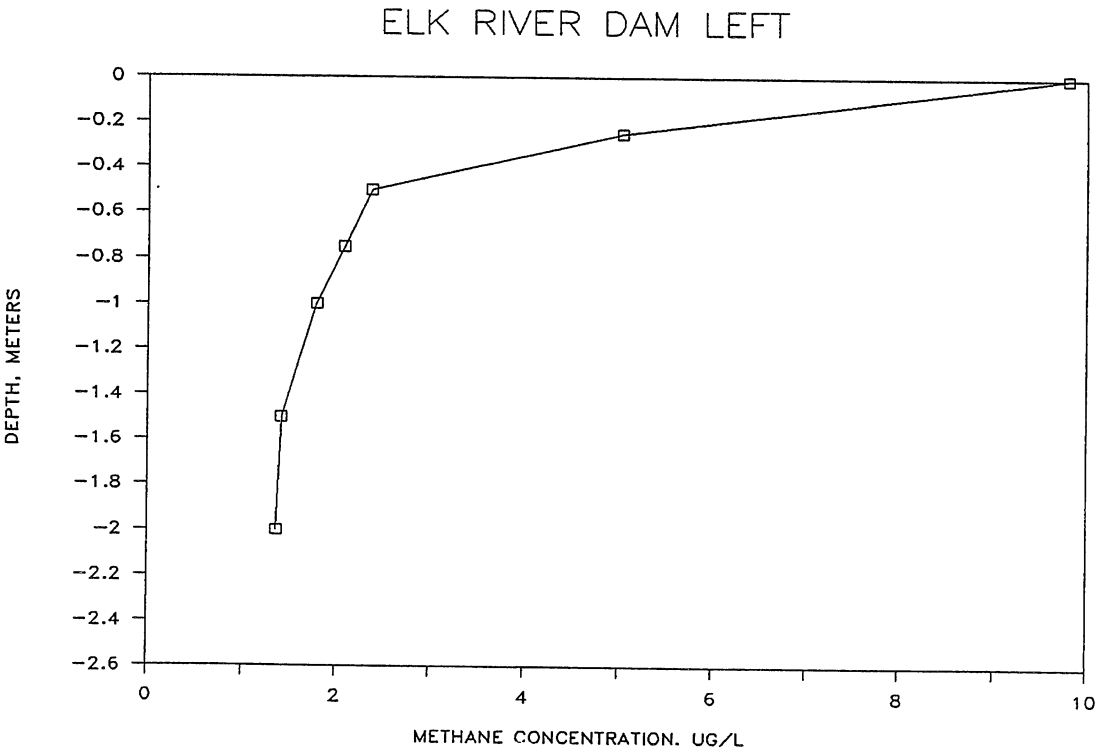

Figure VI–19 D.O. and Methane profiles for left side

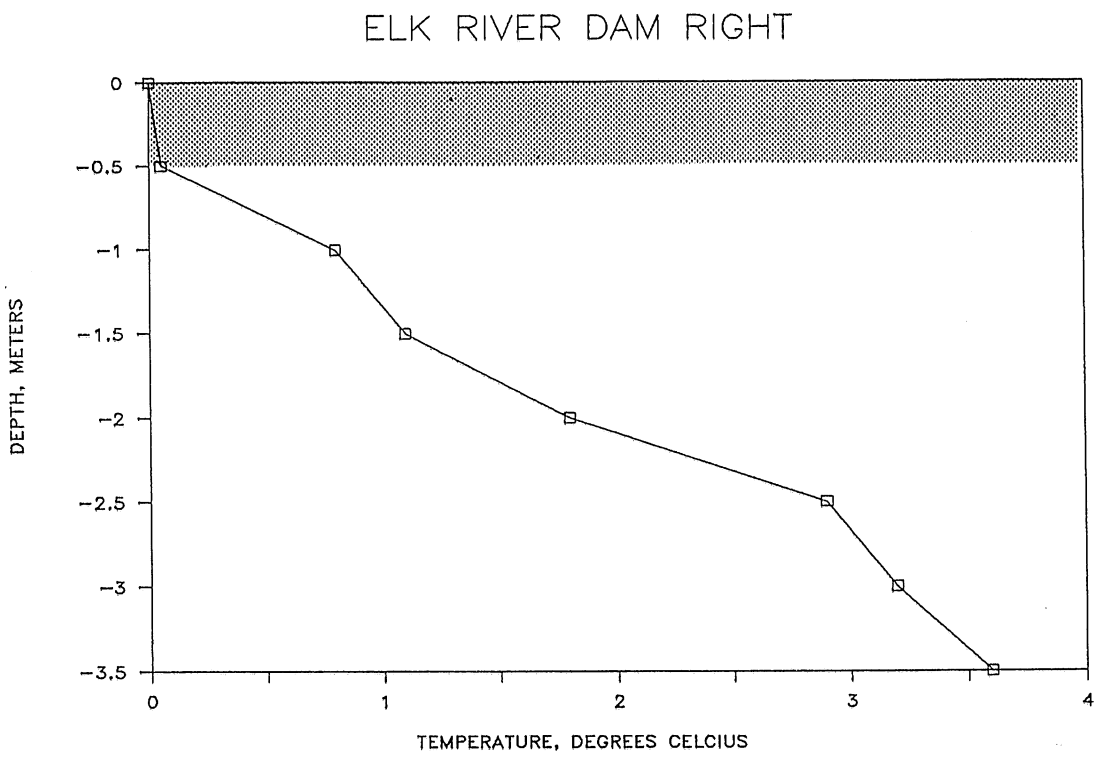

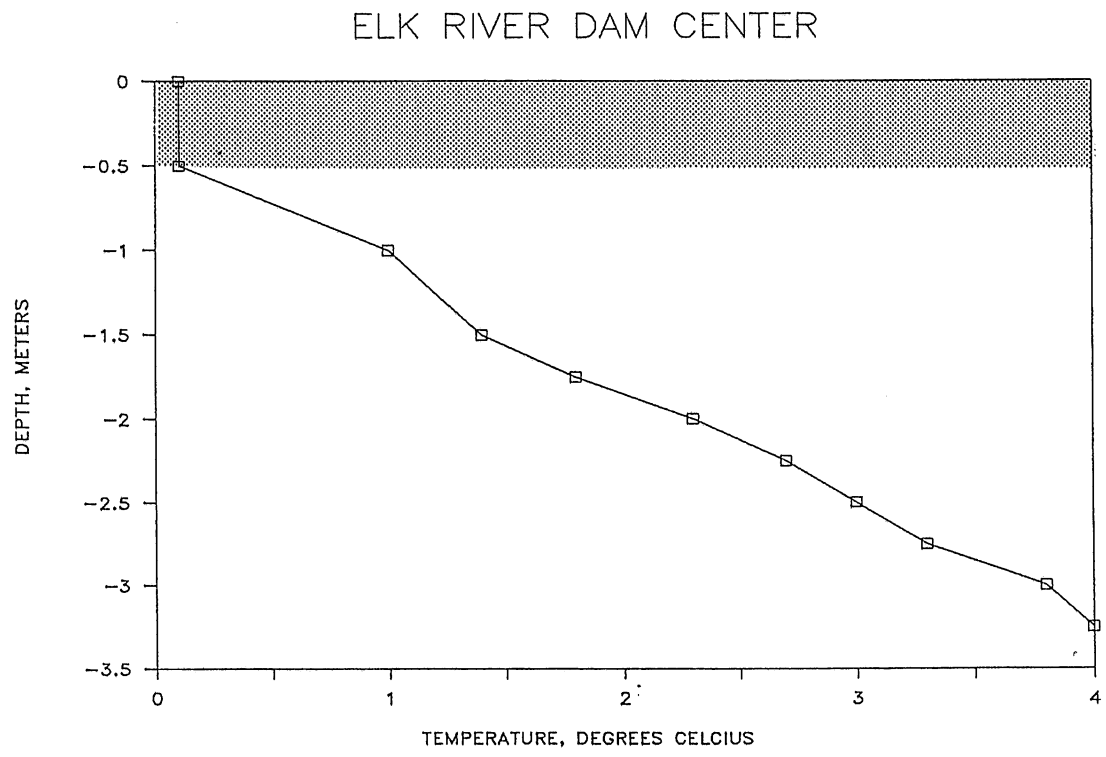

Figure VI–20 Temperature profiles for center and right side

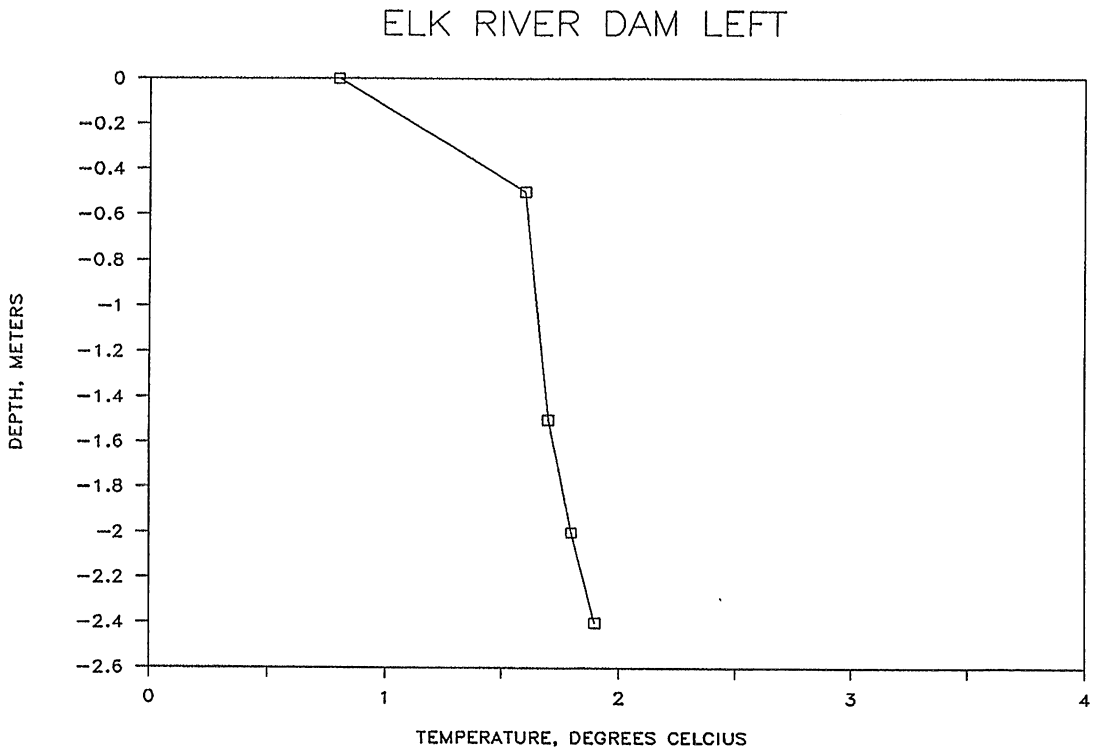

Figure VI–21 Temperature profile for left side

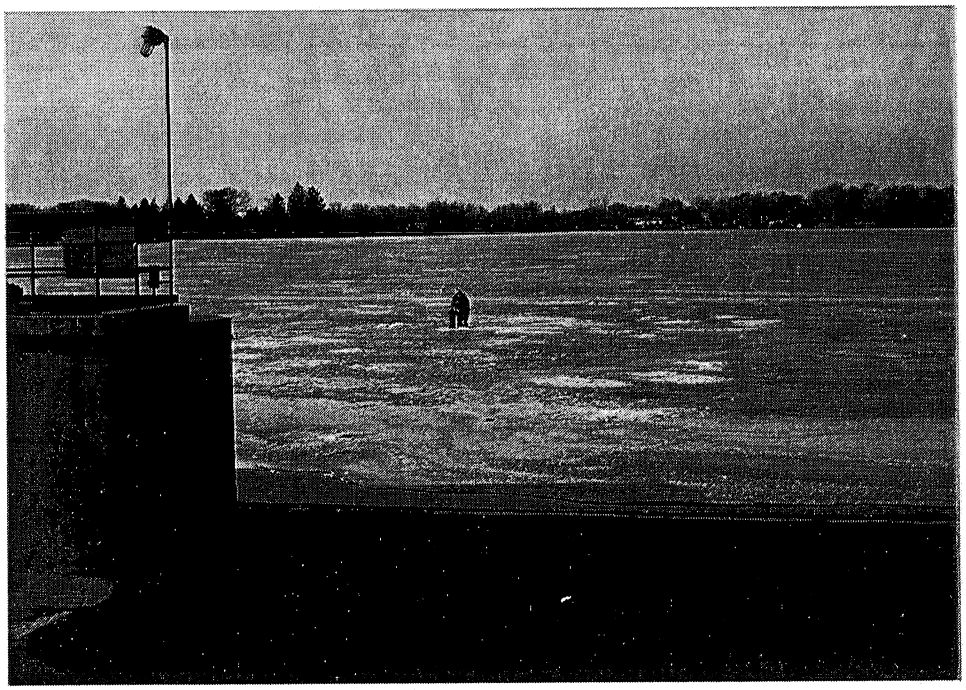

Photo VI–7 Upstream Elk River Dam

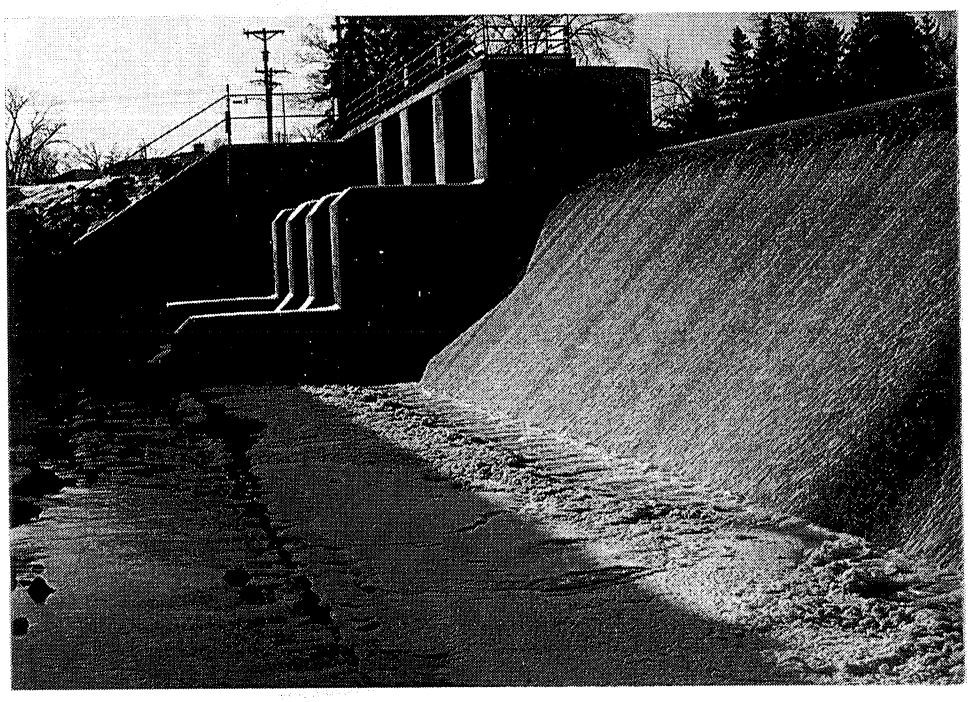

Photo VI–8 Spillway Elk River Dam

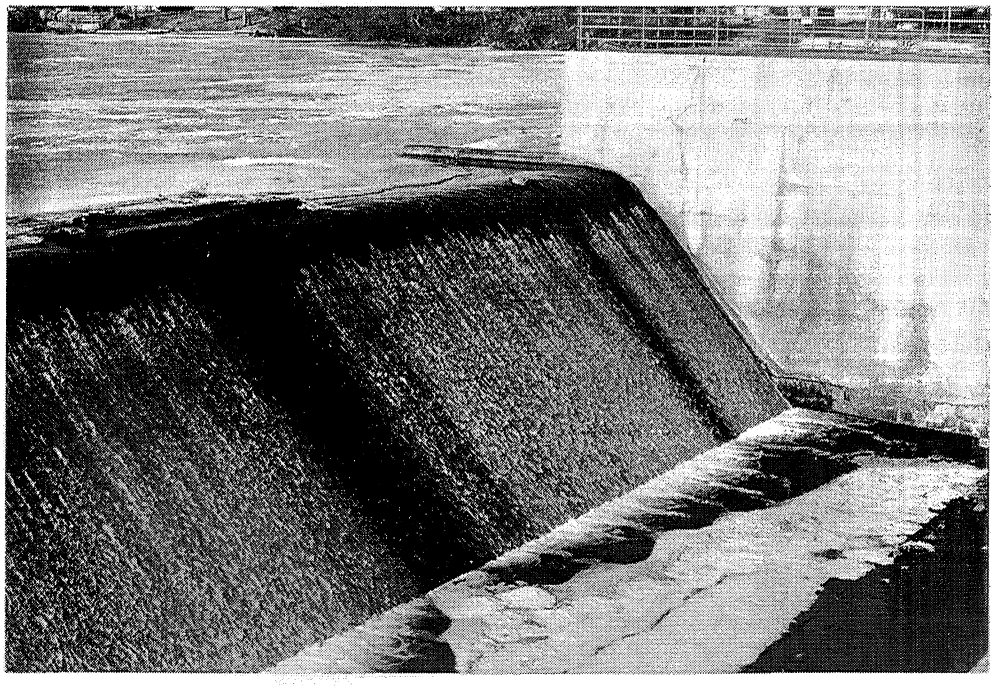

Photo VI–9 Spillway Elk River Dam

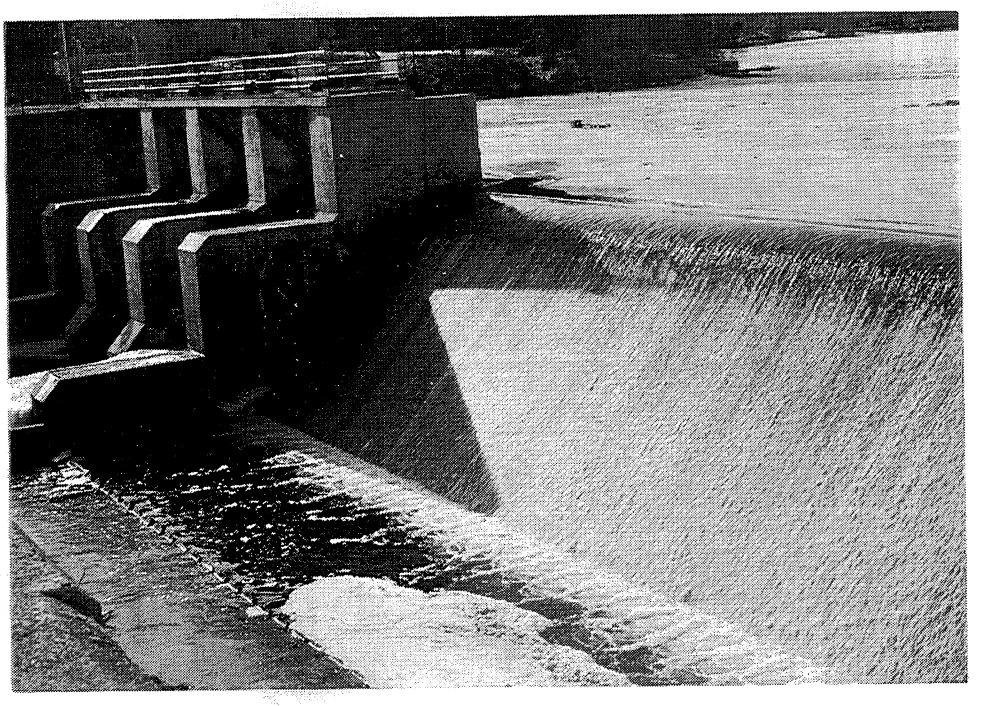

Photo VI–10 Downstream Elk River Dam

E. Kost Dam

The Kost Dam is an earthen dam with a 73.5 ft. uncontrolled ogee spillway located in Chisago County, Minnesota on the Sunrise River. A location plan is shown in Figure VI–22. Previously the dam was used to maintain a reservoir for hydropower purposes. Today the dam is used to maintain a small reservoir for recreational use. The dam is shown in plan view in Figure VI–23 and also in Photos VI–12 to VI–15.

This site was investigated on January 26, 1990. There was no ice over the spillway so a hole was cut through the ice approximately 10 ft. from the crest for the center samples. The samples from the sides were gathered from the side walls approximately 5 ft. from the crest. In performing the survey the crest of the spillway was assumed to be at elevation 100.00.

As with the Elk River results, the methane concentrations exhibit a gradient from the surface to sediments. This is shown in Figures VI–24 to VI–28. SELECT was used to predict upstream concentrations. Transfer efficiencies were calculated and converted to D.O. at 20^{0}C and the results shown in Table VI–5. Using the procedures described in the Elk River section, DEFF was calculated for the three sections. Two of the three sections have comparable effective depths, however the effective depths are greater than the tailwater depth.

Table VI–5 Kost Dam Results

January 26, 1990			
Upstream Water Surface	100.72		
Downstream Water Surface	86.96		
Tailwater Depth	0.66 ft.		
Discharge	0.50 cfs/ft		
Pressure	739.6 mm Hg		
Saturation Concentration	13.73 mg O_2/l		
Location	Right	Center	Left
Upstream (from SELECT)			
D.O.	8.70 mg/l	8.58 mg/l	9.32 mg/l
CH_4	54.01 μg/l	48.84 μg/l	53.55 μg/l
Downstream			
D.O.	10.59 mg/l	10.53 mg/l	11.01 mg/l
CH_4	33.30 μg/l	34.49 μg/l	37.45 μg/l
Downstream			
Temp. from SELECT	0.32° C	0.27° C	0.45° C
Measured Temp.	0.3° C	0.3° C	0.5° C
Transfer Efficiency			
D.O.	0.370	0.373	0.383
Uncertainty	0.027	0.025	0.032
CH_4	0.383	0.294	0.300
Uncertainty	0.065	0.014	0.064
E indexed to D.O. at 20° C			
D.O.	0.526	0.530	0.541
Uncertainty	0.035	0.032	0.036
CH_4	0.589	0.473	0.479
Uncertainty	0.088	0.016	0.078
DEFF, ft.	—	1.77	1.67

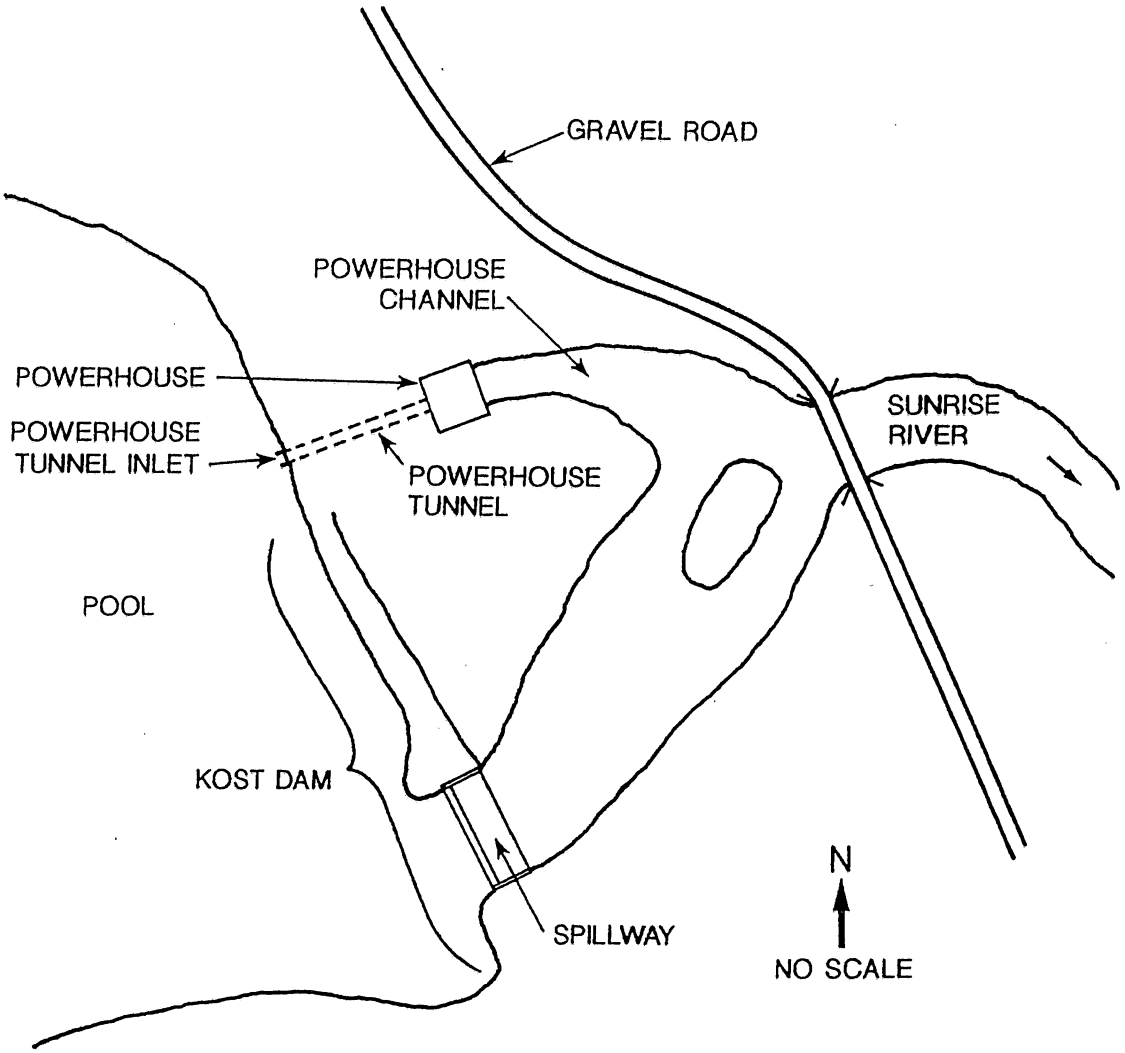

Figure VI–22 Location of Kost Dam

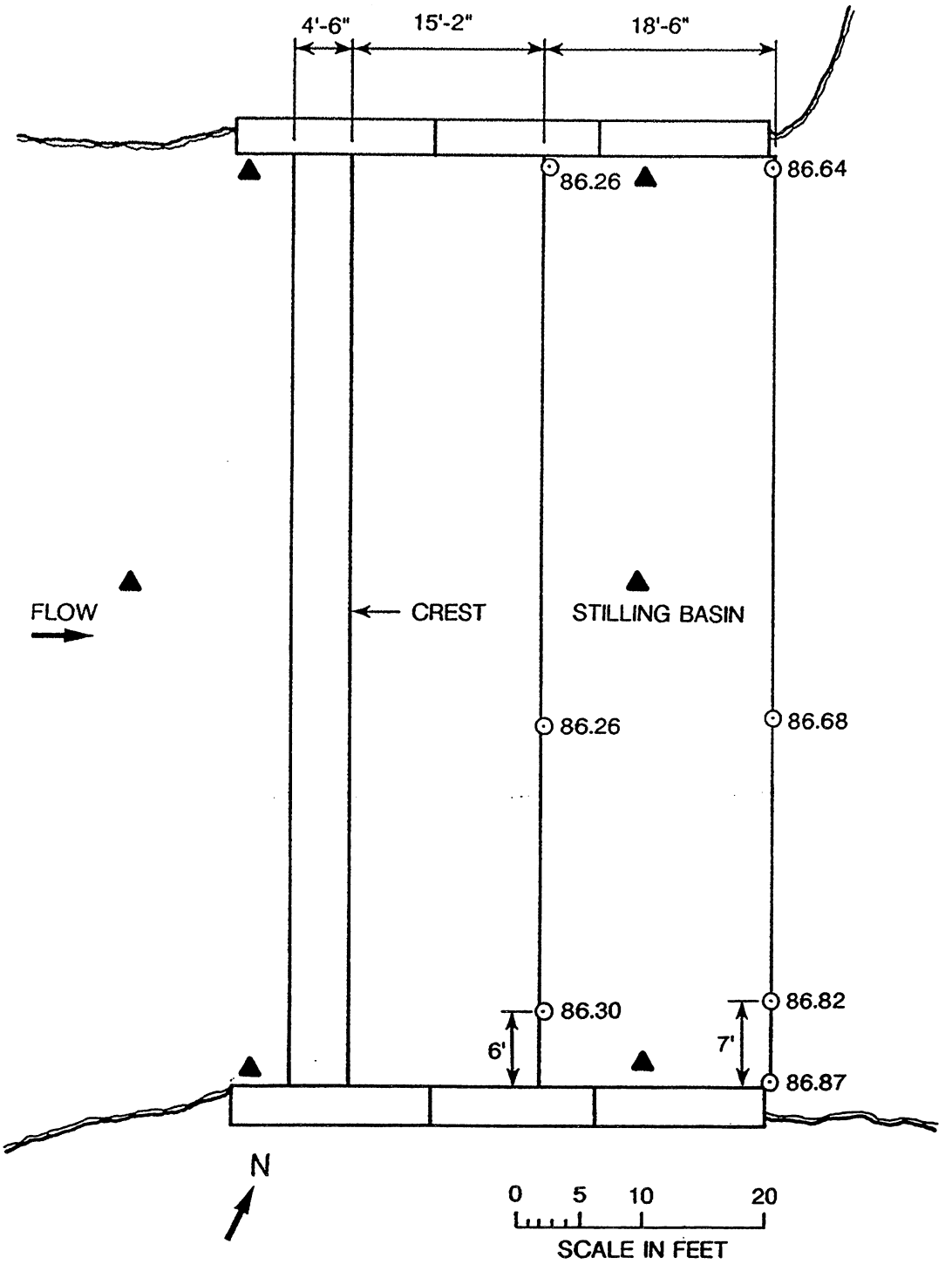

Figure VI–23 Plan view, sampling locations and elevations Kost Dam

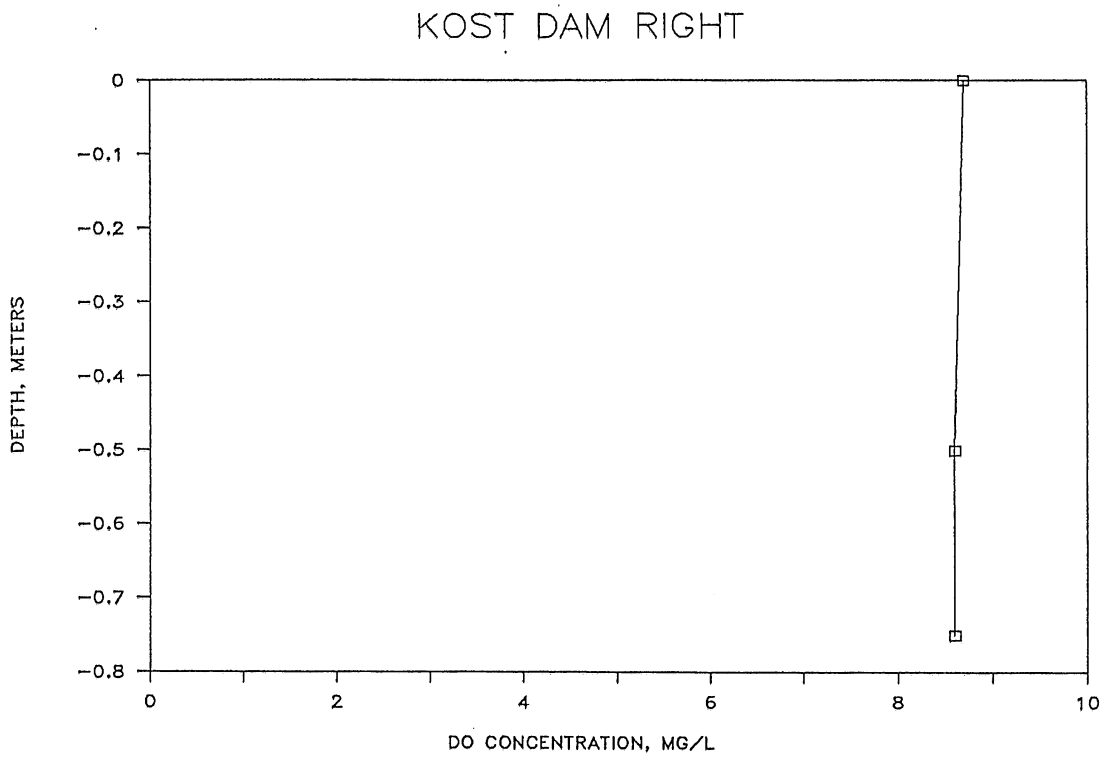

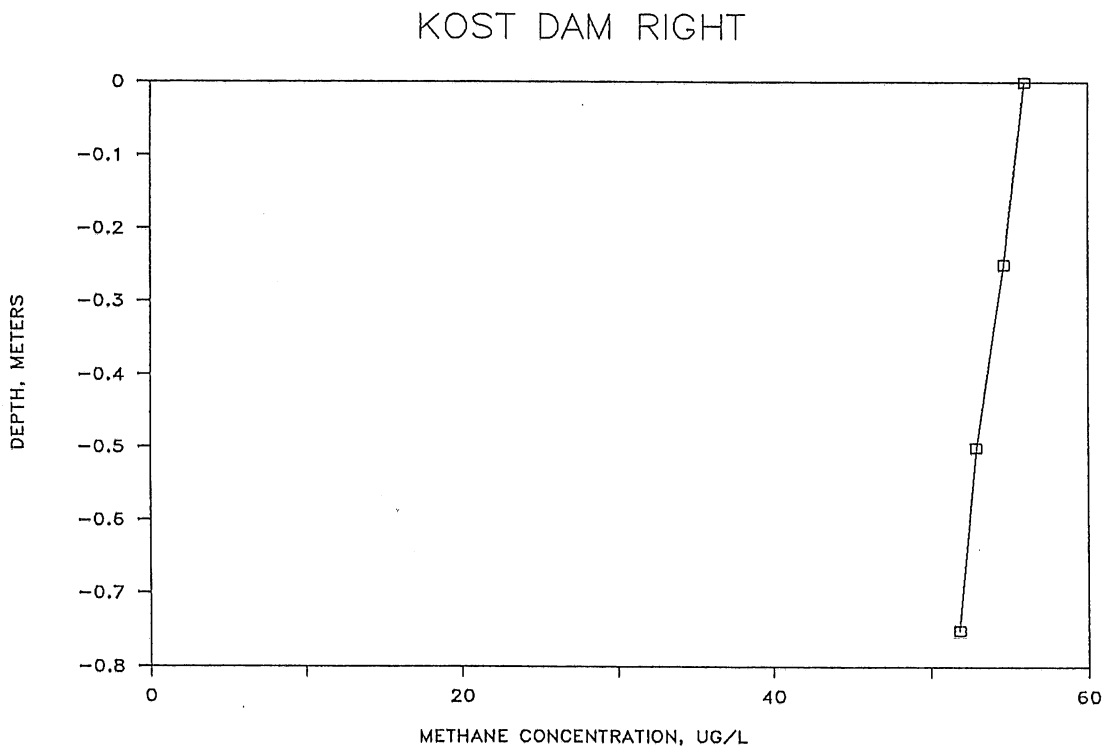

Figure VI–24 D.O. and methane profiles right side

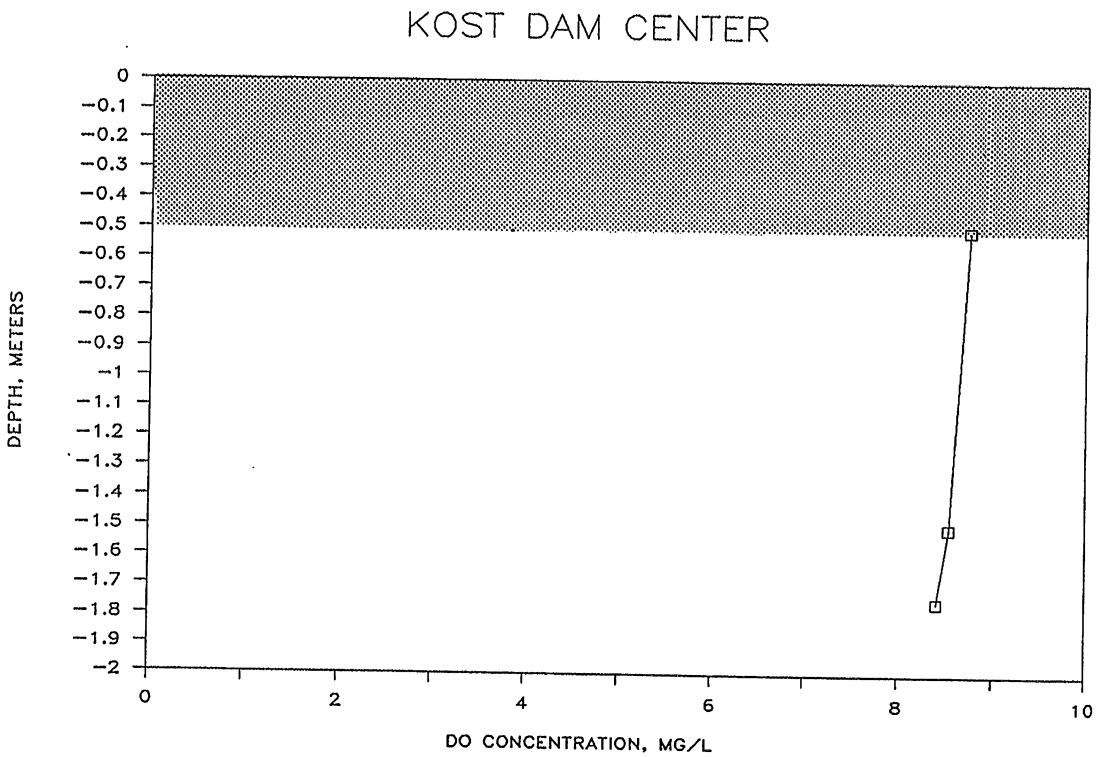

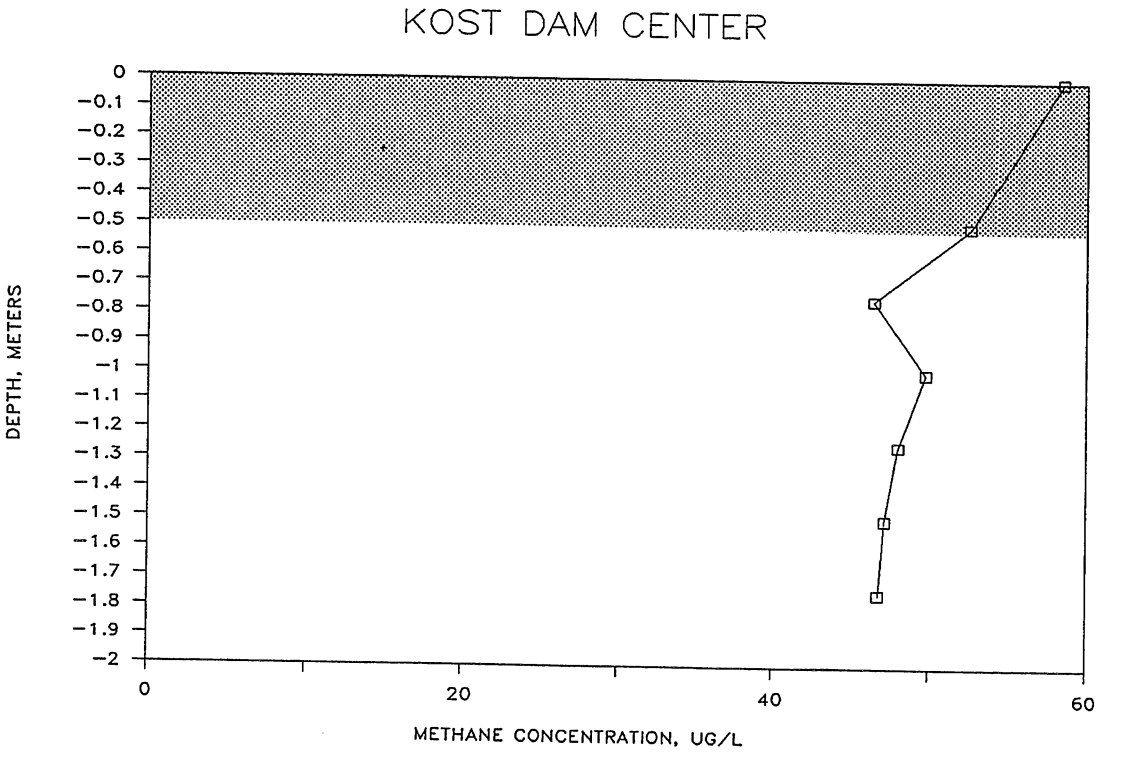

Figure VI–25 D.O. and Methane profiles center

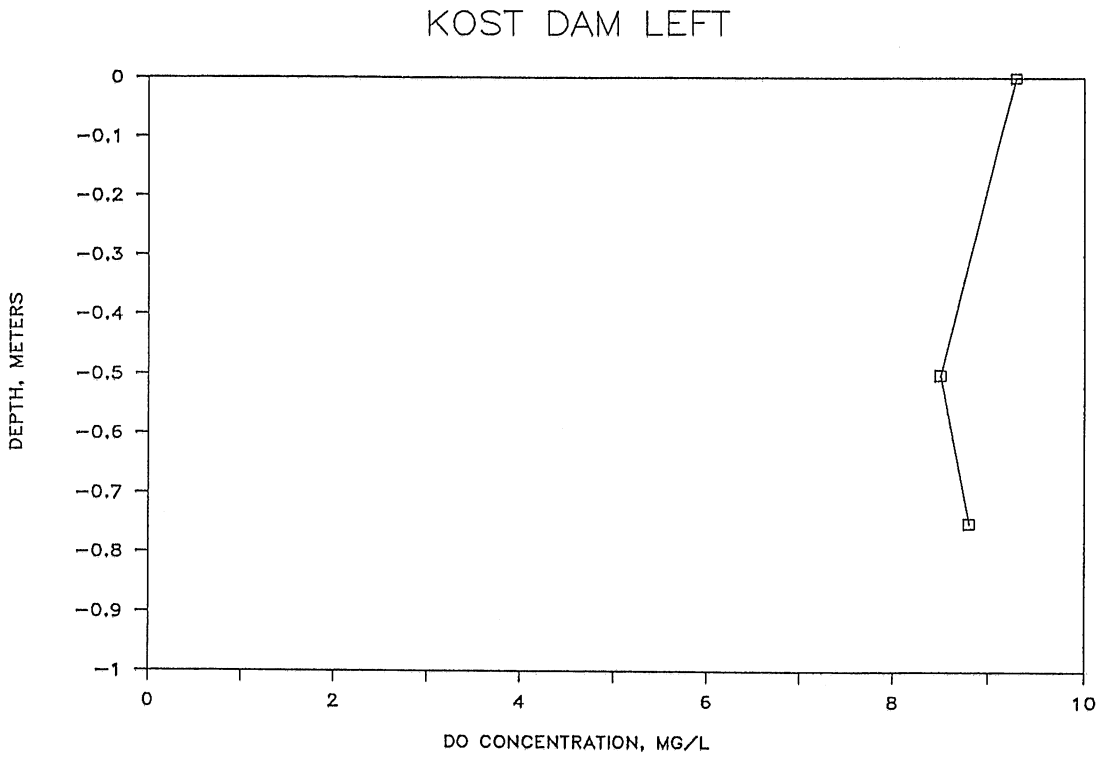

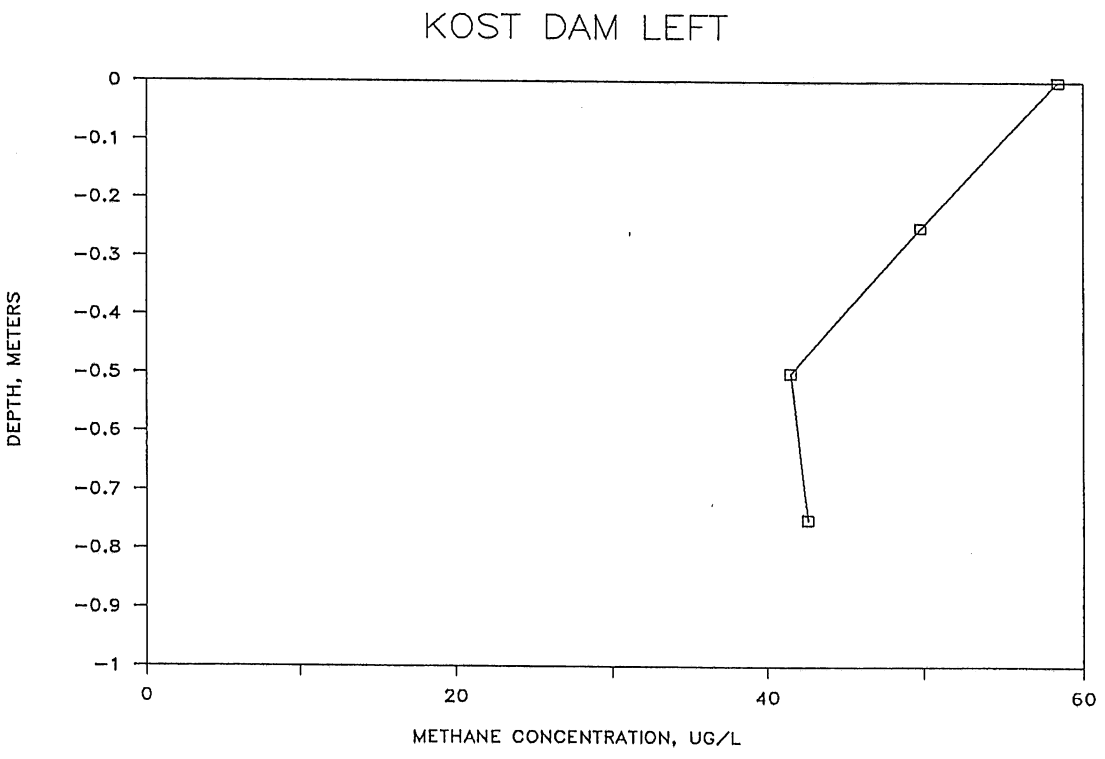

Figure VI–26 D.O. and Methane profiles left side

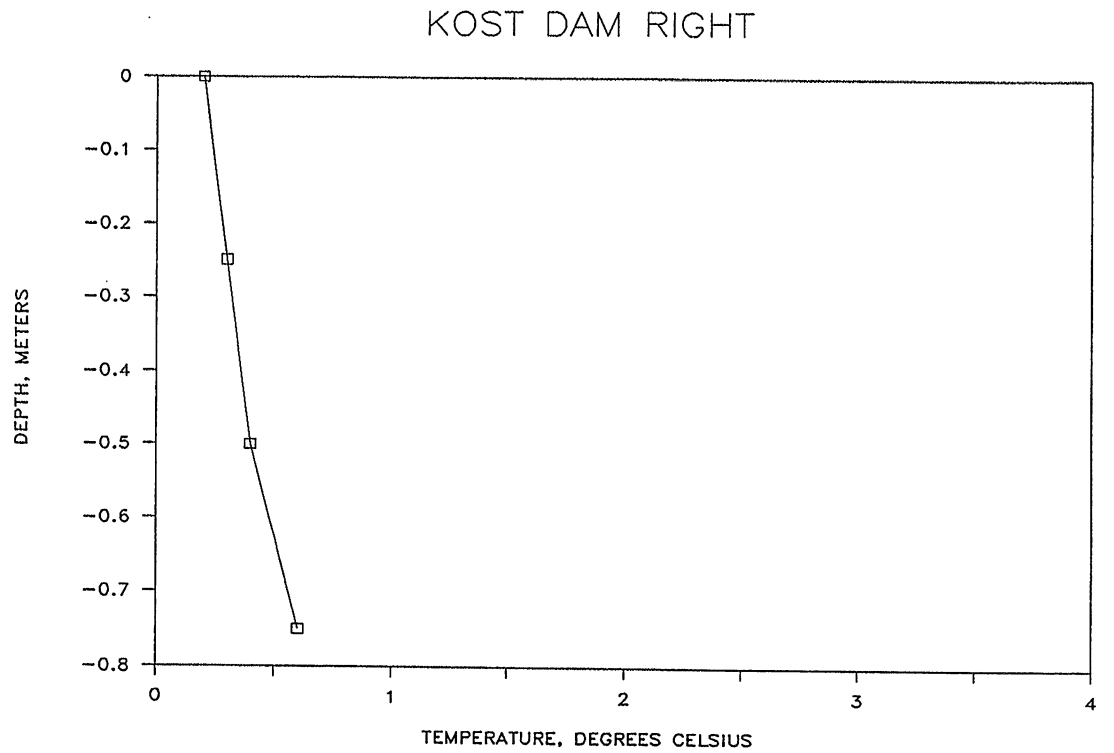

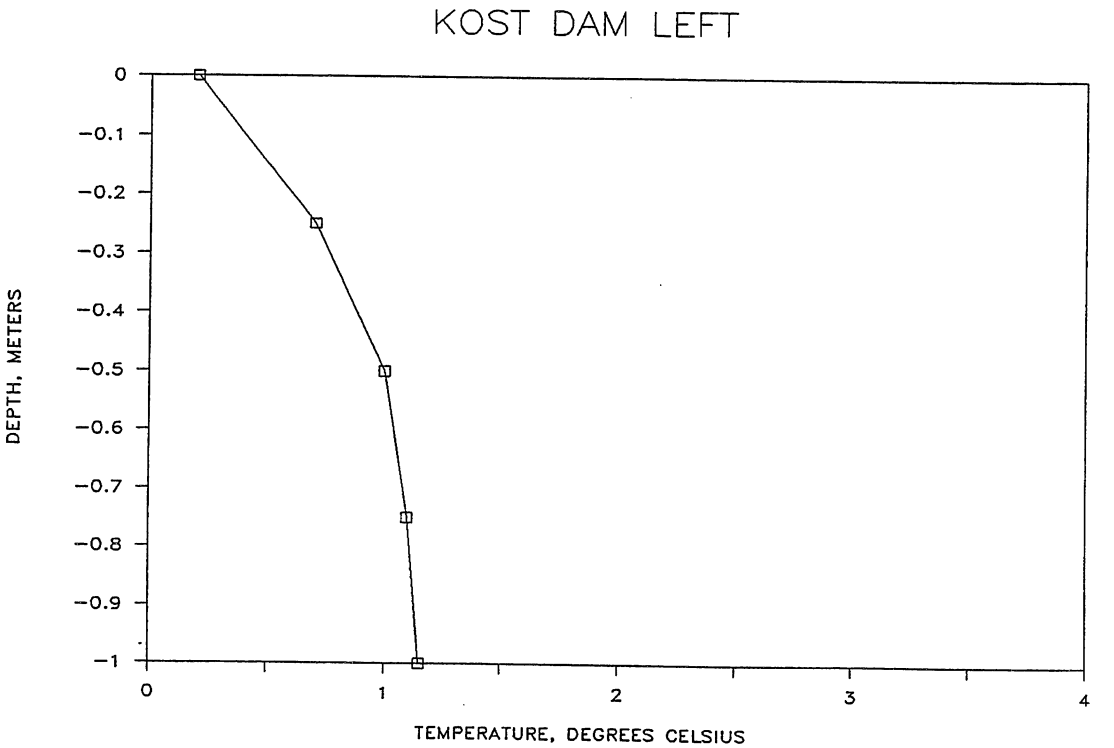

Figure VI–27 Temperature profiles right and left

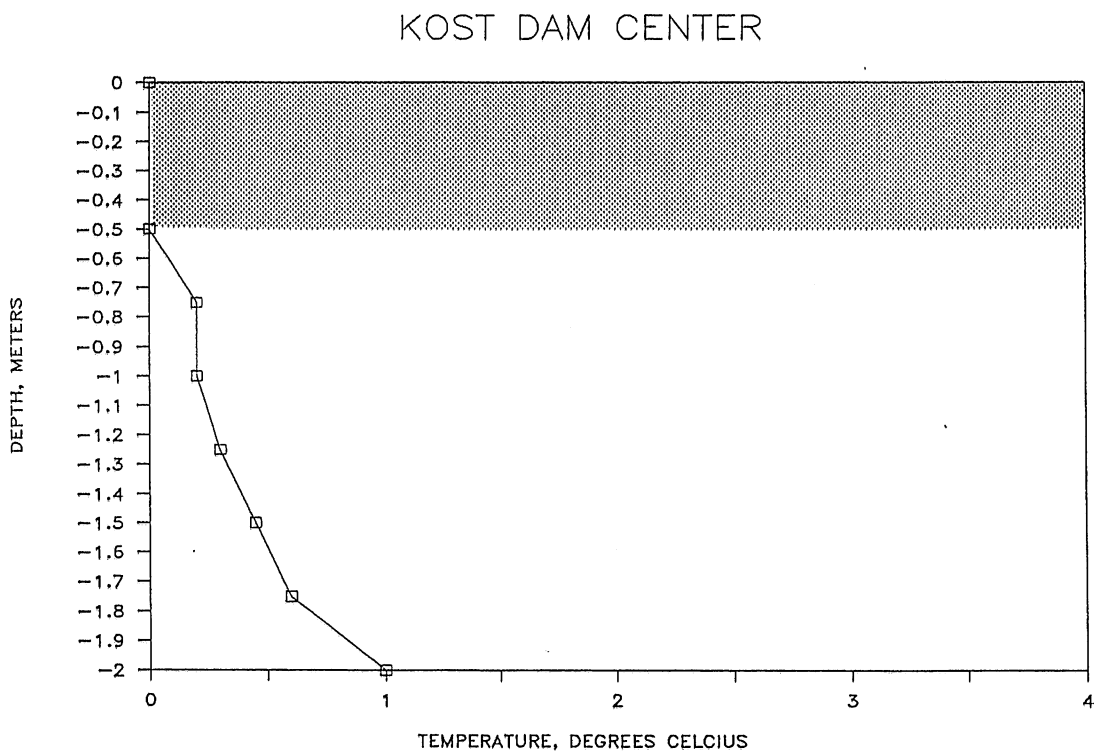

Figure VI–28 Temperature profile center

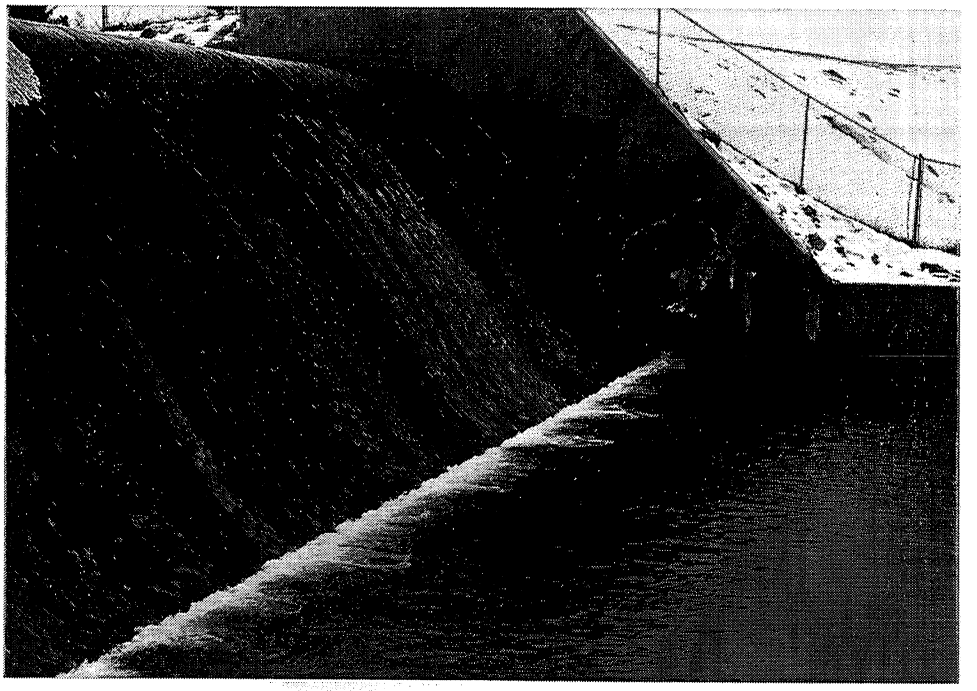

Photo VI–11 Spillway Kost Dam

Photo VI–12 Upstream sampling location

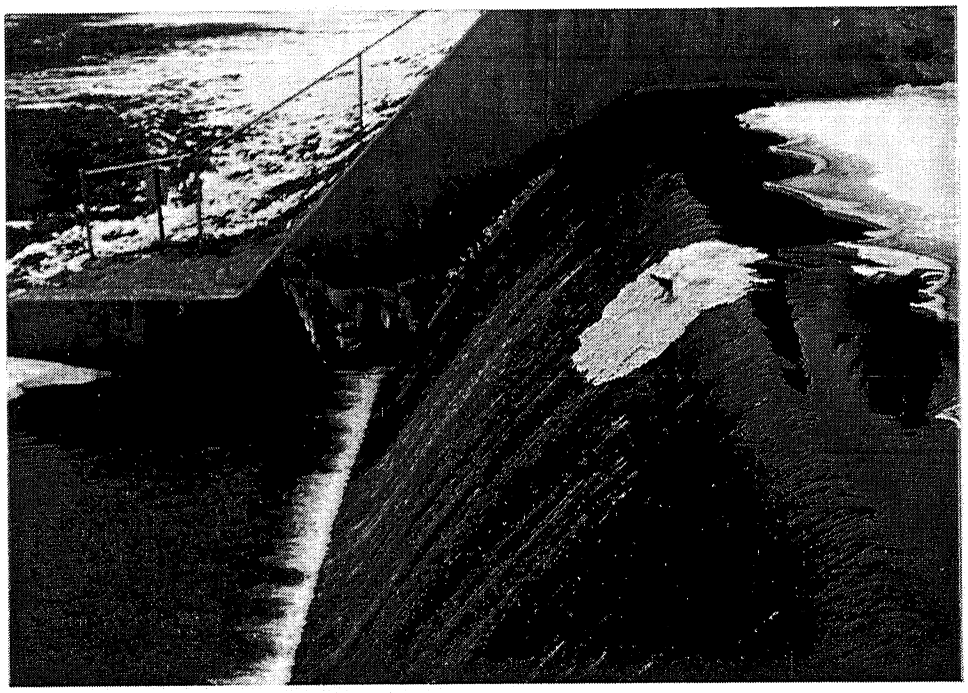

Photo VI–13 Kost Dam

Photo VI–14 Kost Dam

F. Rum River Dam

The Rum River Dam is located in the City of Anoka, approximately 500 ft. upstream from the Main Street bridge. Shown in Figure VI–29, the dam consists of an Ambursen type cross section (ie, hollow) 11.4 ft. high and 236 ft. long with a 20 ft. wide tainter gate spillway on the east bank. This structure is shown in cross section in Figure VI–30. The structure is also shown in Photos VI–15 to VI–20. A hydraulic jump dissipates the excess kinetic energy of the flow at the tainter gate spillway. A free overfall is used for the fixed crest spillway.

This structure was investigated three times, March 22, 1989, February 17, 1990, and March 2, 1990. The first two investigations were performed without opening up the gate, that is, measurements were taken with the gate in one position. Also during the first survey sulfur hexaflouride was also used as a tracer to measure gas transfer. For more information about SF_6 and its use at this structure the reader is referred to McDonald, et al, (1989). During the last investigation the gate was opened and the effect that discharge and tailwater depth have on transfer efficiency and effective depth was investigated.

Results from each of the surveys is given in Table VI–6. During the February 17, 1990 investigation two holes were formed upstream and samples taken at depth to determine if methane and oxygen were stratified similarly to Kost and Elk River. The information plotted in Figures VI–31 and VI–32 shows there is no stratification of methane or D.O. in the reservoir. No temperature profile is plotted as the water was isothermal at 0° C.

During the March 2, 1990 survey, samples were taken upstream before the gate was opened, at the mid–point of the test, and at the end of the test. This was done to see if the upstream concentrations changed during the course of the survey. The upstream concentrations were relatively constant throughout the sampling period.

Also during the March 2, 1990 survey samples were taken on the fixed crest spillway. The results are given in Table VI–7.

Table VI–6 Rum River Dam Results

March 21, 1989		
Upstream Water Surface	841.71	
Downstream Water Surface	831.00	
Tailwater Depth	11.0 ft.	
Discharge	1.7 cfs/ft	
Pressure	741.2 mm Hg	
Saturation Concentration	13.58 mg O_2/l	
Water Temperature	1° C	
	D.O.	CH_4
Upstream	7.41 mg/l	16.25 μg/l
Downstream	11.58 mg/l	8.10 μg/l
Transfer Efficiency	0.686	0.502
Uncertainty	0.034	0.065
E, indexed to D.O. at 20°C	0.834	0.714
Uncertainty	0.028	0.067
DEFF, ft.		2.77
February 17, 1990		
Upstream Water Surface	841.59	
Downstream Water Surface	830.75	
Tailwater Depth	10.75 ft.	
Discharge	1.8 cfs/ft	
Pressure	744.3 mm Hg	
Saturation Concentration	13.86 mg O_2/l	
Water Temperature	0.1° C	
	D.O.	CH_4
Upstream	8.57 mg/l	16.58 μg/l
Downstream	11.97 mg/l	8.72 μg/l
Transfer Efficiency	0.626	0.474
Uncertainty	0.022	0.043
E, indexed to D.O. at 20°C	0.799	0.696
Uncertainty	0.030	0.037
DEFF, ft.		2.72

Table VI–6 Rum River Dam Results (continued)

March 2, 1990
Atmospheric Pressure 738.4 mm Hg
Water Temperature 0.1° C

H, ft	Q, cfs/ft	E,O_2	UE (both indexed to O_2 at 20° C)	E,CH_4	UE	$\frac{C_{se}}{C_s}$	DEFF, ft.	Tailwater Depth, ft.
0.12	1.7	0.840	0.041	0.772	0.018	1.02	1.88	10.5
0.27	3.8	0.799	0.041	0.672	0.017	1.07	3.71	10.75
0.51	7.1	0.732	0.041	0.479	0.018	1.23	9.48	10.95
0.99	13.6	0.686	0.039	0.425	0.020	1.28	9.37	11.25
1.45	19.5	0.620	0.033	0.369	0.019	1.35	10.31	11.5
1.90	24.9	0.589	0.033	0.317	0.019	1.49	12.19	12.1
2.18	27.8	0.436	0.028	0.419	0.020	1.16	0.63	12.15

Table VI–7 Rum River Fixed Weir Results

March 2, 1990
Atmospheric Pressure 738.4 mm Hg
Water Temperature 0.1° C
Saturation Concentration 13.86 mg O_2/l

	Spillway 1	Spillway 2
Tailwater Depth	2.0 ft.	1.0 ft.
Upstream		
D.O.	8.05 mg/l	11.63 mg/l
CH_4	15.13 μg/l	7.66 μg/l
Downstream		
D.O.	11.63 mg/l	12.00 mg/l
CH_4	7.66 μg/l	7.30 μg/l
Transfer Efficiency		
D.O.	0.616	0.166
Uncertainty	0.079	0.110
Transfer Efficiencies, indexed to O_2 at 20° C		
E,O_2	0.790	0.256
Uncertainty	0.089	0.123
E,CH_4	0.819	0.063
Uncertainty	0.045	0.224
DEFF, ft.	——	13.8

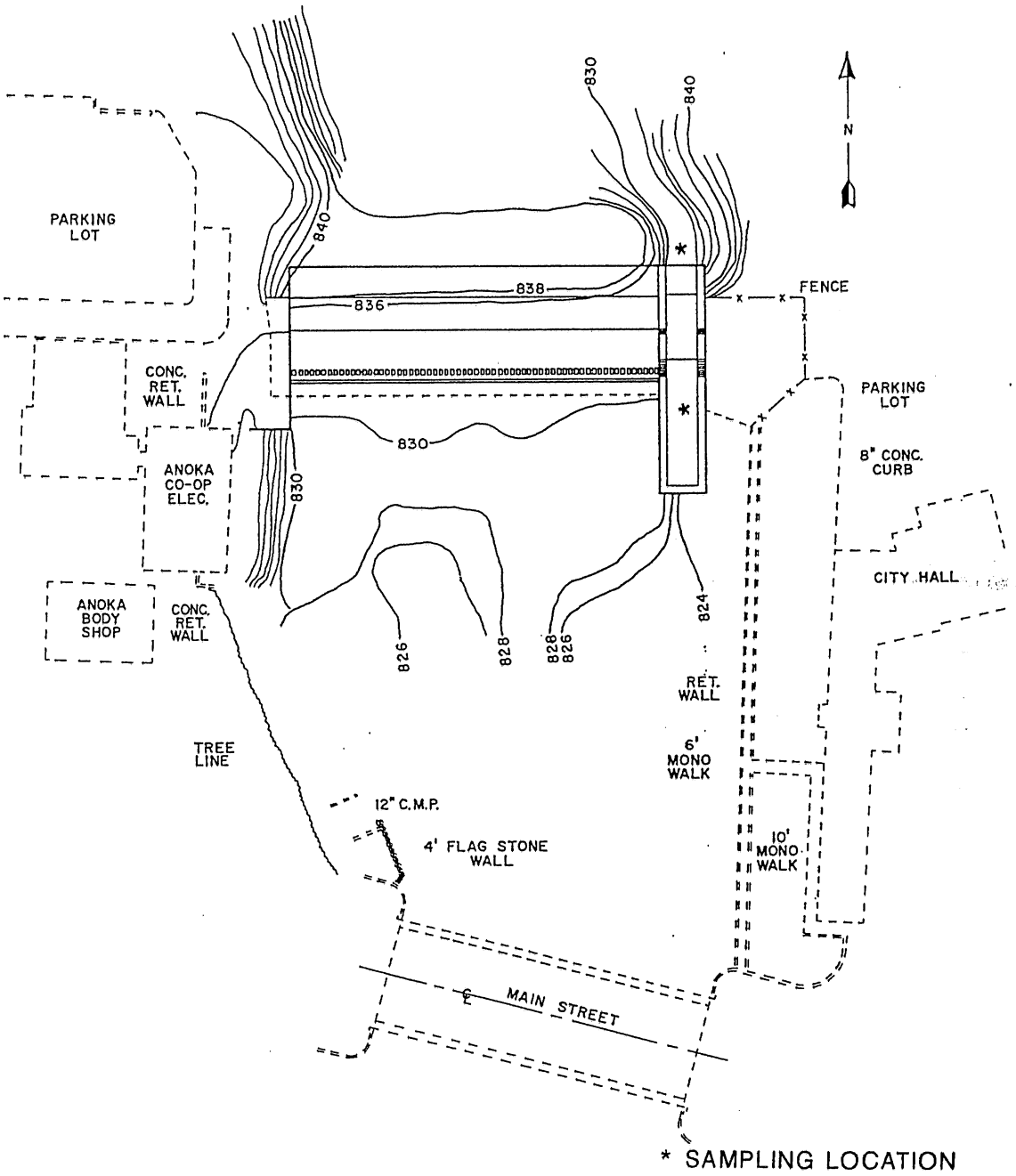

Figure VI–29 Plan view of Rum River Dam at Anoka

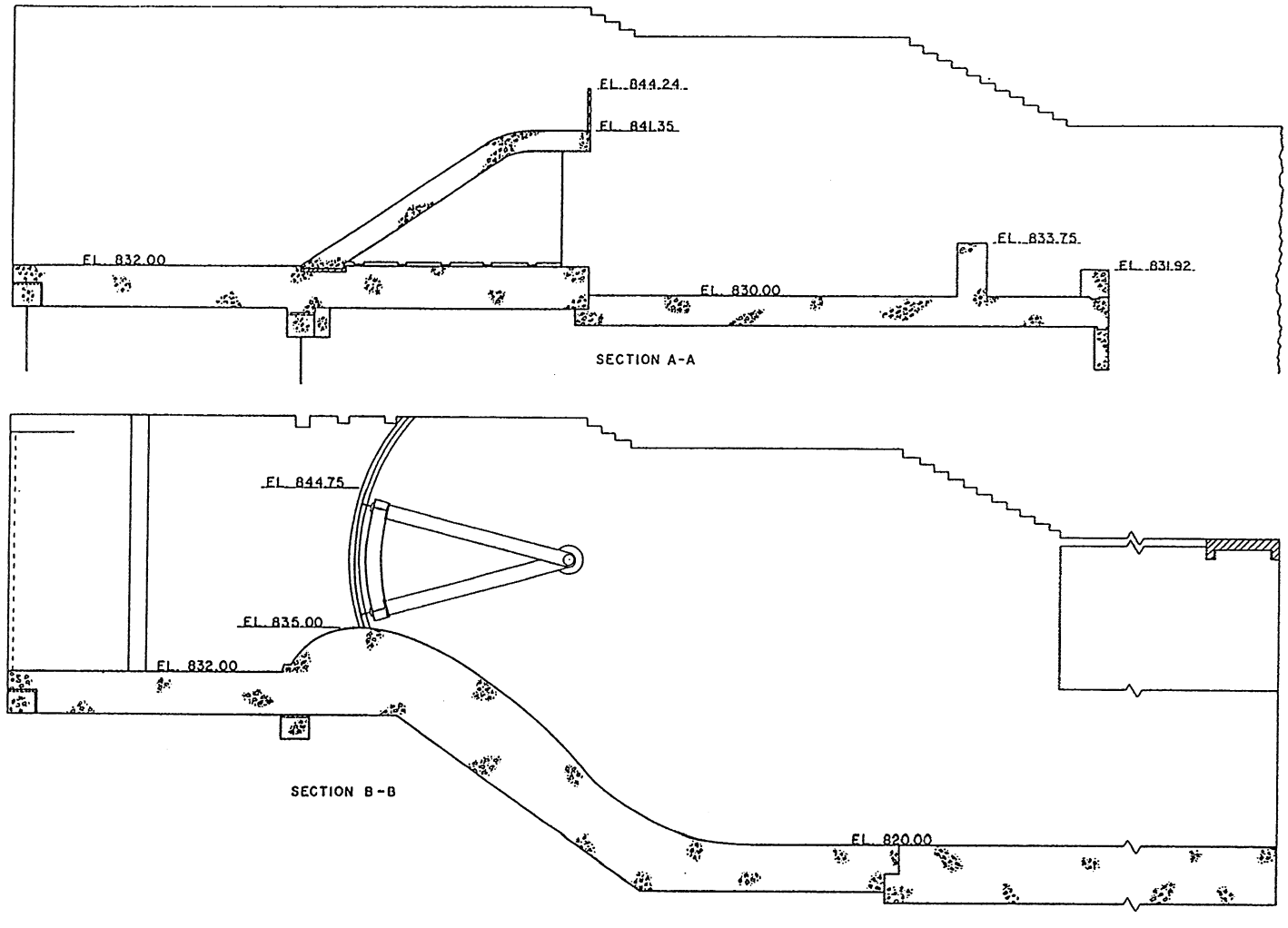

Figure VI–30 Section through tainter gate spillway

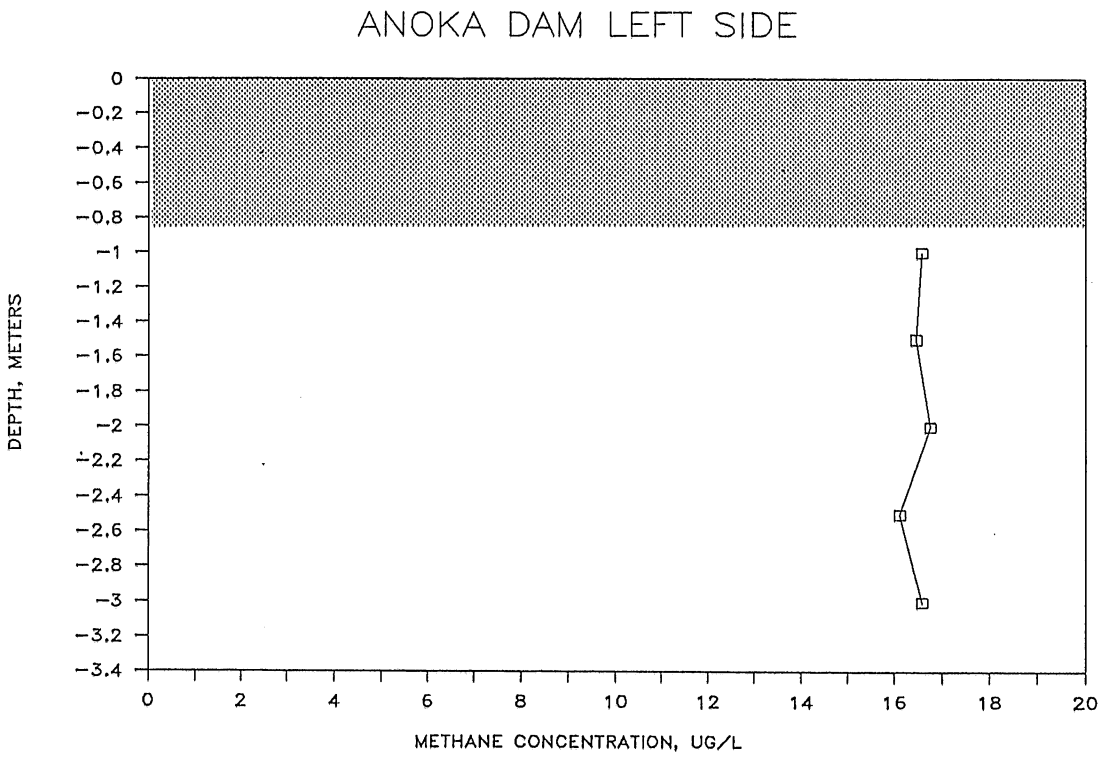

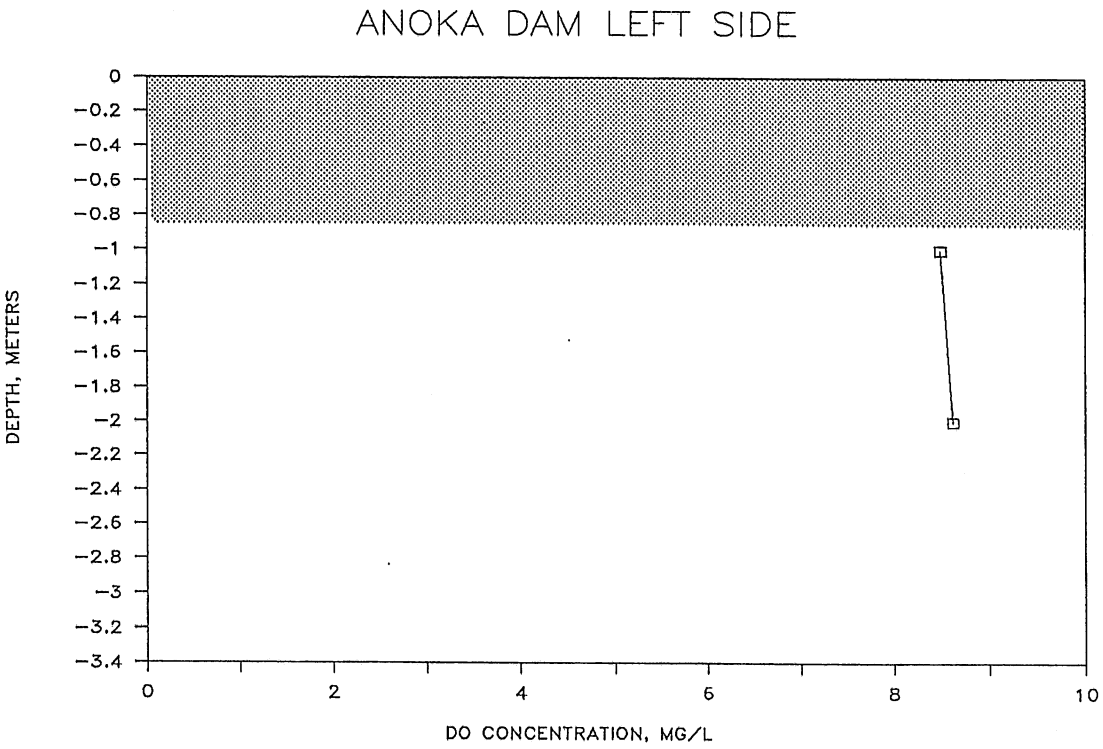

Figure VI–31 Methane and D.O. profiles at Rum River Dam, February 17, 1990

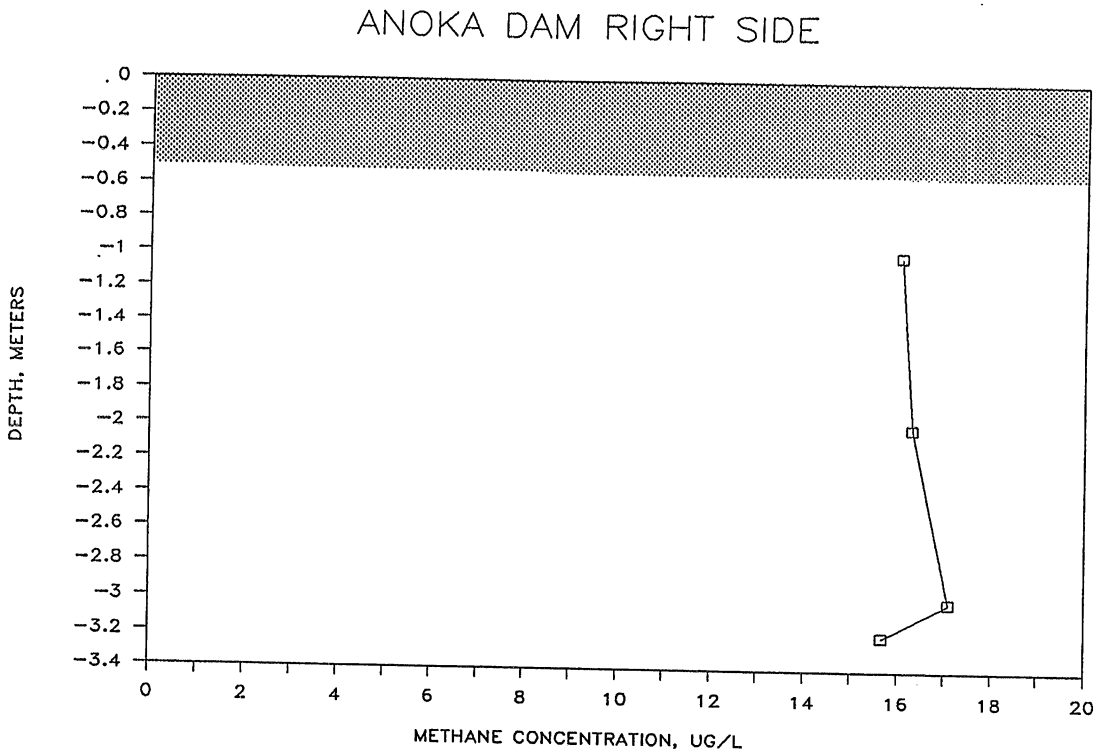

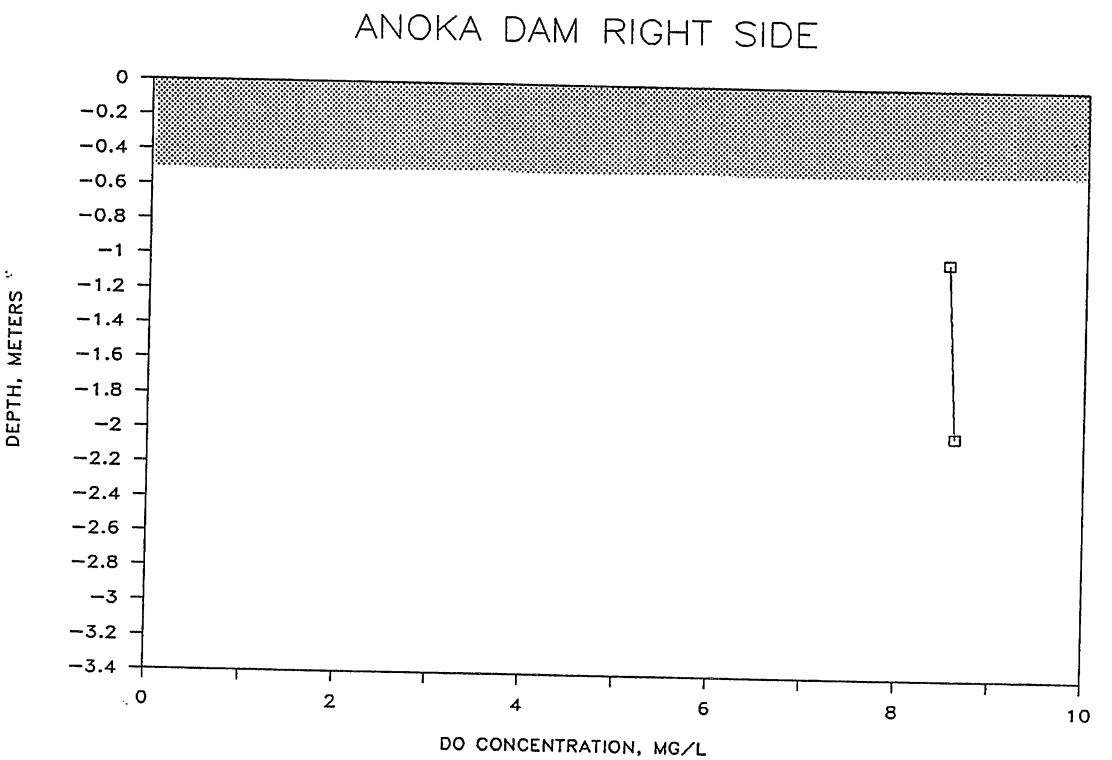

Figure VI–32 Methane and D.O. profiles at Rum River Dam, February 17, 1990

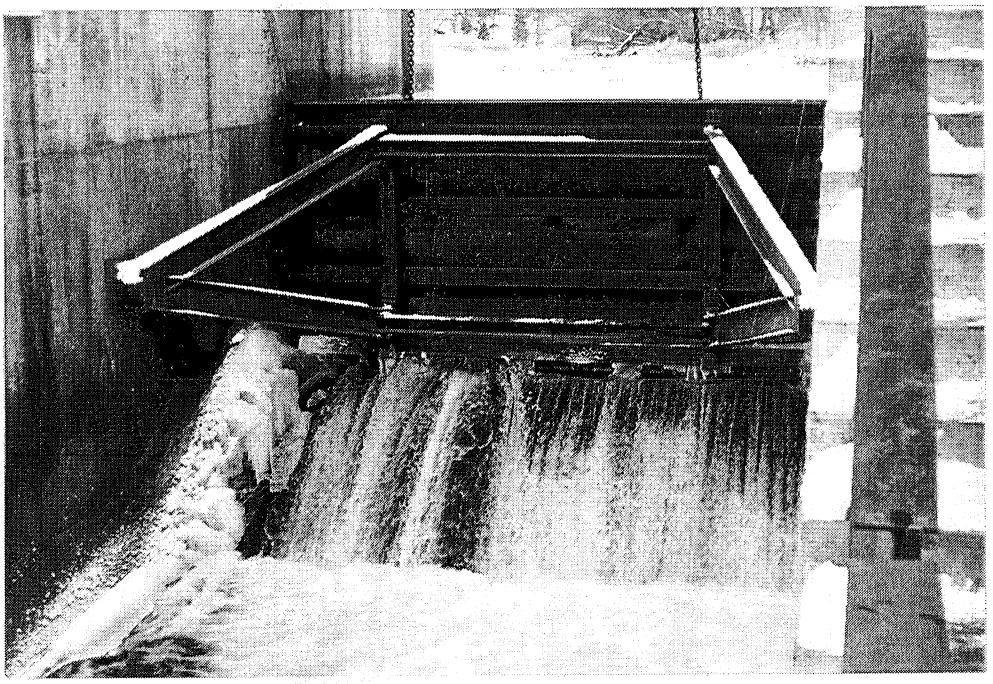

Photo VI–15 Rum River Gated Control Structure in closed position.

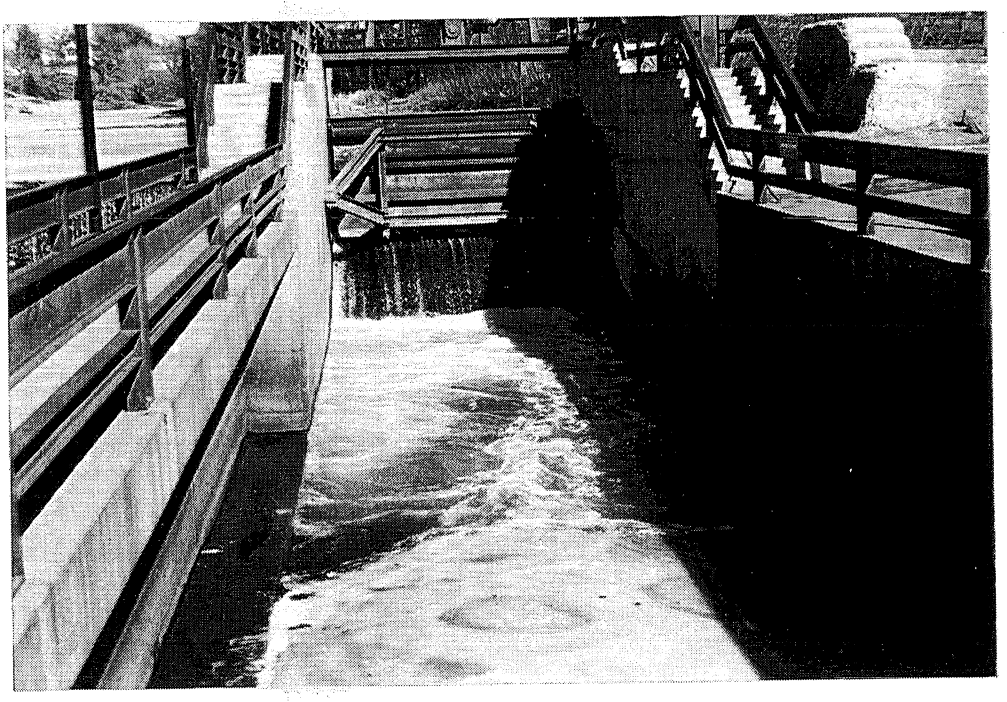

Photo VI–16 Gate open 12".

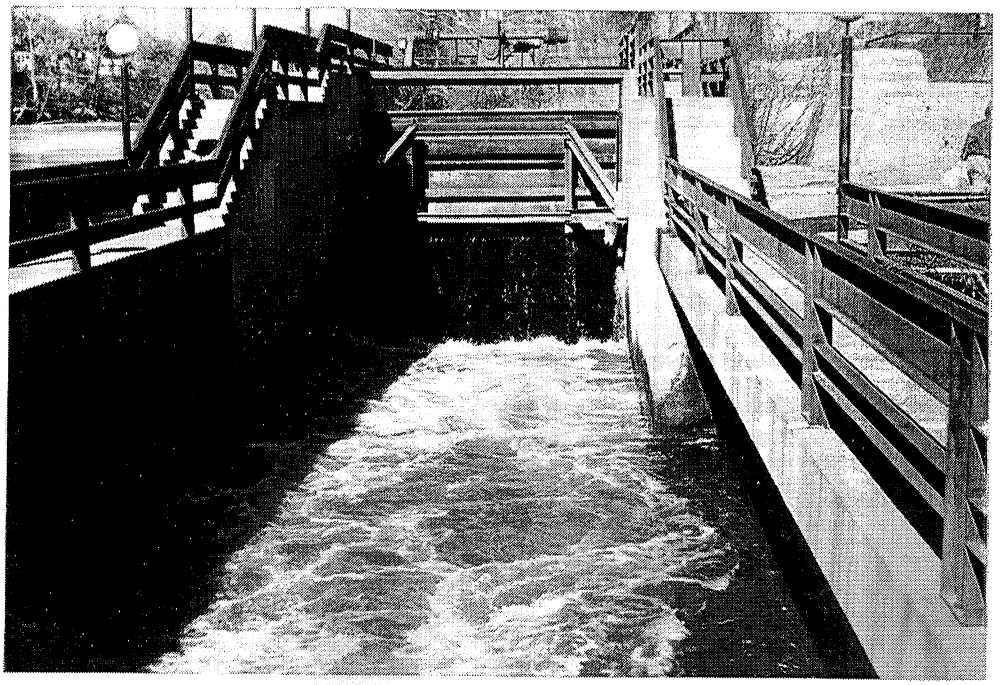

Photo VI–17 Gate open 30".

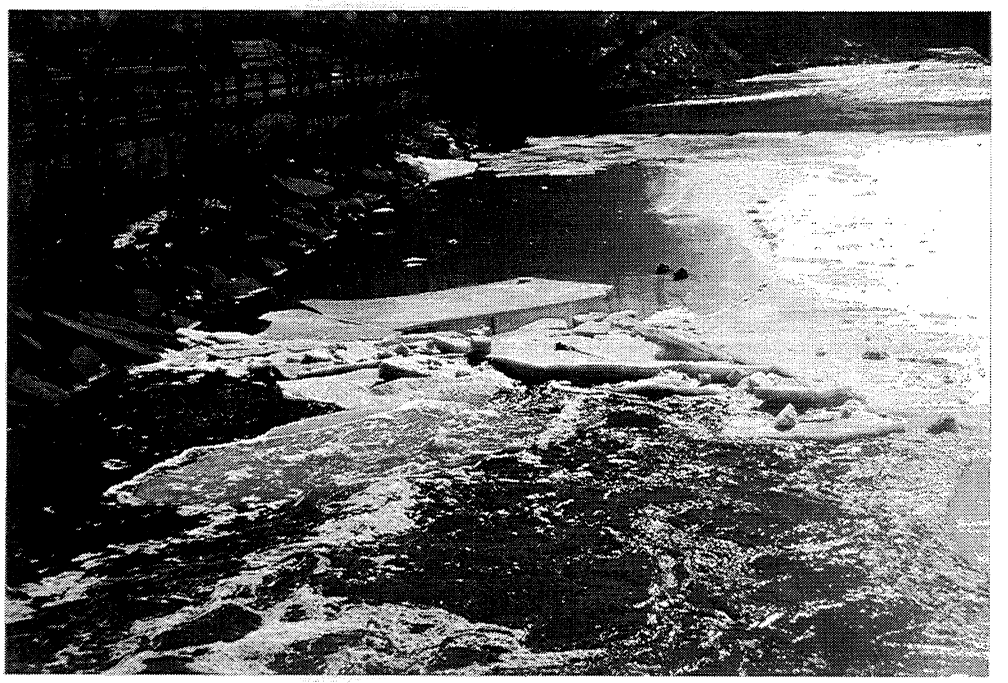

Photo VI–18 Downstream of structure.

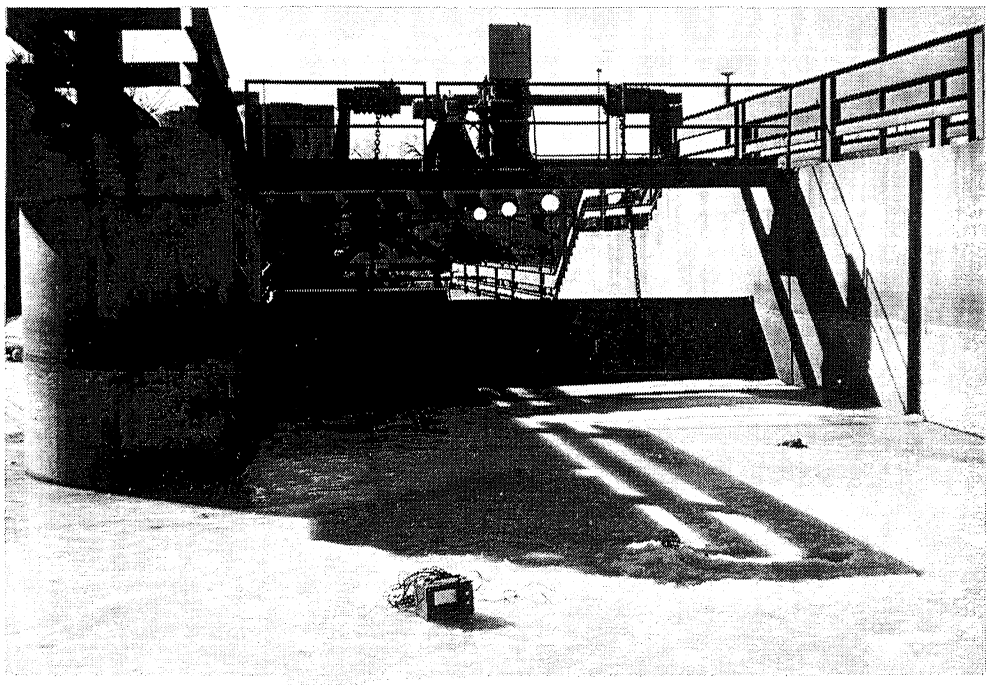

Photo VI–19 Upstream sampling location.

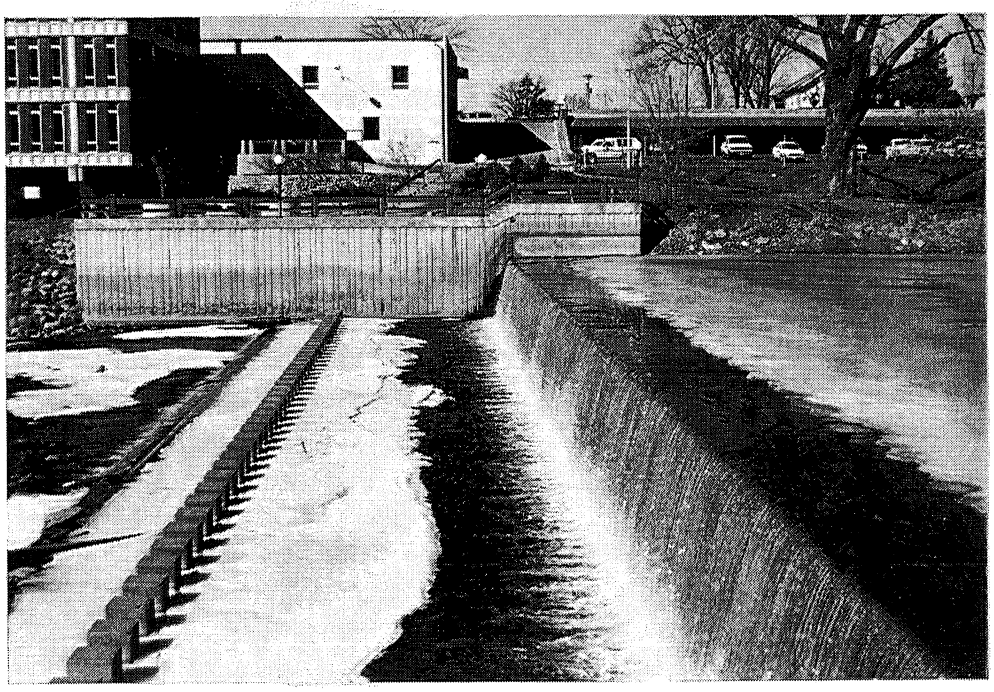

Photo VI–20 Fixed weir at Rum River Dam.

G. St. Cloud Dam

The St. Cloud Dam is located on the Mississippi River within the City of St. Cloud approximately 500 ft. downstream of the 10th Street Bridge. The dam consists of a concrete fixed crest embankment approximately 19.5 ft. high and 500 ft. long. On the left bank a concrete wall and earth embankment extends from the spillway a distance of 200 ft. to high ground. The dam was retrofitted with a hydropower facility on the west bank in 1988. The spillway and hydropower facility are shown in plan view in Figure VI–33.

The structure of interest is the gated spillway associated with the hydropower facility. Samples were taken on March 15, 1990. Samples were gathered upstream at the location shown in Figure VI–33. The gate was then opened to various levels and samples taken downstream. Upstream samples were taken at half–way through the survey and at the end of the sampling period to provide a check on the consistency of the upstream concentrations. The upstream concentrations did not change as evidenced by the profiles shown in Figures VI–34 and VI–35. The results are shown in Table VI–8.

Table VI–8 St. Cloud Results

March 15, 1990
Pressure 724.05 mm Hg
Water Temperature 0.0° C
Saturation Concentration 13.63 mg O_2/l
Upstream Water Surface Elev. 981.7 ft.
Dissolved gas concentrations:

H,ft.	Upstream D.O., mg/l	CH_4,μg/l	Downstream D.O.,mg/l	CH_4,μg/l
0.1	10.05	7.95	11.84	4.20
0.2	10.06	7.95	11.67	4.00
0.4	10.07	7.95	12.08	3.30
0.8	10.09	7.66	12.45	4.14
1.3	10.11	7.66	12.28	4.97
1.8	10.13	7.66	10.67	7.35
2.2	10.15	7.66	10.79	5.21

H,ft	Q, cfs/ft ft.	E,O_2	UE	E,CH_4 (both indexed to O_2 at 20°C)	UE	$\frac{C_{se}}{C_s}$	EFF, ft.	Tailwater Depth, ft.
0.1	1.65	0.678	0.104	0.693	0.035	0.94	—	18.7
0.2	3.35	0.625	0.082	0.720	0.050	0.96	—	18.7
0.4	6.77	0.743	0.089	0.805	0.064	0.97	—	18.9
0.8	13.67	0.834	0.106	0.681	0.080	1.12	3.99	19.0
1.3	22.49	0.791	0.130	0.552	0.100	1.20	6.62	19.0
1.8	31.50	0.240	0.174	0.074	0.131	1.73	24.88	19.0
2.2	38.87	0.283	0.135	0.088	0.119	1.79	24.41	19.0

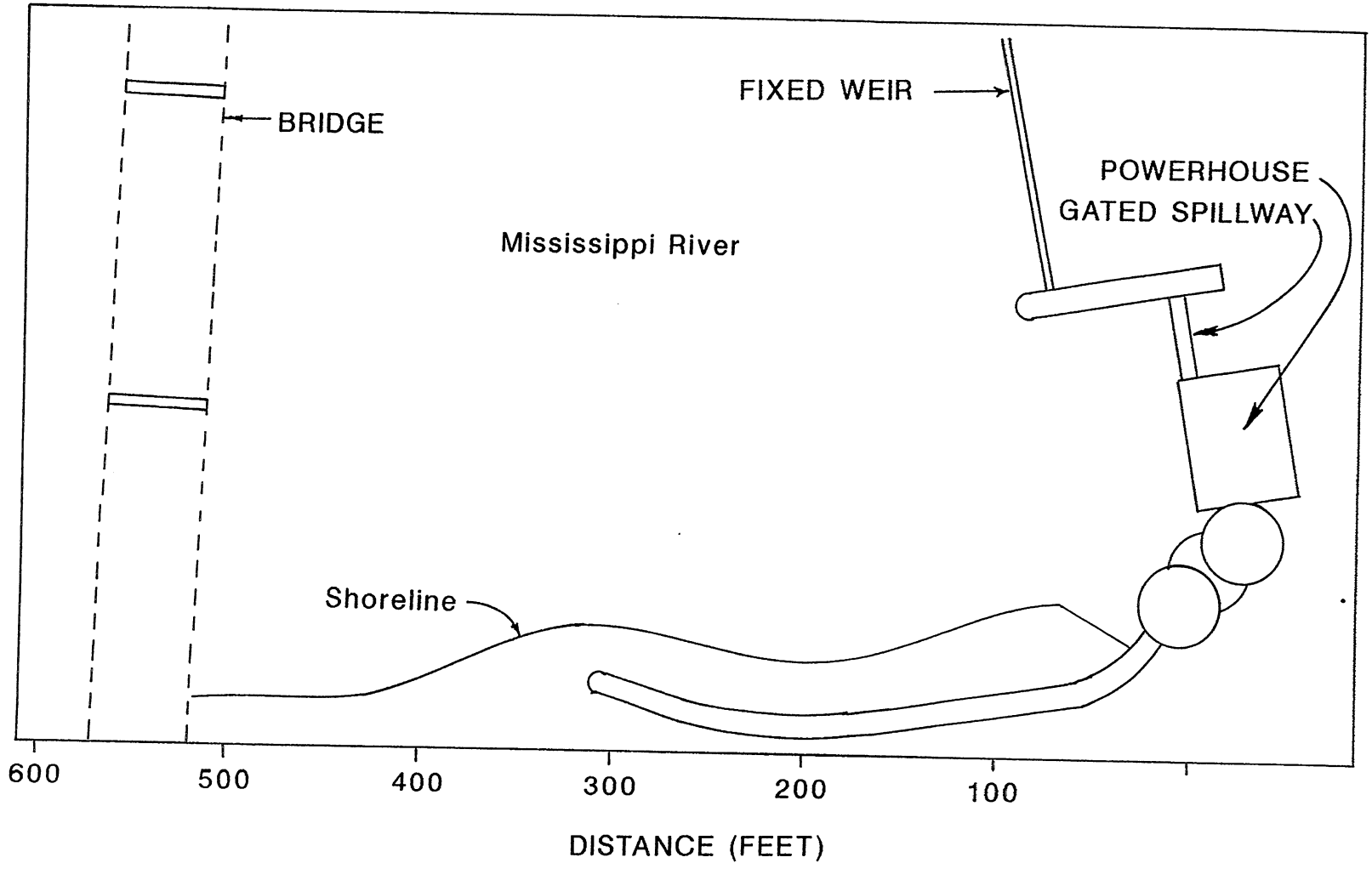

FIGURE VI-33 St. Cloud Dam Plan View

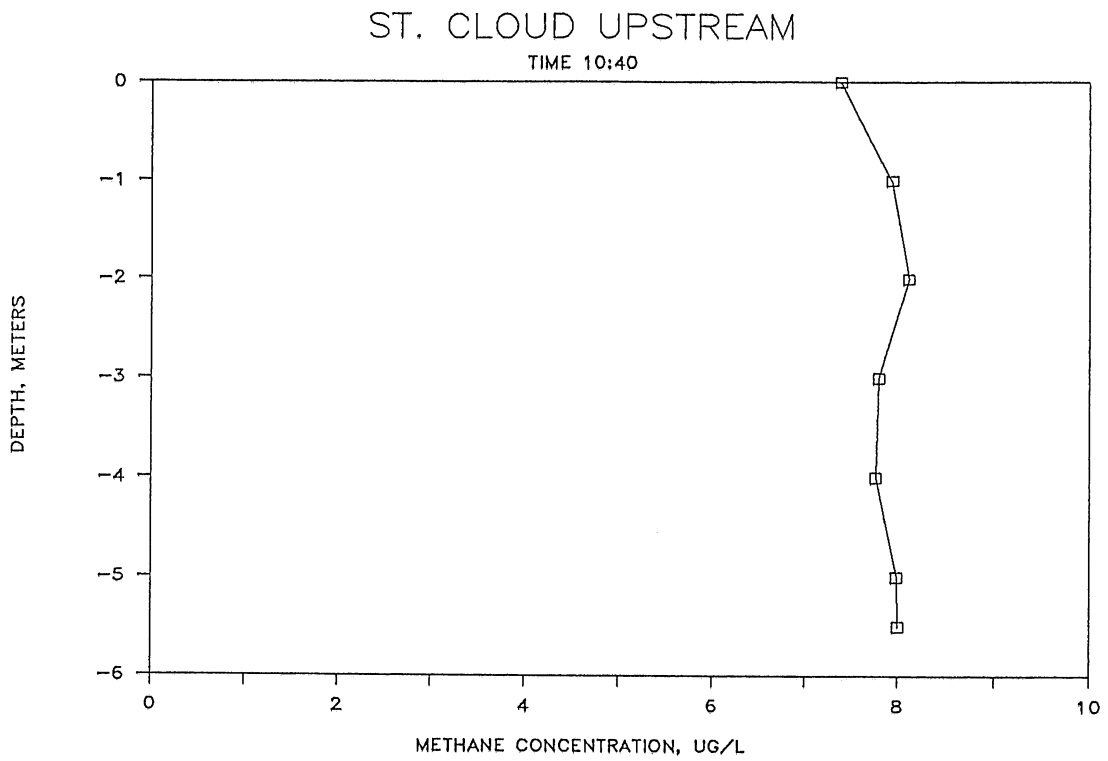

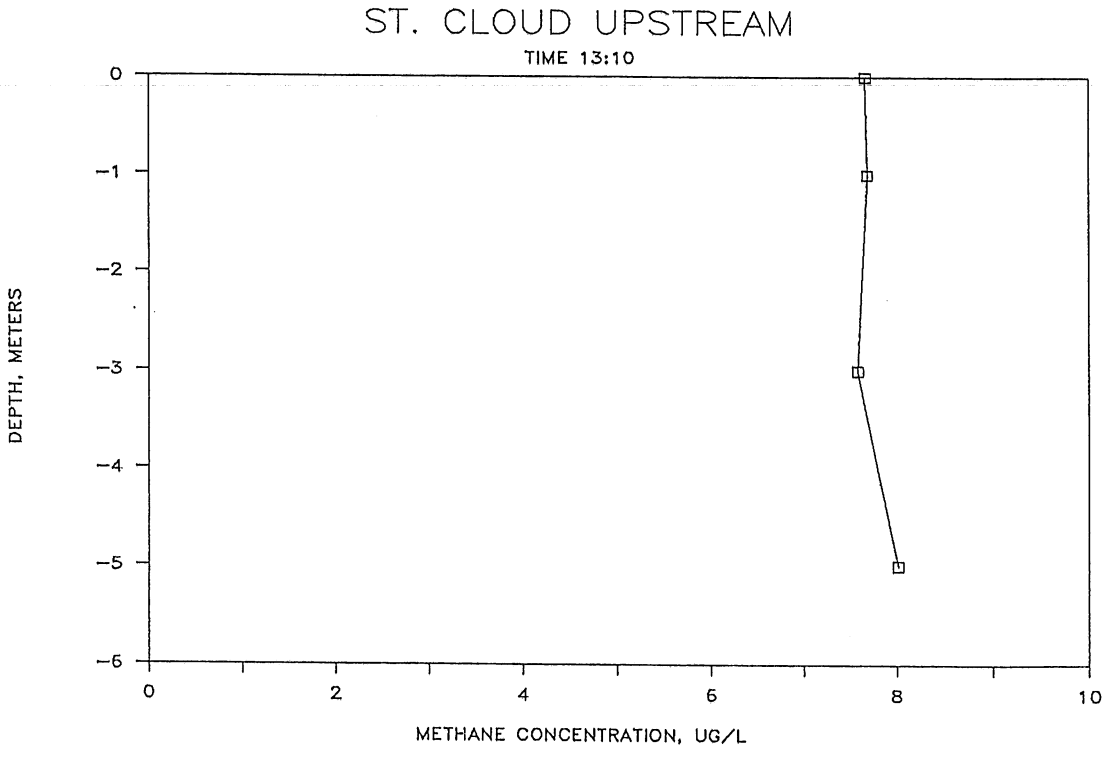

Figure VI–34 Methane concentrations

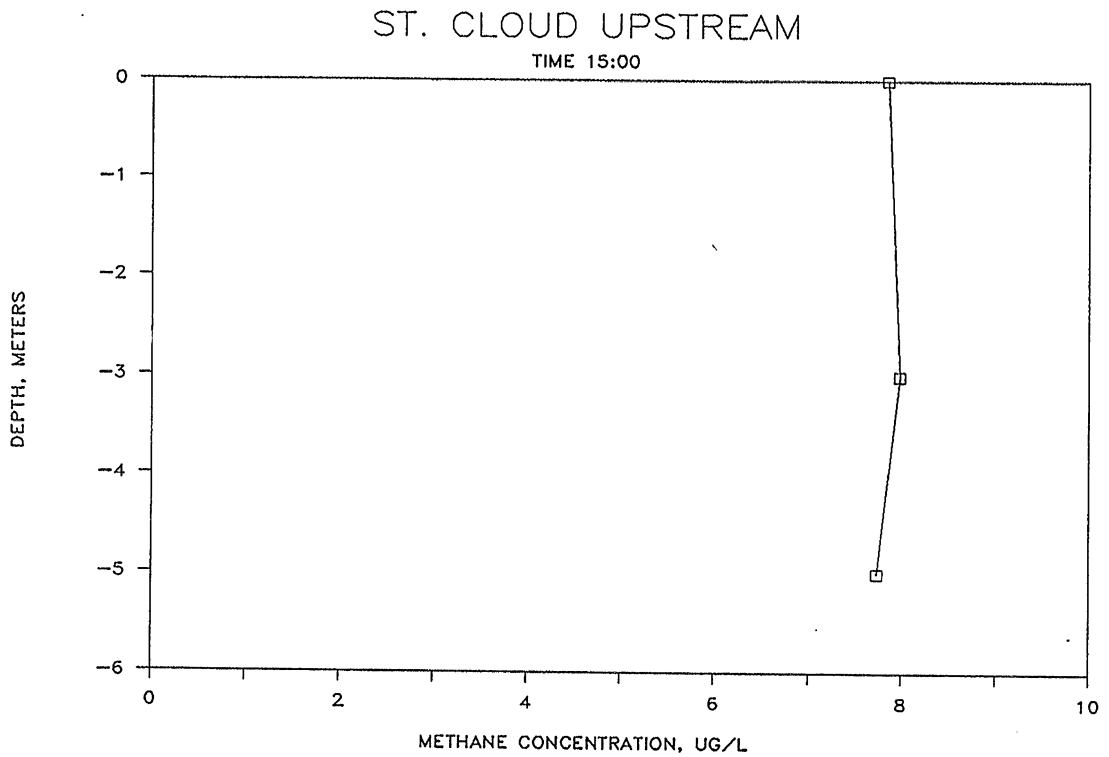

Figure VI–35 Methane concentrations

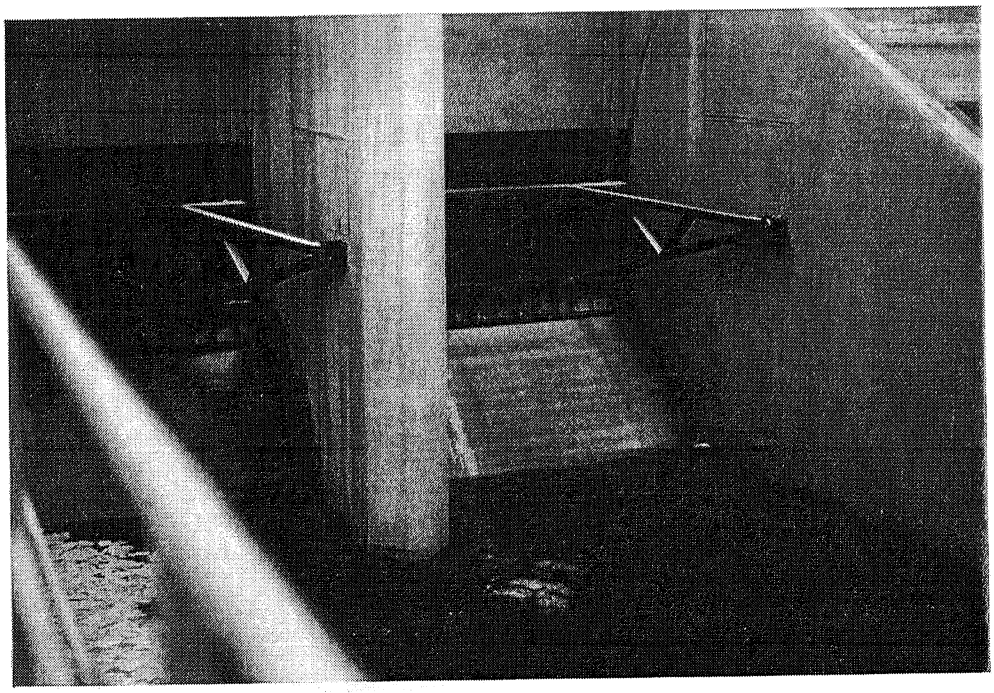

Photo VI–21 Gated Spillway.

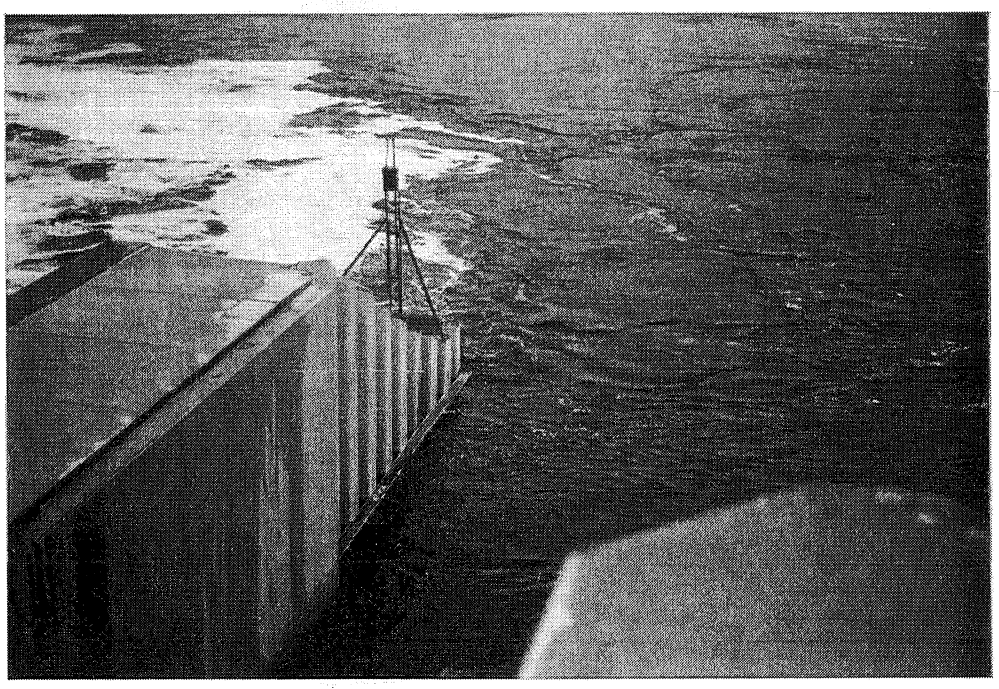

Photo VI–22 Downstream sampling location.

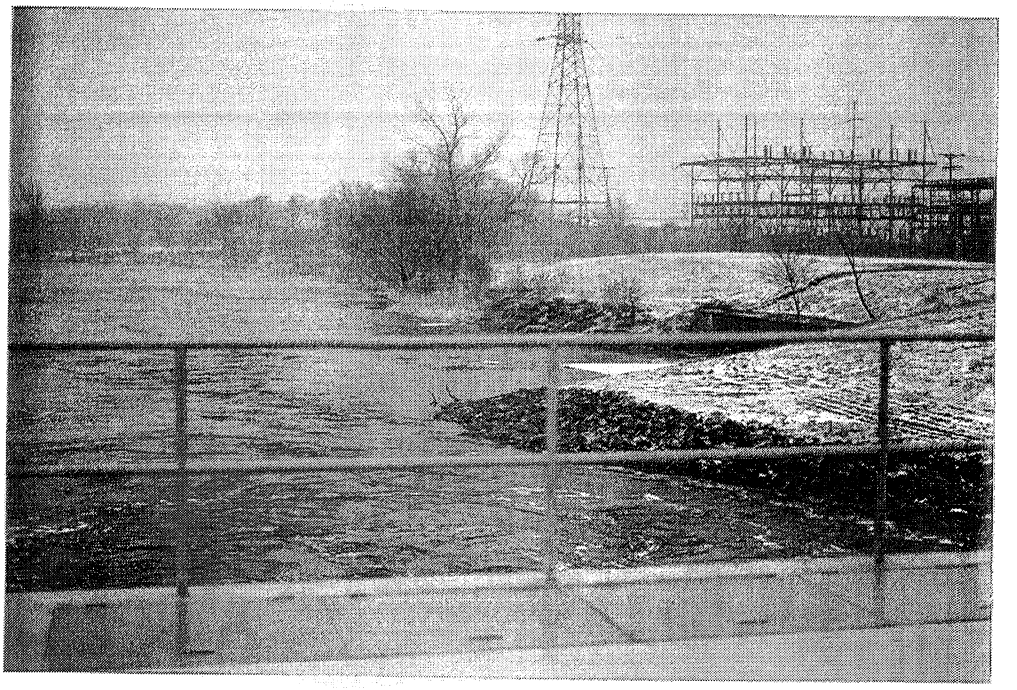

Photo VI–23 View looking downstream.

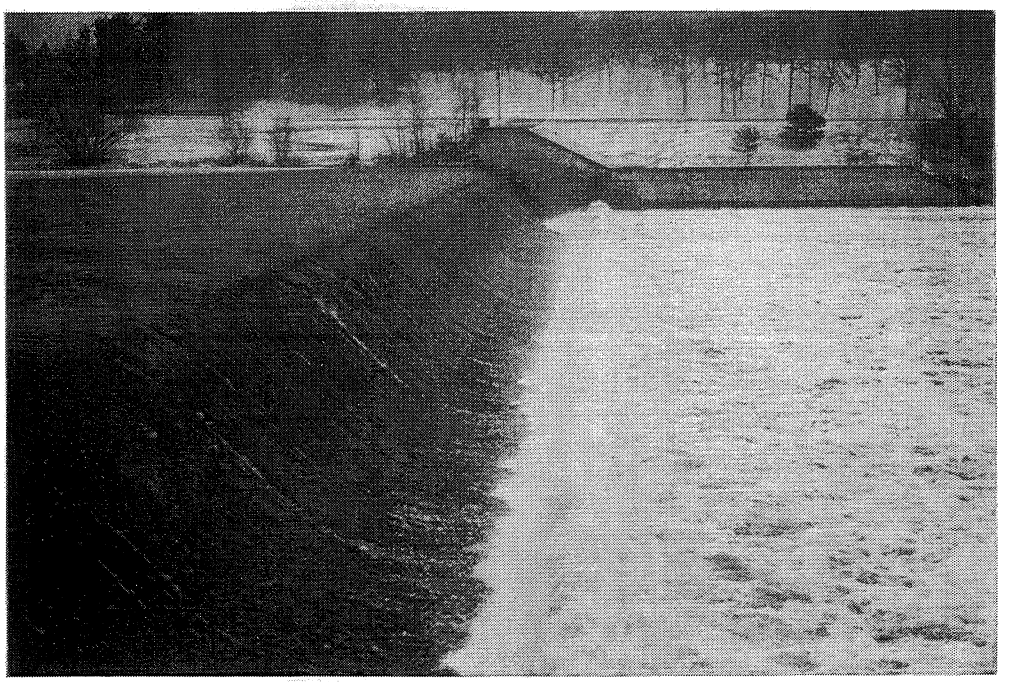

Photo VI–24 Fixed Weir.

VII. RESULTS

The technique used to measure methane concentrations works well. It is easy to perform, doesn't require extensive equipment in the field or in the laboratory, and provides accurate results.

Methane concentrations varied from reservoir to reservoir. De Angelis and Lilley (1989) had similar observations in their survey of methane levels in Oregon rivers and estuaries. They concluded (and I agree) the methane concentration at any point in a river system will be a complex function of many factors including hydrology, drainage basin morphology and vegetation, microbial oxidation and reaeration. The only tool in predicting methane concentrations is sulfate. High sulfate levels indicate low methane concentrations and vice versa.

At all locations methane was supersaturated. This also agrees with results from de Angelis and Lilley. It would seem the bacterial oxidation of methane and methane evasion rates (ie, the pathways by which methane escapes from the water column) are inadequate to remove all the methane from these rivers/reservoirs.

At some sites, under ice cover methane was found at much larger concentrations just under the ice than near the sediments. This may be due to methane bubbles rising from the sediments but, instead of evading to the atmosphere, ice blocks the way thus leaving the water just under the ice at a higher methane concentration. Another thought is that perhaps the ice itself contains a high amount of methane and as it melts the water in contact with the ice will also have a correspondingly high methane concentration. Methane stratification may also be due to inputs into the river/reservoir. At sites without ice cover the methane concentrations were much more uniform. This stratification of methane under ice cover made it difficult to compare the transfer efficiencies of methane and oxygen. When methane concentrations were stratified, a model developed by the U.S. Army Corps of Engineers, SELECT was used. Using temperatures as a guide, SELECT was used to compute an upstream concentration. SELECT was developed using a small model not under ice cover and therefore may not be applicable in this situation.

Overall results of transfer efficiency are shown in Figure VII–1. The transfer efficiency predicted by dissolved oxygen was consistently higher than that predicted by methane. It is felt this may be due to two factors. The first may be that the indexing equation as proposed by Gulliver, et al (1990) does not hold for methane. The suspect term in the indexing equation would be f_g, the term that indexes the transfer to dissolved oxygen. In performing

the calculation this term was assumed to be equal to $\left[\frac{DCH_4}{DO_2}\right]^{1/2}$, where DO_2 is the diffusivity of dissolved oxygen and DCH_4 is the diffusivity of methane. This value is derived from theory coupled with the results of diffusivity experiments.

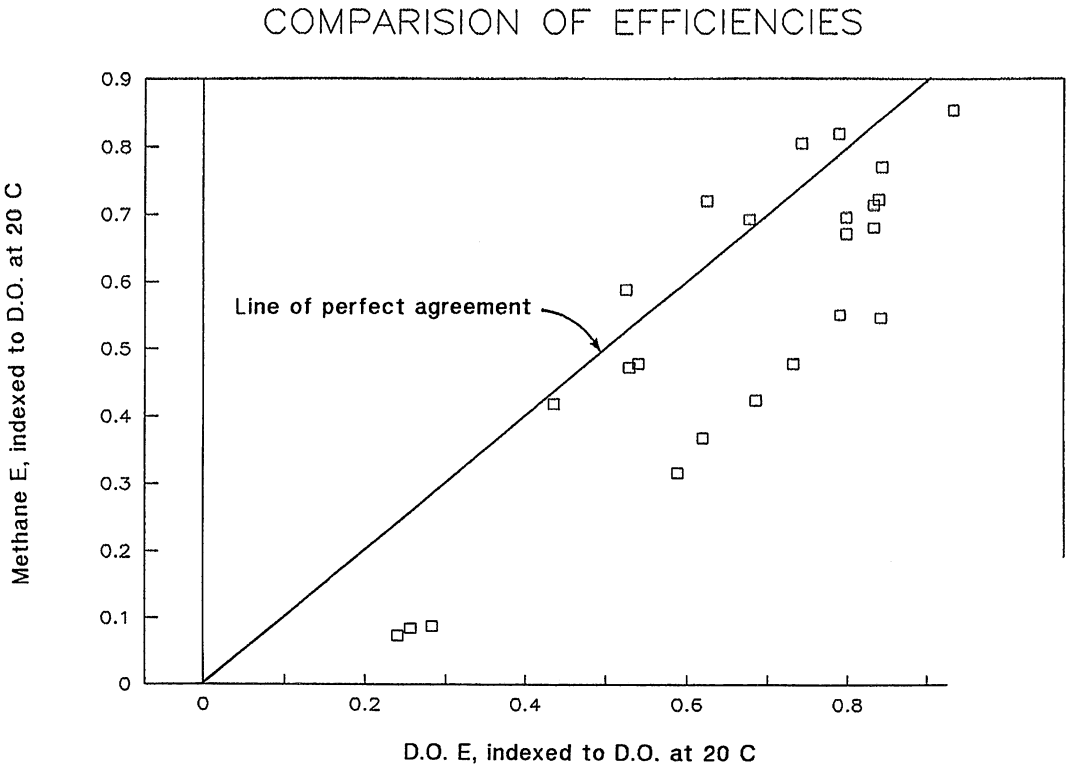

Figure VII–1 Overall E Results

Another thought about the incongruency of the methane and oxygen transfer efficiencies is due to the effect of tailwater on gas transfer. When bubbles are dragged under the surface, the water in contact with the bubble is able to absorb more oxygen (the saturation concentration of oxygen increases with increasing pressure), however, with respect to methane, the bubble receives methane from the water at the same rate no matter how deep the bubble is. A check was performed to verify that methane would not enter into a bubble at a significant rate and affect the gas transfer rate. As a bubble becomes entrained into the flow it contains no methane as there is very little methane in the atmosphere, i.e., $C_s = 0$ for methane. Just prior to leaving the stilling basin, the same bubble will have gained methane from the surrounding water, which is assumed to be insignificant. As there is methane in the bubble, the driving force of the gas transfer is less than what it was when the bubble first entered the flow, or C_s is no longer zero.

Ervine and Elsway (1975) studied the rate of air entrainment caused by a rectangular jet impinging on a free surface. They found the following relationship:

$$\frac{Q_a}{Q_w} = 0.26\left[\frac{b}{p}\right]\left[\frac{h}{t}\right]^{0.446}\left[1 - \frac{v_o}{v}\right] \qquad \text{(VII–1)}$$

where Q_a is the discharge of entrained air, Q_w is the discharge of water, b is the width of the jet (20' at the Rum River dam), p is the perimeter of the jet (for our purposes the length of jet exposed to the surface at the Rum River Dam or 20' was used), h is the fall height, t is the thickness of the jet, v is the velocity at impact and v_o is the minimum velocity needed to entrain air. The minimum velocity to entrain air was found by Ervine and Elsway to be 1.1 m/s.

To determine if the amount of methane in a bubble is significant the mass flow rate of methane from the water is calculated as:

$$C_m = \frac{Q_w\,(C_u - C_d)}{Q_a} \qquad \text{(VII–2)}$$

where C_m = concentration of methane in a bubble, Q_w = water flow rate, Q_a = air entrainment rate, from Ervine and Elsway, C_u = concentration of methane in water upstream, and C_d = concentration of methane in water downstream. From the above equation and using the concentrations and flow rate measured at the Rum River Dam on March 21, 1989, C_m = 10.3 μg/l. This would be the methane concentration in a bubble downstream.

The saturation concentration of a bubble downstream can be found from the ideal gas law and the relationship that 1 gram–mole of an ideal gas at 0^0C and 760 mm Hg will occupy 22.414 liters. If the downstream concentration of methane is 8.1 μg/l then the water concentration can be corrected to the partial pressure of methane in a bubble by Henry's Law. Assuming T=1° C Henry's Law constant is found by:

$$HLC = \frac{M_w\ P}{C_s\ M_m\ \rho} = 25.11\ \ 1\ \text{atm/gram}$$

then the partial pressure of methane in a bubble is then:

$$p = HLC\ C_{CH_4} \qquad \text{(VII–3)}$$

From above p is 2.185 x 10^{-4} atm. The equation for the saturation concentration of methane in a bubble is then:

$$C_{sm} = M_{CH_4}\frac{p}{P}\frac{1\text{g mole}}{22.4141} \qquad \text{(VII–4)}$$

where C_{sm} = saturation concentration of methane in a bubble, M_{CH_4} = molar mass of methane, p = partial pressure of methane found above, P = total pressure. Using the above equation, C_{sm} = 145.6 μg/l. As C_{sm} is an order of magnitude greater than C_m it is assumed that concentration change in bubbles in the flow does not significantly affect transfer efficiency of the tracer gas.

When D.O. predicted a larger E value than methane, an effective depth for bubbles was calculated. This was discussed in detail in Section VI–D. This value is the mean depth at which bubbles get to in the stilling basin. The implications of effective depth are shown in Figure VII–2. The gated control structure at the Rum River Dam was opened to various levels and the transfer efficiencies for D.O. and methane calculated along with the effective depth. A greater discharge should result in the flow having more momentum and thus bubbles should be carried deeper into the flow. Figure VII–2 shows this; as the gate was opened the effective depth increased until it reached the depth of the tailwater. A similar trend was noted with the St. Cloud data (Table VI–7), except that at low discharge the effective depth is negative, and at high discharge it is greater than the tailwater depth. Neither of these seem plausible, and the methane–oxygen comparison of transfer efficiency needs to be studied further.

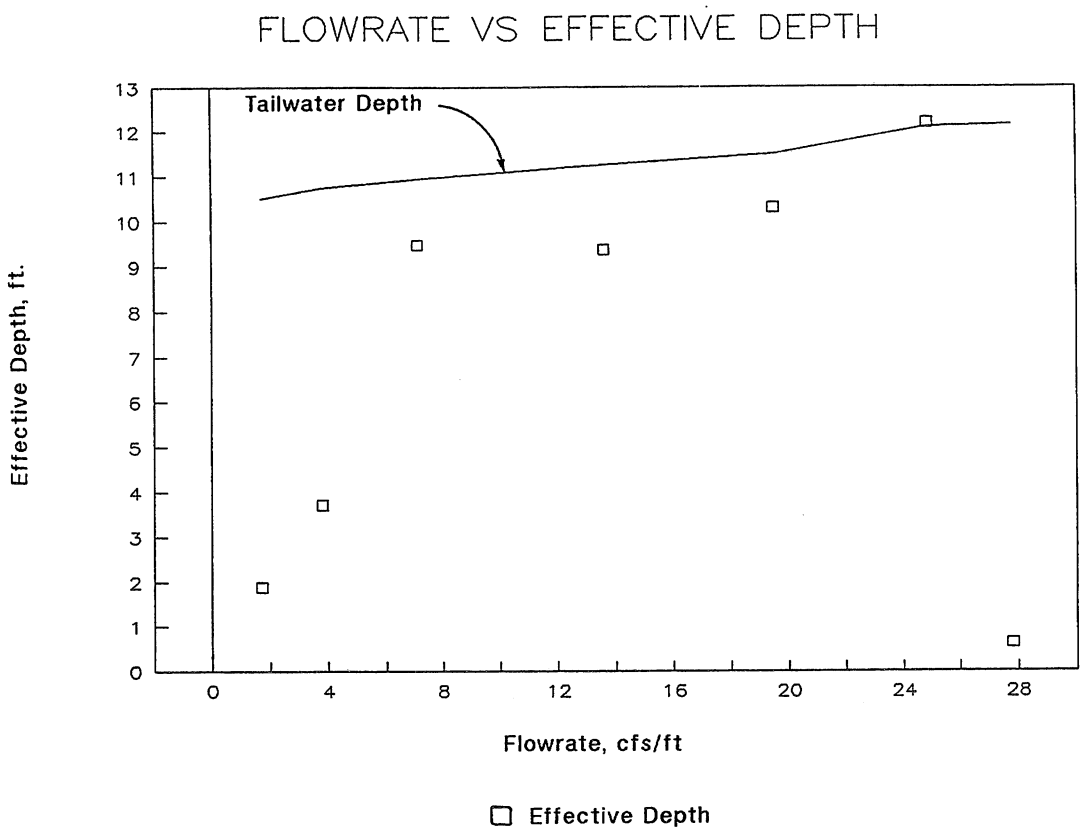

Figure VII–2 Tailwater vs. Effective Depth at Rum River Dam

As stated above, the saturation concentration of water in contact with a bubble changes as a completes its path through a stilling basin. This changes the rate of transfer as a bubble passes through a stilling basin. However the tracer gas saturation concentration of water in contact with bubbles does not change and thus the driving force of gas transfer remains constant. This is a stumbling block in comparing tracer gas transfer to D.O. transfer at hydraulic structures. One does not know how far bubbles are dragged into the stilling basin and thus the saturation concentration of dissolved oxygen is not known.

The very low flows encountered during this study may have had an effect on the results. More flow would have resulted in more mixing, and perhaps the stratification seen with methane under ice cover would not have occurred. Methane stratification occurred when a thermal gradient was observed. That is, when the temperature at the sediment/water interface was higher than that at the ice/water interface there was stratification of methane. More flow might have resulted in a uniform temperature distribution.

VIII. CONCLUSIONS AND RECOMMENDATIONS

The indexing equation proposed by Gulliver et al (1990) could not be sufficiently tested to compare the E values from D.O. and methane. The dissolved gas indexing term, f_g, used was derived from theory together with the results of diffusion tests. Therefore, more research should be in the direction of determining f_g for methane. A test similar to what Rathbun et al (1978) did for propane and ethylene should be done for methane. A tank of water should be deoxygenated and methane added either by bubbling natural gas through the tank or by adding water saturated with natural gas. Propane should be added to the deoxygenated and methane saturated water. This would provide another check on f_g of methane. Measurements should be taken of the reaeration together with the evasion of methane and propane. Thene and Gulliver (1989) have described the headspace analysis method for propane analysis in detail. The results of the methane evasion could be checked with those of propane evasion as the f_g for propane is well documented.

The impact that tailwater depth has on the measurement of transfer efficiency has yet to be quantified. Transfer efficiencies could be taken at a small weir in a laboratory with a varied tailwater which would provide more data to determine the effect of tailwater on E. Propane could be injected into the water to provide an additional check on effective depth. That is, effective depth could be calculated using both methane and propane. If f_g for both gases is correct, the effective depths should be the same.

More structures could be surveyed to provide further information as to the validity of using methane as a tracer for gas transfer. Perhaps more flow would be available and the stratification of methane under ice cover that was measured during this survey period would not occur. If this is the case, (no stratification of methane under ice) then ideal conditions to measure E would occur. Accurate measurements of E using D.O. and methane would be possible and the indexing equation could be used to compare the results.

IX. REFERENCES

Abernathy, R.B., R.P. Benedict, and R.B. Dowell, 1985. "Measurement uncertainty," *Journal of Fluids Engineering*, ASME Vol. 107,pp. 161–167.

Abram, Jeremy W. and David B. Nedwell, 1978. "Inhibition of Methanogenesis by Sulphate Reducing Bacteria Competing for Transferred Hydrogen," *Archives of Microbiology*, Vol. 117, p. 89–92.

American Public Health Association, 1980. *Standard Methods for the Examination of Water and Wastewater (1981). 15th Edition*, New York.

de Angelis, Marie A. and Marvin D. Lilley, 1987. "Methane in surface waters of Oregon estuaries and rivers," *Limnology and Oceanography*, Vol 32, No. 3, pp. 716–722.

Baker–Blocker, Anita, Thomas M. Donahue, and Khalil H. Mancy, 1976. "Methane flux from wetlands areas," *Tellus*, Vol. 29, 245–250.

Barker, H. Albert, 1936. "On the biochemistry of the methane fermentation," *Archives of Microbiology*, Vol. 7, pp. 420–438.

Brownlee, K.A., 1960. *Statistical Theory and Methodology in Science and Engineering*, John Wiley and Sons, New York.

Boylen, Charles W., and Thomas D. Brock, 1973. "Bacterial Decomposition process in Lake Winga sediments during winter," *Limnology and Oceanography*, Vol. 18, No. 4, pp. 628–634.

Broecker, W.S., and T.H. Peng, 1974. "Gas exchange rates between air and sea," *Tellus*, Vol. 26, pp. 21–35.

Bureau of Reclamation, 1974. *Design of Small Dams*, Denver, CO.

Danckwerts, P.V., 1951. "Significance of Liquid Film coefficients in Gas Absorption," *Industrial and Chemical Engineering Chemistry*, Vol. 43, pp. 1460–1467.

Daniil, I., 1983. "Molecular diffusivity of dissolved oxygen in water and water mixtures," Unpublished review, University of Minnesota, St. Anthony Falls Hydraulic Laboratory, Minneapolis, MN

Davis, J.E., J.D. Holland, M.L. Schneider, and S.C. Wilhelms, 1987. "Select: A Numerical One–Dimensional Model for Selective Withdrawal," Report E–87–2, U.S. Army Corps of Engineers Waterways Experiment Station, Vicksburg, MS.

Devol, Allan H., 1983. "Methane oxidation rates in the anaerobic sediments of Saanich Inlet," *Limnology and Oceanography*, Vol. 28, No. 4, pp. 738–742.

Dobbins, W.E. 1956. The Nature of the Oxygen Transfer Coefficient in Aeration Systems, in *Biological Treatment of Sewage and Industrial Wastes,* Reinhold Book Corp., New York, NY, pp. 141–253.

Ehhalt, D.H., 1973. "The atmospheric cycle of methane," *Tellus*, Vol. 24, pp. 58–70.

Electric Power Research Institute, 1989. *Quality Assurance and Quality Control for Environmental Laboratories,* Palo Alto, CA.

Ervine, D.A. and E.M. Elsway, 1975. "The effect of a falling nappe in river aeration," Proceeding, XVI Congress IAHR, Paper C45.

Fallon , R.D., S. Harrits, and R.S. Hanson, 1980. "The role of methane in internal cycling in Lake Mendota during summer stratification," *Limnology and Oceanography*, Vol. 25, pp. 757–760.

Gameson, A., 1957. "Weirs and the aeration of rivers," *Journal of the Institute of Water Engineers*, 11, 447–490.

Gebhart, B. and J.C. Mollendorf, 1977. "A new density relation for pure and saline water," *Deep Sea Research*, Vol. 24, pp. 831–848.

Goldstick, T.K., and Fatt, J, 1970. "Diffusion of oxygen in solutions of blood proteins," Chemical Eng. Progress Symposium Series, Vol. 66, pp. 101–113.

Gulliver, J.S., J.R. Thene, and A.J. Rindels, 1990. "Indexing Gas Transfer in Self–Aerated Flows," *Journal of Environmental Engineering,* ASCE, Vol. 116(3).

Harrits, Susan M. and Richard S. Hanson, 1980. "Stratification of aerobic methane–oxidizing organisms in Lake Mendota, Madison, Wisconsin," *Limnology and Oceanography*, Vol. 25, No. 3, pp. 412–421.

Iversen, Niels, Ronald S. Oremland, and Michael J. Klug, 1987. "Big Soda Lake (Nevada). 3. Pelagic methanogenesis and anaerobic methane oxidation," *Limnology and Oceanography*, Vol. 32, No. 4, pp. 804–814.

Jannasch, Holger W., 1976. "Methane oxidation in Lake Kivu (central Africa)," *Limnology and Oceanography,* Vol. 21, No. 2, pp. 860–864.

Kuivila, K.M., J.W. Murray, A.H. Devol, M.E. Lidstrom, and C.E. Reimers, 1988. "Methane cycling in the sediments of Lake Washington," *Limnology and Oceanography,* Vol. 33, No. 4, pp. 571–581.

Lamontagne, R.A., J.W. Swinnerton, V.J. Linnenbom, and W.D. Smith, 1973. "Methane Concentrations in Various Marine Environments," *Journal of Geophysical Research,* Vol. 24, No. 24, pp. 5817–5324.

Lewis, W.K. and Whitman, W.G., 1924. "Principles of Gas Absorption," *Industrial and Engineering Chemistry*, Vol. 16, pp. 1215–1220.

Lovley, Derek R., Daryl F. Dwyer, and Michael J. Klug, 1982. "Kinetic Analysis of Competition Between Sulfate Reducers and Methanogens for Hydrogen in Sediments," *Applied and Environmental Microbiology,* Vol. 43, No. 6, pp. 1373–1379.

Martens, Christopher, and Robert A. Berner, 1976. "Interstitial water chemistry of anoxic Long Island Sound sediments. 1. Dissolved gases," *Limnology and Oceanography*, Vol. 24, No. 2, pp. 10–25.

McDonald, J.P., J.S. Gulliver, and S.C. Wilhelms, 1989. "Gas Transfer at the Anoka Dam Gated Control Structure," Internal Memorandum, St. Anthony Falls Hydraulic Laboratory, Minneapolis, MN.

Mountfort, Douglas O. and Rodney A. Asher, 1981. "Role of Sulfate Reduction Versus Methanogenesis in Terminal Carbon Flow in Polluted Intertidal Sediment of Waimea Inlet, Nelson, New Zealand," *Applied and Environmental Microbiology*, Vol. 42, No. 2, pp. 252–258.

Oremland, Ronald S., Laurence G. Miller, and Michael J. Whiticar, 1987. "Sources and flux of natural gases from Mono Lake, California," *Geochimica et Cosmochimica Acta*, Vol. 52, pp. 2915–2929.

Phelps, T.J. and J.G. Zeikus, 1984. "Influence of pH on Terminal Carbon Metabolism in Anoxic Sediments from a Mildly Acidic Lake," *Applied and Environmental Microbiology,* Vol. 48, No. 6, pp. 1088–1095.

Rainwater, Kenneth A. and Edward Holley, 1983. "Laboratory Studies on the Hydrocarbon Gas Tracer Technique for Reaeration Measurement," Technical Report CRWR–189, Austin, TX.

Rathbun, R.C., D.W. Stephens, D.J. Schultz, and D.Y. Tai, 1978. "Laboratory Studies of gas tracers for reaeration," *Journal of Environmental Engineering Division*, ASCE, Vol. 104, No. EE2, pp. 1215–1220.

Reeburgh, William and David T. Heggie, 1977. "Microbial methane consumption reactions and their effect on methane distributions in freshwater and marine environments," *Limnology and Oceanography*, Vol. 22, No. 1, pp. 1–9.

Rindels, Alan J. and John S. Gulliver, 1986. "Air–Water Transfer at Spillways and Hydraulic Jumps," *Water Forum '86,* ASCE.

Rindels, Alan J. and John S. Gulliver, 1989. "Measurements of Oxygen Transfer at Spillways and Overfalls," Project Report 266, St. Anthony Falls Hydraulic Laboratory, Minneapolis, MN.

Rudd, John W.M., Akira Furutani, R.J. Flett, and R.D. Hamilton, 1976. "Factors controlling methane oxidation in shield lakes: The role of nitrogen fixation and oxygen concentration," *Limnology and Oceanography*, Vol. 21, No. 3, pp. 357–364.

Rudd, John W.M., and R.D. Hamilton, 1977. "Methane cycling in a eutropic shield lake and its effect on whole lake metabolism," *Limnology and Oceanography,* Vol. 23, pp. 337–345.

Rudd, John W.M., R.D. Hamilton, N.E.R. Campbell, 1974. "Measurement of microbial oxidation of methane in lake water," *Limnology and Oceanography,* Vol. 19, No. 3, pp. 519–524.

Sebacher, Daniel L. Robert C. Harriss and Karen B. Bartlett, 1982. "Methane flux across the air–water interface: air velocity effects," *Tellus,* Vol. 35B, pp. 102–109.

Sheppard, J.C., H Westberg, J.F. Hopper, and K. Ganesan, 1982. "Inventory of Global Methane Sources and Their Production Rates," *Journal of Geophysical Research,* Vol. 87(c2), pp. 1305–1312.

Smith, Richard L. and Michael J. Klug, 1981. "Reduction of Sulfur Compounds in the Sediments of a Eutrophic Lake Basin," *Applied and Environmental Microbiology,* Vol. 41, No. 5, pp. 1230–1237.

Strayer, Richard F. and James M. Tiedge, 1978. "In situ methane production in a small, hypereutrophic, hard–water lake: Loss of methane from sediments by vertical diffusion and ebullition," *Limnology and Oceanography,* Vol. 28, No. 6, 1201–1206.

Thene, John R. 1988. "Gas Transfer at Weirs using the Hydrocarbon Gas Tracer Method with Headspace Analysis," M.S. Thesis, University of Minnesota, Minneapolis, MN.

Thene, John R. and John S. Gulliver, 1989. "Gas Transfer at Weirs Using the Hydrocarbon Gas Tracer Method with Headspace Analysis," Project Report 273, St. Anthony Falls Hydraulic Laboratory, Minneapolis, MN.

Thene, John R., 1989. Personal communication.

Tsivoglou, E.C., 1968. "Tracer Measurement of Stream Reaeration: II Field Studies," *Journal of the Water Pollution Control Federation,* Vol. 77, No. 2, pp. 219–262.

Turekain, K.K., 1969. *Handbook of Geochemistry; volume 1,* Springer–Verlag, New York, p. 318.

U.S. Environmental Protection Agency, *Treatability Manual: Volume 5 Summary,* EPA–600/2–82–001e, Sept. 1981.

Wetzel, Robert G., 1983. *Limnology,* CBS College Publishing, New York.

Wilhelms, S.C., 1984. "Measurements of Dissolved Gases at Corps of Engineers Projects," Technical Report E–84–6, U. S. Army Corps of Engineers Waterways Experiment Station, CE, Vicksburg, MS.

Wilhelms, S.C., 1980. "Tracer Measurement of Reaeration: Application to Hydraulic Models Investigation," Technical Report E–80–5, U.S. Army Corps of Engineers Waterways Experiment Station, CE, Vicksburg, MS.

Woltemate, I., M.J. Whiticar, and M. Schoell, 1984. "Carbon and hydrogen isotopic composition of bacterial methane in a shallow freshwater lake," *Limnology and Oceanography,* Vol. 29, No. 5, pp. 985–992.

Young, C.L., R. Battino, and H.L. Clever, 1986. *Solubility Data Series: Methane,* Vol. 27/28, pp. 1–3, Peramagon Press, New York.

Zehnder, Alexander J.B. and Thomas D. Brock, 1980. "Anaerobic Methane Oxidation: Occurrence and Ecology," *Applied and Environmental Microbiology,* Vol. 44. No. 1, pp. 194–203.

Zehnder, Alexander J.B. and Thomas D. Brock, 1979. "Methane Formation and Methane Oxidation by Methanogenic Bacteria," *Journal of Bacteriology,* Vol. 137, No. 1, pp. 420–432.

Zeikus, J.G. and M.R. Winfrey, 1976. "Temperature Limitation of Methanogenesis in Aquatic Sediments," *Applied and Environmental Microbiology,* Vol. 31, pp. 99–107.

APPENDIX A

```
                        $debug
C
C     THIS PROGRAM COMPUTES THE ORIGINAL WATER CONCENTRATIONS FOR
C     METHANE ANALYZED BY THE HEADSPACE GAS CHROMATOGRAPHIC TECHNIQUE
C       ADDITIONALLY IT COMPUTES THE TRANSFER NUMBER, E, AND
C       THE UNCERTAINTY ASSOCIATED WITH THAT NUMBER
C       FILES NEEDED:
C             BODAT : THE NUMBER OF BOTTLES, THE WEIGHT OF THE
C                   BOTTLES (GM) AND THEIR VOLUMES (ML)
C           EXPDAT : WHERE EXPDAT IS THE NAME OF A FILE
C          WITH THE NUMBER OF SAMPLES, THE SAMPLING AND ANALYSIS
C          THE BOTTLE NUMBER, THE MASS WITH H.S. (GM), THE G.C.
C          TEMPERATURES(^C), EACH CALIBRATION IS GIVEN WITH VOLUME
C          AND ITS AREA COUNT, THEN, PER SAMPLE:
C          AREA COUNTS, THE VOLUME INJECTED (UL), AND A 25 SYMBOL
C          DESCRIPTION IN QUOTES EX: 'UPSTREAM,12:15,6/25/87'
C
      PARAMETER(NB=117,MAXINJ=10)
      DIMENSION BOWT(NB),BOVOL(NB),VW(NB),WWHS(NB),VH(NB)
      DIMENSION NOTINC(NB),WCM(NB),NINJ(NB),CAVG(NB)
      DIMENSION X(50),Y(50),C(50)
      DIMENSION PERTUS(NB),AREA(NB,MAXINJ),VINJ(NB,MAXINJ)
      DIMENSION CENV(NB,MAXINJ)
      DIMENSION INCLUD(NB,MAXINJ),CONFIN(NB),UC(NB)
      CHARACTER BODAT*18,EXPDAT2*18,RESULTS*18,overall*18,sample*18
      CHARACTER DESC(NB)*60,GCNOTE(NB,MAXINJ)*45,TESTD(3)*60
      CHARACTER DES*10,RESFN*14,SAMFN*14
      INTEGER BOTN(NB)
      REAL MMETH,MWATER,MCAP,MSEPTA
      PARAMETER(MMETH=16.0403,  MWATER=18.0152,   RUNIV=0.082057)
      PARAMETER(TKO=273.15, MCAP=3.036, MSEPTA=0.736)
C
C RUNIV = UNIVERSAL GAS CONSTANT
C CRATIO = GAS TRANSFER RATIO FOR METHANE TO OXYGEN, TKO = TEMPERATURE CONSTANT
C
      write(*,'(a\)')' enter bottle data file name '
      read(*,'(a)')bodat
      open(unit=1,file=bodat)
C
      READ(1,*)NOBOT
      READ(1,*)(BOWT(I),BOVOL(I),I=1,NOBOT)
C
      write(*,'(a\)')' enter data file '
      read(*,'(a)')expdat2
      open(unit=2,file=expdat2)
C
      READ(2,*)(TESTD(I),I=1,3)
      READ(2,*)NCAL,NSAMP,NUPS,NDNS
C     NCAL=NUMBER CALIBRATIONS, NSAMP=NUMBER SAMPLES
C     NUPS=NUMBER UPSTREAM, NDNS=NUMBER DOWNSTREAM
      READ(2,*)TENV,TLAB,PRESS
      READ(2,*)TK,TA,TB,SIGMA
C     TK,TA, AND TB ARE CONSTANTS ASSOCIATED WITH CALIBRATION LINE
C     THESE CONSTANTS WERE COMPUTED USING LOTUS
C     SIGMA IS STD DEVIATION OF VOLUME OF STANDARD INJECTED
C     TENV=TEMP OF ENVIRONMENT, TLAB=LAB TEMP, PRESS=PRESSURE IN MM HG
      DO 130 I = 1,NCAL
      READ(2,*) X(I),Y(I),C(I)
130   CONTINUE
C
```

Appendix A. FORTRAN program used to compute methane concentrations, transfer efficiencies and uncertainties.

```
C     X IS AREA COUNTS & Y VOLUME [UL] & C IS IN PPM
C
      DO 200 I=1,NSAMP
      READ(2,*) BOTN(I),WWHS(I),NINJ(I),DESC(I)
      DO 150 J=1,NINJ(I)
      READ(2,*) AREA(I,J),VINJ(I,J),INCLUD(I,J),GCNOTE(I,J)
150   CONTINUE
200   CONTINUE
C
      close(unit=2)
C
      TENV=TENV+TKO
      TLAB=TLAB+TKO
      RHOLAB=RHO(TLAB)
      RHOENV=RHO(TENV)
C     RHOLAB=DENSITY OF WATER IN LAB, RHOENV=WATER DENSITY INSITU
C
C     ***************************************************************
C     **  CALCULATE TERMS USED IN FINDING CALIBRATION UNCERTIANTY   **
C     ***************************************************************
C
      FIRST = 0
      SECOND = 0
      THIRD = 0
      COMBINE = 0
C
      DO 300 I=1,NCAL
C
C     THE FOLLOWING COMPONENTS WHICH WILL BE USED TO FIND
C     THE UNCERTAINTY IN THE CALIBRATION
C
      FIRST=FIRST + X(I)
      SECOND=SECOND + X(I)**2
      THIRD = THIRD + SECOND**2
      COMBINE = COMBINE + X(I)*X(I)**2
C
300   CONTINUE
C
C    ********************************************
C    ** CALCULATE C(I,J), CAVG(I), AND WCM(I)   **
C    ********************************************
C
C     COMPUTE H IN ATM*L/G, NOTE RTOMMH IS UNITLESS
C
      HC=HENRY(TLAB,RHOLAB)
      RTOMMH=(RUNIV*TLAB)/(MMETH*HC)
      SLFAC=MMETH*PRESS/760/RUNIV/TLAB/1000000
C
C    COMPUTE CONCENTRATION IN MICROGRAMS PER LITER
C
      DO 700 I=1,NSAMP
      VW(I)=(WWHS(I)-BOWT(BOTN(I))-MCAP-MSEPTA-0.50)/RHOLAB
C     0.5 ACCOUNTS FOR FORMADEHYDE ADDED AS PERSERVATIVE
      VH(I)=BOVOL(BOTN(I))/1000-VW(I)-0.000550
      UCAL=0
      UCAL2=0
      CSUM=0
      CSUM2=0
      NOTINC(I)=NINJ(I)
      DO 500 J=1, NINJ(I)
```

```
         VOLSTD = TK + TA*AREA(I,J) + TB*AREA(I,J)**2
C     VOLSTD IS EQUIVILENT AMOUNT OF STANDARD INJECTED
         CSYR = VOLSTD*SLFAC*C(1)/VINJ(I,J)
C     CSYR = CONCENTRATION IN SYRINGE
         UPPERA = ((AREA(I,J)-0)**2)*THIRD
         UPPERB = 2*(AREA(I,J)-0)*(AREA(I,J)**2-0)*COMBINE
         UPPERC = UPPERA - UPPERB + AREA(I,J)**4*SECOND
         VAR = UPPERC / (SECOND*THIRD - COMBINE**2)
         UM = SIGMA * SLFAC * 99 * TSCORE(NCAL-3) * (1/NCAL + VAR)**0.5
C      UM = UNCERTAINTY IN MASS
         CHSI=  CSYR*1000000
         CLAB=CHSI*(RTOMMH+VH(I)/VW(I))
         CENV(I,J)=CLAB*RHOLAB/RHOENV
         CSUM=CSUM+INCLUD(I,J)*CENV(I,J)
         CSUM2=CSUM2+INCLUD(I,J)*CENV(I,J)**2
         NOTINC(I)=NOTINC(I)-INCLUD(I,J)
         UCAL = UM / VINJ(I,J) *(RTOMMH + VH(I)/VW(I))*1000000
         UCAL2 = UCAL2+(UCAL/NINJ(I)*INCLUD(I,J))**2
C
C      UCAL=UNCERTIANTY IN CONCENTRATION INJECTION
C
500   CONTINUE
C
      NINC=NINJ(I)-NOTINC(I)
      UC(I) = (UCAL2/(NINC**2))**0.5
C     UC IS UNCERTAINTY IN CONCENTRATION OF BOTTLE DUE TO CALIBRATION
      UC2 = UC2 + UC(I)**2
      IF (I.EQ.NUPS) THEN
       WCUC=UC2**0.5/NUPS
       UC2=0
      ELSE IF (I.EQ.NUPS+NDNS) THEN
       WCDC=UC2**0.5/NDNS
      END IF
C
      CAVG(I)=CSUM/NINC
C
      SDCI=((CSUM2-CSUM**2/NINC)/(NINC-1))**0.5
      CONFIN(I) = SDCI*TSCORE(NINC-1)
      WCM(I) = CONFIN(I)/NINC**0.5
C     WCM IS PRECISION UNCERTAINTY OF BOTTLE
      PERTUS(I) = 100*WCM(I)/CAVG(I)
700   CONTINUE
C
      close(unit=1)
C
C     ******************************************************
C     ** COMPUTE PREC UNC'S: WCUM, WCDM, WEP IN CU, CD, E **
C     ******************************************************
C
      WSUM=0
      CSUM=0
      DO 800 I=1,NUPS
        CSUM=CSUM+CAVG(I)
       WSUM=WSUM+WCM(I)**2
800   CONTINUE
      CU=CSUM/NUPS
      WCUM=WSUM**(0.5)/NUPS
C
C     COMPARE THIS UNCERTAINTY TO BOTTLE AVG UNCERTAINTY
C
```

```
      CSUM =0
      DO 825 I = 1,NUPS
      CSUM = (CAVG(I)-CU)**2+CSUM
825   CONTINUE
      IF (NUPS .NE.1) GO TO 826
      S=0
      WCU=0
      GO TO 828
C
826   S=(CSUM**0.5)/(NUPS-1)**0.5
      WCU=TSCORE(NUPS-1)*S/(NUPS)**0.5
828   IF (WCUM .GT. WCU) GO TO 830
      WCUM = WCU
C
830   CSUM=0
      WSUM=0
      DO 900 I=NUPS+1,NUPS+NDNS
        CSUM=CSUM+CAVG(I)
        WSUM=WSUM+WCM(I)**2
900   CONTINUE
      CD=CSUM/NDNS
      WCDM=WSUM**(0.5)/NDNS
C
C     COMPARE THIS UNCERTAINTY TO DOWNSTREAM BOTTLE AVG UNCERTAINTY
C
      CSUM = 0
      DO 850 I = NUPS+1,NDNS+NUPS
      CSUM=CSUM+(CAVG(I)-CD)**2
850   CONTINUE
      IF (NDNS .NE.1) GO TO 832
      WCD=0
      GO TO 834
c
832   S=((CSUM**0.5)/(NDNS-1))**0.5
      WCD=TSCORE(NDNS-1)*S/(NDNS**0.5)
834   IF (WCDM .GT. WCD) GO TO 875
      WCDM = WCD
C
875   E=1-CD/CU
C
C     E IS TRANSFER EFFICIENCY
C
      WEP=((- WCDM/CU)**2+(CD*WCUM/CU**2)**2)**0.5
C     WEP IS PRECISION UNCERTAINTY IN SAMPLES
C ************************************************************
C **              COMPUTE WEY                                 **
C ** WEY IS THE UNC IN E DUE TO AN UNC IN THE CALIBRATION  **
C ************************************************************
C
      WEY = ((WCDC/CU)**2 + (CD/CU**2*WCUC)**2)**0.5
C
C   ************************************************
C   ** COMPUTE BEVSYR: THE BIAS IN E DUE TO A BIAS   **
C   **                 SYRINGE VOLUME                **
C   ************************************************
C
      BEVSYR=0.02*CD/CU
C
C   ************************************************
C   ** COMPUTE WEFW: THE UNCERTAINTY DUE TO THE TERM **
```

```
C   **                FW=(RTOMMH + VH(I)/VW(I)          **
C   ************************************************
      A = NUPS
      B = NDNS
C
      WEFW = CD/CU * 0.01 * (1/A + 1/B)**0.5
C
C   ************************************************
C   ** COMPUTE BEH: THE BIAS IN E DUE TO BIAS IN H **
C   ************************************************
C
      BCHS=0
      DO 1000 I=1,NUPS
        CHS=CAVG(I)/(RTOMMH+VH(I)/VW(I))
        BCH=CHS*RTOMMH*0.0017
        BCHS=BCHS+BCH
1000  CONTINUE
      BCUH=BCHS/NUPS
C
      BCHS=0
      DO 1100 I=NUPS+1,NUPS+NDNS
        CHS=CAVG(I)/(RTOMMH+VH(I)/VW(I))
        BCH=CHS*RTOMMH*0.0017
        BCHS=BCHS+BCH
1100  CONTINUE
      BCDH=BCHS/NDNS
C
      BEH=((-BCDH/CU + BCUH*CD/CU**2)**2)**0.5
C
C   ************************************************
C   ** COMBINE WEP, WEY, WEFW, BEVSYR AND BEH TO GIVE **
C   **            THE TOTAL UNCERTAINTY IN E = UE       **
C   ************************************************
C
      BEVSYR=0
      UE2= WEP**2 +WEFW**2 + BEH**2+WEY**2+BEVSYR**2 + WECAL**2
      UE=UE2**0.5
C
C   ****************************************
C   ** CONVERT E(METHANE,TENV) TO E(O2,20C) **
C   ****************************************
C
      FG=0.880
      FT=0.6124+0.01773*(TENV-TKO)+0.00008261*(TENV-TKO)**2
      FI=FG*FT
      EOX=1-(1-E)**(1/FI)
      UEOX=UE*1/FI*(1-E)**(1/FI-1)
C
C   ************************************************
C   * OUTPUT CU, CD, E, UE AND THE COMPONENT WE'S  **
C   ************************************************
C
C   WRITE RESULTS TO SCREEN
      WRITE(*,1800)
      WRITE(*,1900)(TESTD(I),I=1,3)
      WRITE(*,1800)
      WRITE(*,1950)TENV-TKO
      WRITE(*,2000)CU
      WRITE(*,2010)WCUM
      WRITE(*,2020)CD
```

```
      WRITE(*,2025)WCDM
      WRITE(*,2100)E
      WRITE(*,2120)UE
      WRITE(*,2140)100*UE/E
      WRITE(*,2200)WEP
      WRITE(*,2250)WEY
      WRITE(*,2301)WEFW
      WRITE(*,2400)NDNS
      WRITE(*,2500)NUPS
      WRITE(*,2600)BEH
      WRITE(*,2625)
      WRITE(*,2650)EOX
      WRITE(*,2700)UEOX
C
      write(*,'(a\)')' ENTER OVERALL RESULTS FILE NAME (.RES)'
      read(*,'(a)')results
      overall=results//'.res'
      open(unit=3,file=overall,status='new')
C
      write(*,'(a\)')' ENTER SAMPLE RESULTS FILE NAME (.SAM)'
      read(*,'(a)')results
      sample=results//'.sam'
      open(unit=4,file=sample,status='new')
c
      WRITE(3,1800)
      WRITE(3,1900)(TESTD(I),I=1,3)
      WRITE(4,1900)(TESTD(I),I=1,3)
      WRITE(3,1800)
      WRITE(3,1950)TENV-TKO
      WRITE(3,2000)CU
      WRITE(3,2010)WCUM
      WRITE(3,2020)CD
      WRITE(3,2025)WCDM
      WRITE(3,2100)E
      WRITE(3,2120)UE
      WRITE(3,2140)100*UE/E
      WRITE(3,2200)WEP
      WRITE(3,2250)WEY
      WRITE(3,2301)WEFW
      WRITE(3,2400)NDNS
      WRITE(3,2500)NUPS
      WRITE(3,2600)BEH
      WRITE(3,2625)
      WRITE(3,2650)EOX
      WRITE(3,2700)UEOX
C   ***************************************************
C   **  OUTPUT INDIVIDUAL CONCENTRATIONS AND WCM(I)   **
C   ***************************************************
C
      DO 1300 I=1,NSAMP
      WRITE(4,3000)BOTN(I)
      WRITE(4,3020)DESC(I)
      WRITE(4,3100)CAVG(I)
      WRITE(4,3120)PERTUS(I)
      WRITE(4,3123)WCM(I)
      WRITE(4,3125)UC(I)
      WRITE(4,3126)VH(I)/VW(I)+RTOMMH
      WRITE(4,3135)CONFIN(I)
      WRITE(4,3150)
      WRITE(4,3200)(CENV(I,J),GCNOTE(I,J),J=1,NINJ(I))
```

```
1300  CONTINUE
C
1800  FORMAT(/)
1900  FORMAT(A60)
1950  FORMAT(' WATER TEMPERATURE [^C]',F7.1)
2000  FORMAT(/' UPS CONC [UG/L]      ',F10.2)
2010  FORMAT(' UPS CONC UNC [UG/L]   'F8.2)
2020  FORMAT(' DNS CONC [UG/L]      ',F10.2)
2025  FORMAT(' DNC CONC UNC [UG/L]   'F8.2)
2100  FORMAT(' TRANSFER #, E [-] ',F10.3)
2120  FORMAT(' TOTAL UNC IN E [-]',F10.3)
2140  FORMAT(' PERCENT UNC [-]',F14.3)
2200  FORMAT(' PRECISION UNCERTAINTY IN E',F10.5)
2250  FORMAT(' WE DUE TO CALIBRATION',F10.5)
2301  FORMAT(' WE DUE TO HCF ',F10.5)
2400  FORMAT(' NUMBER SAMPLES DOWNSTREAM    ',I2)
2500  FORMAT(' NUMBER SAMPLES UPSTREAM  ',I2)
2600  FORMAT(' BE DUE TO H         ',F15.5)
2625  FORMAT(/' TRANSFER EFF., DEF RATIOS:, OXYGEN AT 20^C')
2650  FORMAT(/' MEASURED E          ',F6.3)
2700  FORMAT(' TOTAL UNC IN E     ',F6.3)
3000  FORMAT(/' SAMPLE NO          ',I3)
3020  FORMAT(' DESCRIPTION       ',A45)
3100  FORMAT(' AVG CONC [UG/L]',F7.2)
3110  FORMAT(' TOTAL UNC         ',F6.2)
3120  FORMAT(' PERCENT UNC       ',F6.2)
3123  FORMAT(' PRECISION UNC IN SAMPLE',F7.2)
3125  FORMAT(' UNC DUE TO CALIBRATION',F10.2)
3126  FORMAT(' HEADSPACE CORRECTON FACTOR',F10.3)
3135  FORMAT(' CONFIDENCE INTERVAL',F6.2)
3150  FORMAT(' INDIVIDUAL G.C. RUNS:')
3200  FORMAT(3X,F6.2,8X,A45)
      close(unit=3)
      close(unit=4)
C
C
      END
C *****************
C **** FUNCTIONS **
C *****************
      FUNCTION HENRY(T,R)
C
C     HENRY'S CONST. HAS UNITS OF LITER*ATMOSPHERE/GRAM
C     MOLE FRACTION (MFRAC) IS UNITLESS
C
      REAL MFRAC,MWATER,MMETH
      PARAMETER(MMETH=16.0430,MWATER=18.0152)
      MFRAC=EXP(-78.1564+104.4791/(T/100)+29.7802*LOG(T/100))
C
C     MFRAC IS FROM PAPER BY BATTINO, R IS DENSITY OF WATER (RHO)
C
      HENRY=MWATER/(MFRAC*MMETH* R)
      END
C
C
      FUNCTION RHO(T)
C
C     RHO IS DENSITY IN G/L, GIVEN BY EQUATION FROM HENDERSON-SELLERS
C
      PARAMETER(uu=999.9726,xx=277.029325,yy=1.89482)


      RHO=uu*(1-0.000009297173*(ABS(T-xx))**yy)
C     RHO IS ACCURATE TO WITHIN 0.00035
      END
C
      FUNCTION TSCORE(IDEGFR)
      TSCORE=1.96+2.36/IDEGFR+3.2/IDEGFR**2+5.2/IDEGFR**3.84
      END
```